"The other day, as I will swear
I saw some salt that was not there.
It was not there again today –
How do I prove it went away?."

-John Van Couvering

University of Alberta

HONDO EVAPORITES WITHIN THE GROSMONT HEAVY OIL
CARBONATE PLATFORM, ALBERTA, CANADA

by

MARY LUZ BORRERO

A thesis submitted to the Faculty of Graduate Studies and Research
in partial fulfillment of the requirements for the degree of

MASTER OF SCIENCE

DEPARTMENT OF EARTH AND ATMOSPHERIC SCIENCES

©Mary Luz Borrero
Fall 2010
Edmonton, Alberta

Examining Committee

Dr. Hans G. Machel, Department of Earth and Atmospheric Sciences

Dr. S. George Pemberton, Department of Earth and Atmospheric Sciences

Dr. Douglas Schmitt, Department of Physics

To my parents Rafael and Graciela, you are the light of my eyes. Thanks
for the unconditional love, guidance, patience, and care.

In loving memory of my brother Henry.

A mis padres quienes son el pilar de mi vida y mi alegría.
A mi hermano Henry, siempre vivirás en mi memoria.

ABSTRACT

The Upper Devonian Grosmont shelf complex is the world's largest heavy oil deposit hosted in carbonates, with an estimated >50 billion cubic meters (318 to probably 406 bbls) of initial volume in place. At present the Grosmont is not yet under production. This study involves log interpretation, core examination; facies description; strontium, sulphur, carbon, and oxygen isotope analysis. The Grosmont is subdivided into four shallowing-upward cycles. Most Hondo evaporites are part of the Upper Grosmont 3 and Lower Grosmont and were deposited in a series of small, shallow subaqueous brine ponds or in an extensive lagoon. In the eastern part of the area, the Hondo appears to be dissolved resulting in solution-collapse breccias. Other diagenetic processes that were important in shaping the present reservoir characteristics were pervasive dolomitization and dolomite recrystallization, fracturing, and karstification.

ACKNOWLEDGEMENTS

TABLE OF CONTENTS

CHAPTER 5:   GEOCHEMISTRY

CHAPTER 6:   DISTRIBUTION AND DEPOSITIONAL

ENVIRONMENT OF HONDO

CHAPTER 7:   **CONCLUSIONS AND FUTURE WORK**

LIST OF TABLES

LIST OF FIGURES

PAGE

CHAPTER 1

INTRODUCTION

The Upper Devonian Grosmont shelf complex is the world's largest heavy oil deposit hosted in carbonates, with an estimated > 50 billion cubic meters (318 to probably 406 bbls) of initial volume in place (Hein, 2006; ERCB, 2010). At present, the Grosmont reservoir is not under production but is under consideration for several in-situ thermal recovery schemes.

The Grosmont reservoir is located in east-central Alberta at depths of 250 m to approximately 1200 m in the up-dip limit of the Alberta Basin (Figure 1.1). The Grosmont shelf complex represents a shallow marine carbonate platform (Cutler, 1983; Machel and Hunter, 1994; Huebscher, 1996), and is subdivided into four shallowing-upward cycles: Lower Grosmont (LGM), Upper Grosmont1 (UGM1), Upper Grosmont2 (UGM2), and Upper Grosmont3 (UGM3). These units are separated by layers of marl of the Lower Ireton Formation that are named consecutively SB1, SB2, and SB3, and can be identified on gamma ray and resistivity well logs. The Hondo "Formation" (not recognized as a Formation in the Canadian Stratigraphic Code) is an evaporitic sub-unit within the Grosmont and replaces part of the four cycles in certain portions of the complex, especially at the top of the UGM3. Diagenetic processes, such as dolomitization, dissolution, and karstification have affected the succession especially in the upper stratigraphic units (Huebscher, 1996). Also, brecciation took place mainly in the eastern part of the complex, near the pre-Cretaceous erosional edge.

Several studies regarding characterization of the reservoir properties have been conducted in the Grosmont Platform, mainly in the east and central portions (Machel and Hawlader, 1990; Dembicki and Machel, 1996; Huebscher, 1996). However, the southern and western areas near the western limit of the Grosmont platform have not been studied in great detail, and therefore, the spatial distribution of the Hondo is not well known in that area.

The Hondo evaporites were first described by Belyea (1952) as the Hondo "member", which is stratigraphically equivalent to the upper part of the Grosmont Formation. Local studies of the Hondo have been undertaken by Cutler (1983), and a sketch of the possible areal distribution of the Hondo is shown in Chapter 12 of the Geological Atlas of the Western Canada Sedimentary Basin by Mossop and Shetsen (1994). However, it is important to note that no data was provided to support the Hondo distribution. Moreover, the Hondo is not formally stratigraphically defined as part of the Grosmont or the Ireton Formations, probably because data is sparse in the area and evaporite facies had been observed in only five cores. Thus, the depositional nature and areal distribution of the Hondo evaporites remain somewhat enigmatic.

1.1 Objectives and importance of this project

Currently, with the decrease in global conventional oil reserves, heavy oil has become the new frontier of exploration. The Grosmont Formation is known for its large bitumen reserves but a lack of geological understanding as well as high production costs had made the reservoir not commercially viable until now.

2

This study attempts to provide new insights into the depositional environment and distribution of the Hondo, its relationship with the Grosmont Formation, and to supplement the understanding of the geometry and oil trapping characteristics in the Grosmont. Specific objectives of this study include:

1. Delineation of the spatial distribution of Hondo evaporites.

2. Better define the western margin of the Grosmont platform.

3. Investigate the sedimentological and diagenetic characteristics of the Hondo.

4. Determine the depositional and sedimentological evolution of the Hondo evaporites, and to suggest possible recent analogs for the Hondo.

5. Determine the role of the Hondo evaporites as a potential reservoir seal.

1.2 Study Area

The study area spans approximately 24,700 km^2 and is located in the subsurface of north-central Alberta. The north-south limits are townships 68 to 89 and east-west limits are between range 22W4 and range 10W5 (Figure 1.1).

1.3 Methods

This study involves core examination; facies description; log interpretation; strontium, sulphur, carbon, and oxygen isotope analysis.

Based on the density of well control, the study area can be subdivided in two geographic regions, northeastern and southwestern. The density of wells is lower

in the southwestern part of the study area. In the northeastern part, the density of wells penetrating the Devonian is approximately one to two wells per township, and density increases towards the eastern limit of the platform approaching the erosional edge. An important issue with the dataset is the quality and reliability of the cores and cuttings, as most of the wells in the area were drilled during the 1950's, 1960's, and 1970's. Seismic information was not available for the study area.

1. 3.1 Core and cuttings description

Data was collected from 32 cored wells and 105 wells with only cuttings. All rock material is stored in the Alberta Energy and Utilities Board (EUB) Core Research Centre (CRC), located in Calgary. Basic core data is summarized in Table 1; a list of the wells with only cuttings is presented in Appendix 1.
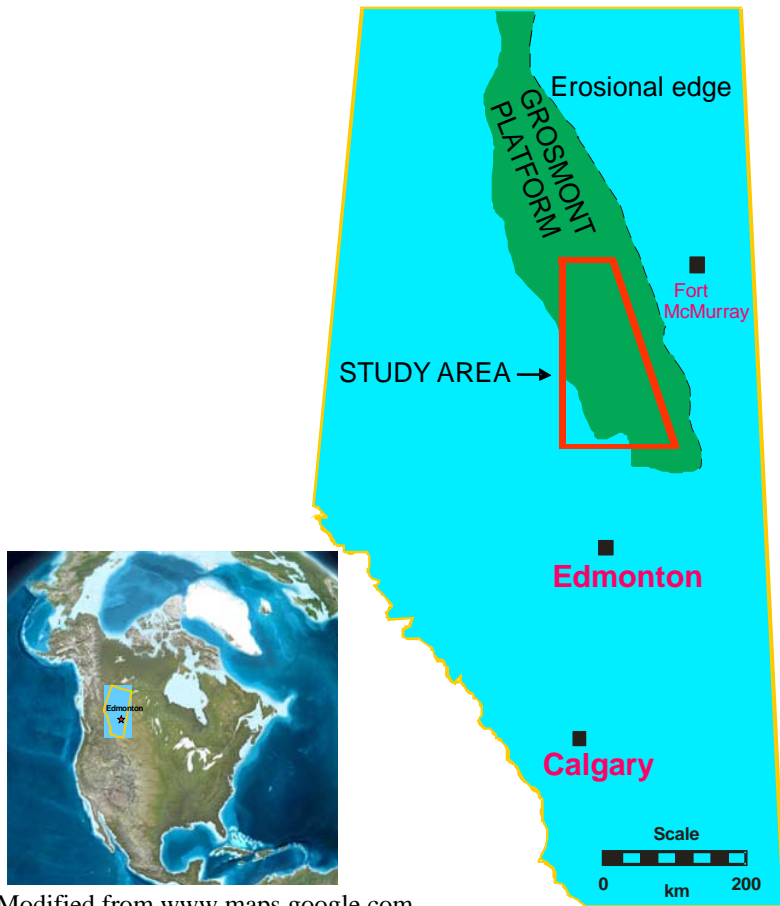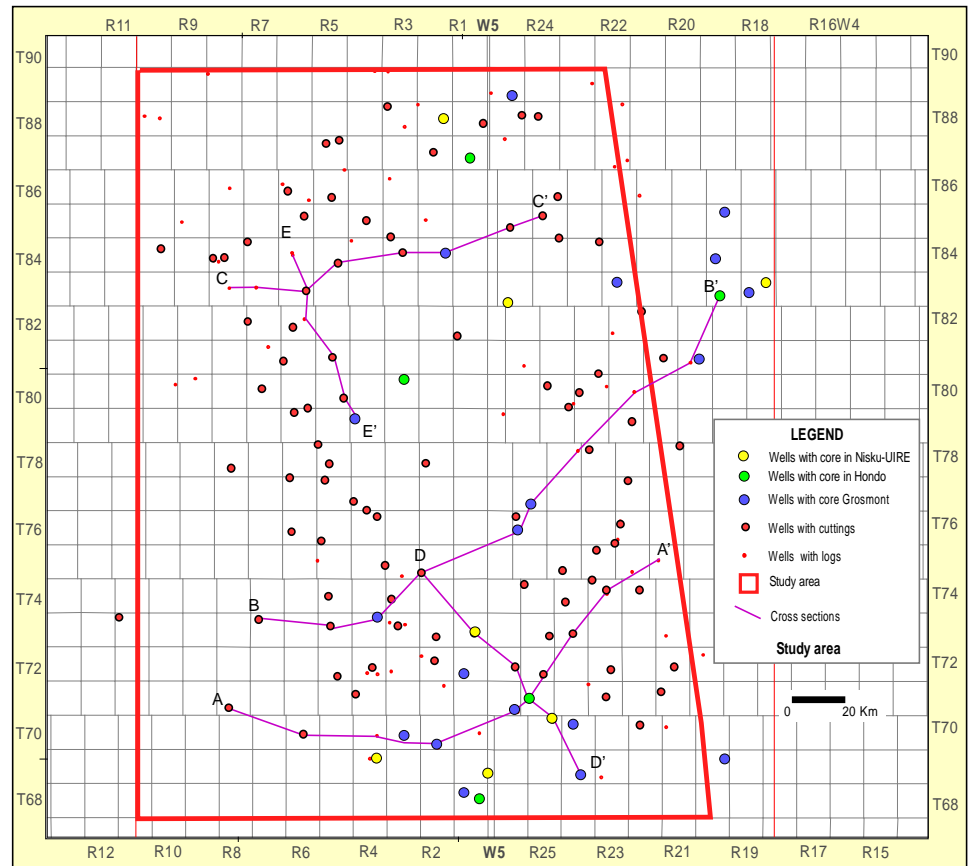
Figure1.1 Location of the study area.

Well ID	Core Depth (m)	Formation	Observation
02-29-68-01W5	1127.7-1139.05	UIRE -UGM3	
02/15-23-68-01W5	1096-1127	UGM3, UGM2?	No logs. Contains Hondo
08-28-69-04W5	1305-1337	Nisku-UIRE	
01-12-69-01W5	964.80-1043.0	UIRE-Nisku	
05-25-69-20W5	626-738.24	UGM3, UGM2, UGM1	
04-15-69-24W4	1005.84-1019.60	LIRE-LGM	
03-28-70-24W4	740.7-751.9, 854.7-868.4	Nisku, UGM3, UGM2	
11-35-70-25W4	893.05-901.09	Nisku-UIRE	
02-23-70-01W5	879.3-880.87	Nisku	
06-03-70-02W5	1215-1253.7	UGM3	
01-09-70-03W5	1155.40-1161.5	GM3	
15-17-71-25W4	888.5-918.20, 1012-1047.9	UGM3, LGM	"Hondo type well"
10-01-71-26W4	928.11-932.38	UGM3	
05-09-72-01W4	881.5-1026	Nisku, UGM3, UGM2	
10-35-73-04W5	1012.9-1121.70	Nisku-UGM2	
10-18-76-25W4	1043.7-1066.8	UGM3	
06-10-77-25W4	1052.47-1057.04	LGM	
02-30-79-04W5	1065-1076.74	UGM3	
11-34-80-03W5	831.20-976.63	UGM3, UGM2	Contains Hondo, Incomplete logs
11-14-81-20W4	380-389, 449.0-455	UGM3, UGM1	
16-24-81-20W4	430-433.1	Grosmont	
06-24-83-18W4	295.7-300.8	UIRE	
10-17-83-18W4	370.25-460.5	UGM3-LGM	
10-09-83-19W4	371.0-438.35	UGM2, UGM1, LGM	
13-22-83-22W4	555.0-584.32	UGM3, UGM2	
08-05-83-25W4	416.0-419.0	Nisku	
13-24-84-02W5	856-860	UGM1	

Table 3.1 Core wells summary

Well ID	Core Depth (m)	Formation	Observation
10-17-84-19W4	371.5-521	Grosmont	Grosmont type well Contains Hondo
06-34-85-19W4	322-406.5	UIRE?, UGM3, UGM2	
08-16-87-01W5	652-900	Calmar to UGM2	No logs below Nisku. Contains Hondo
10-14-88-02W5	672.8-725.5	Nisku - UIRE	
06-11-89-25W4	529.0-585.5, 624-638	UGM2, UGM1, LGM,	

A total of five wells contain "evaporite" facies, four of them within the Upper Grosmont, and one of them within the Lower Grosmont (in the Grosmont type section well). Well 15-17-71-25W4 is informally considered the "type well" of the Hondo, because it contains the most complete evaporite succession (25 m) in the study area. An additional 27 wells with core contain intervals of the Nisku, Ireton, and Grosmont formations but no "evaporites" were found. Recognition of Grosmont units and facies is based on the Grosmont subdivision made by Union Oil, later refined by Cutler (1983), for the Grosmont type section well 10-17-84-19W4, which contains the entire Grosmont Formation. Facies descriptions are based on the lithofacies types defined by Machel and Hunter (1994).

Approximately 25,000 m of drill cuttings were examined; cuttings are generally taken every 3 m (10 ft). The main purpose for examining the cuttings was the identification of the sulphate minerals, anhydrite and gypsum. Part of the coarse fraction (1-2mm) of the cuttings was dipped into a 10% HCL solution and parts of the fraction into an Alizarin Red-S solution to identify calcite or dolomite

which were examined under binocular microscope. Determining the presence of sulphates was done using a binocular microscope; anhydrite and gypsum chips were dipped into a solutional-mix of acid and water. If needle-shaped minerals were formed as the chips were dried, they were identified as sulphate bearing (anhydrite or gypsum) (Figure 1.2). For each interval of ten feet, minerals of chips were classified and counted to determine the relative abundance of the rock types (expressed as a percentage).

Some wells have poor recovery and/or show poor sample quality. The poor quality is attributed to loss of circulation when drilling, and contamination from overlying intervals (cavings). Nevertheless, cuttings were useful to identify marl/shale (layers) within the Grosmont units and were calibrated against geophysical wireline logs where available, with gamma ray or resistivity logs being the most useful.

1.3.2 Well log analysis

A total of 140 wells with geophysical wireline logs were available for the Grosmont-Hondo interval within the study area from ACCUMAP. The main well logs used for identification of the evaporites in the area were gamma ray, density, resistivity, and neutron. However, most of the wells within the study area had only spontaneous potential (SP) and Gamma ray (GR) and outdated electrical logs available. For the identification of the Hondo evaporites the best logs are density and sonic, but these are rarely available. For these reasons, the interpretation of lithology was based mainly on cores and cuttings.
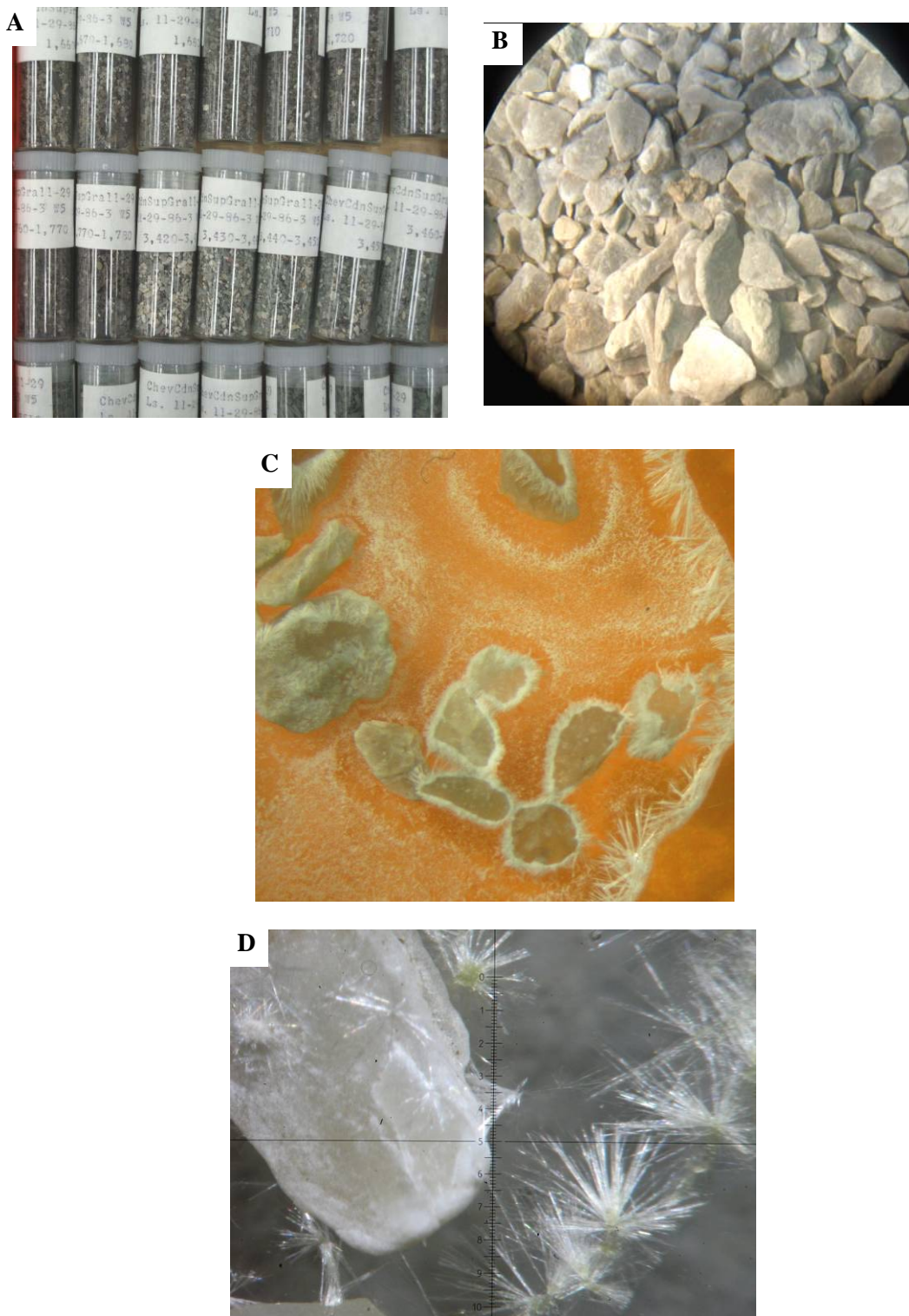
Figure 1.2 Drill cuttings. A) cuttings from well 11-29-86-03W5. B) Chips from the Upper Grosmont 3 (anhydrite mostly). C) Sulphates (anhydrite and gypsum) after treatment with HCl 10% and dried. D) Gypsum needles, magnification 20X.

9

The information from logs, cores, and cuttings was used to produce three dip-oriented and two strike-oriented stratigraphic cross sections (locations marked in Figure 1.1). Isopach and structural maps were produced using the contouring software Surfer©. Contours were then edited by hand to interpret geological features not captured by computer contouring, and then redrawn using a drawing program. These cross sections are discussed in Chapter 6.

1.3.3 Petrography

Petrographic analyses were performed on core and on 75 thin sections. Most sections were impregnated with blue epoxy and stained with Alizarin red-S. Eighteen samples were finely powdered and packed for mineral identification by XRD in the X-Ray diffraction laboratory at the Earth and Atmospheric Sciences Department at the University of Alberta.

1.3.4 Isotope analyses

$\delta^{18}O$, $\delta^{13}C$ and $\delta^{34}S$ isotopic compositions for dolomites, calcite, and sulphates (n=19) from the Upper Grosmont units were obtained in the Isotope Science Laboratory of the University of Calgary. Radiogenic strontium isotopes $^{87}Sr/^{86}Sr$ of 15 samples of anhydrite/gypsum, calcite and dolomite, were determined in the radiogenic isotope facility in the Earth and Atmospheric Sciences Department at the University of Alberta. The analytical procedures are described in Chapter 5.

CHAPTER 2

GEOLOGICAL FRAMEWORK

2.1 Introduction

The Grosmont platform, including the Grosmont Formation and the Hondo evaporites, is part of the Woodbend Group, an economically important interval that contained approximately 32 percent of the initial unconventional oil and gas in place found within the Paleozoic in the Alberta Basin (Mossop and Shetsen, 1994). Significant accumulations of heavy oil and bitumen are located in the eastern part of the Grosmont platform close to sub-Cretaceous unconformity. The Grosmont platform is underlain by Leduc-age reef complexes of varying size and shape, deposited during the major late-Frasnian regression in the Western Canada Sedimentary Basin (Stoakes, 1980). The carbonate platform has been recognized in the subsurface of northeastern and north-central Alberta to be about 150 km wide by 600 km long, covering approximately 100,000 km^2 (Theriault, 1988) (Figure 2.1).

2.2 Previous Work

Studies of the Grosmont platform began in 1949 with the drilling of the Imperial Grosmont No. 1 Well 13-17-67-23W4, approximately 10 km northeast
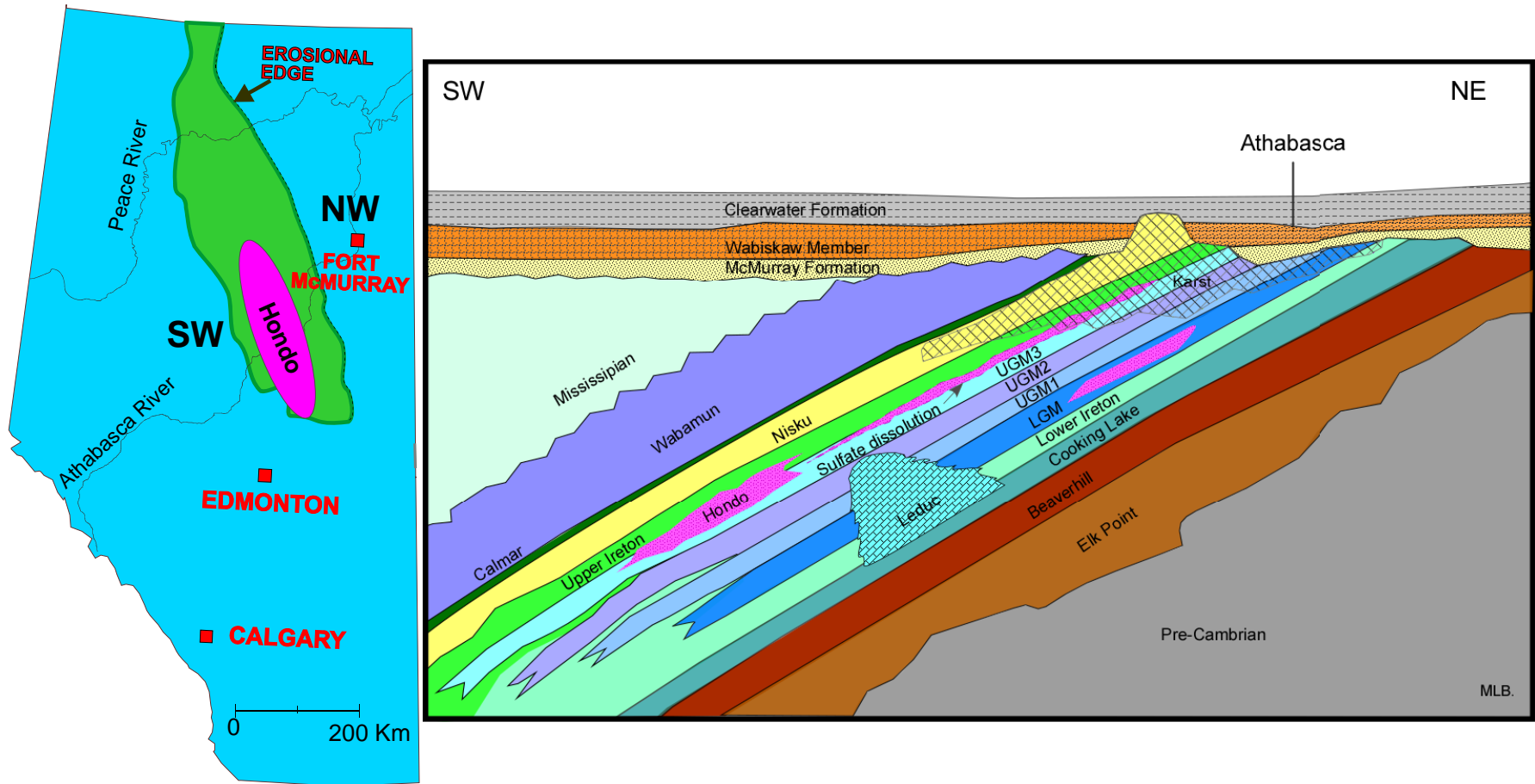
Figure 2.1 Map of the Grosmont Platform and Hondo "evaporites" (modified from Switzer et al., 1994); schematic stratigraphic cross section through the region (some concepts taken from Cuttler, 1983 and Dembicki and Machel, 1996).

12

of the abandoned village of Grosmont, Alberta. Belyea (1952) used information from this and other wells to further define the stratigraphy of the Grosmont Formation. Belyea (1952) also provided the first description of the Hondo, then informally assigned to be a member, as found in a 318 feet interval in well 11-17-78-02W5. (Harrison and McIntyre (1981) and Harrison (1982, 1984) summarized the then-available geological research of the region using the stratigraphic nomenclature established by Union Oil. They also reported the first bitumen occurrence from tar-saturated cuttings in well Wabasca 6-9-87-20W4.

Techniques of bitumen recovery such as steam drive, steam stimulation and forward combustion were initiated in two pilot wells, Chipewyan River 14-21-88-19W4 and Buffalo Creek 14-5-88-19W4. In 1982, the Energy Resources and Conservation board (ERCB) reported an estimation of in place total gas reserves of 29,851 x $10^6 m^3$ and crude bitumen reserves of 50,500 x $10^6 m^3$.

During test production in 1975 the daily peak of production was 20 bbls, increasing to 440 bbls during 1980-1981, by using thermal recovery and steam stimulation methods (Harrison and McIntyre, 1981). However, these yields were low and inconsistent. Thus, despite the at times encouraging production results from pilot operations and large estimated reserves, bitumen production from the Grosmont Formation has never become commercial. Factors such as reservoir variability (associated with complex reservoir architecture), high viscosity of the oil (bitumen), a lack of understanding of the lithology changes within Grosmont units, rendered the Grosmont economically nonviable at that time.

Cutler (1983) studied the stratigraphy and sedimentology of the southern part of the platform. Theriault and Hutcheon (1987) and Theriault (1988) studied the same area defining the relationship between lithofacies and crude oil properties, and Hoffmann and Strausz (1986) studied the bitumen geochemistry. In 1990, Dr. Hans Machel and graduate students of the Petroleum Geology Research Group at the University of Alberta started a major project in an area surrounding the wells drilled by UNOCAL. Machel and Hawlader (1990) established the major diagenetic features and processes in the central part of the platform. Dembicki (1994) recognized and delineated paleokarst zones using well log data. Luo and Machel (1995) determined the effects of dolomitization on petrophysical properties, and Huebscher (1996) provided a core-based investigation of the reservoir diagenesis in the central to southern part of the platform. However, none of these studies endeavoured to define the extent of the carbonate platform, specifically its western edge, nor of the Hondo. A map produced by an anonymous author and published in Harrison (1982) delineated the western platform margin and areal distribution of the Hondo as shown in Figure 2.1 in the absence of supporting evidence.

The Hondo evaporites have not been investigated in detail before, and only two studies reported information about them. Belyea (1952) first described the Hondo as member. Cutler (1983) provided additional petrographic observations from the Hondo between townships 55 and 75 and ranges 12W4 and 8W5, and its distribution in the southern part of the present study area.

After a 10 year of inactivity in the Grosmont region, advances in recovery technology and the worldwide decrease of conventional oil reserves, the Grosmont reservoir has again become an attractive target. Several oil companies, including Shell-SURE (Houston), Husky, Laricina, and Osum Corporation are presently investigating the viability of development. Laricina recently demonstrated a significant recovery potential using steam, and it was found that the Grosmont reservoir shows viability for application of SAGD, especially in the karstified areas (Cimolai et al., 2009). Shell-SURE has been studying other techniques for bitumen recovery and has invested several hundred million of dollars in land and experimental studies. Since 2006, Shell-SURE has supported this MSc. thesis but most of the information from this company remains confidential. Zhao (2009) studied the bitumen properties in the Shell-SURE area and concluded that viscosity varies along depth and probably is stratigraphically controlled.

2.3 Stratigraphy of the Woodbend Group

The Grosmont platform is part of the Devonian Woodbend Group (Figure 2.2). The Upper Devonian Woodbend Group represents an aggradational succession of carbonates with shales filling the basinal areas. This group comprises the Cooking Lake and Grosmont Formations, shallow marine carbonates; the Leduc Formation, reefal buildups; and the Ireton Formation, basin-filling marls (commonly referred as shales). The succession was deposited

in a period of overall increasing sea level with higher order eustatic sea level oscillations Basin (Mossop and Shetsen, 1994).

Through time, there was an increase in the rate of accumulation of sediments, including the development of thick and extensive reef complexes (Wendte, 1994).
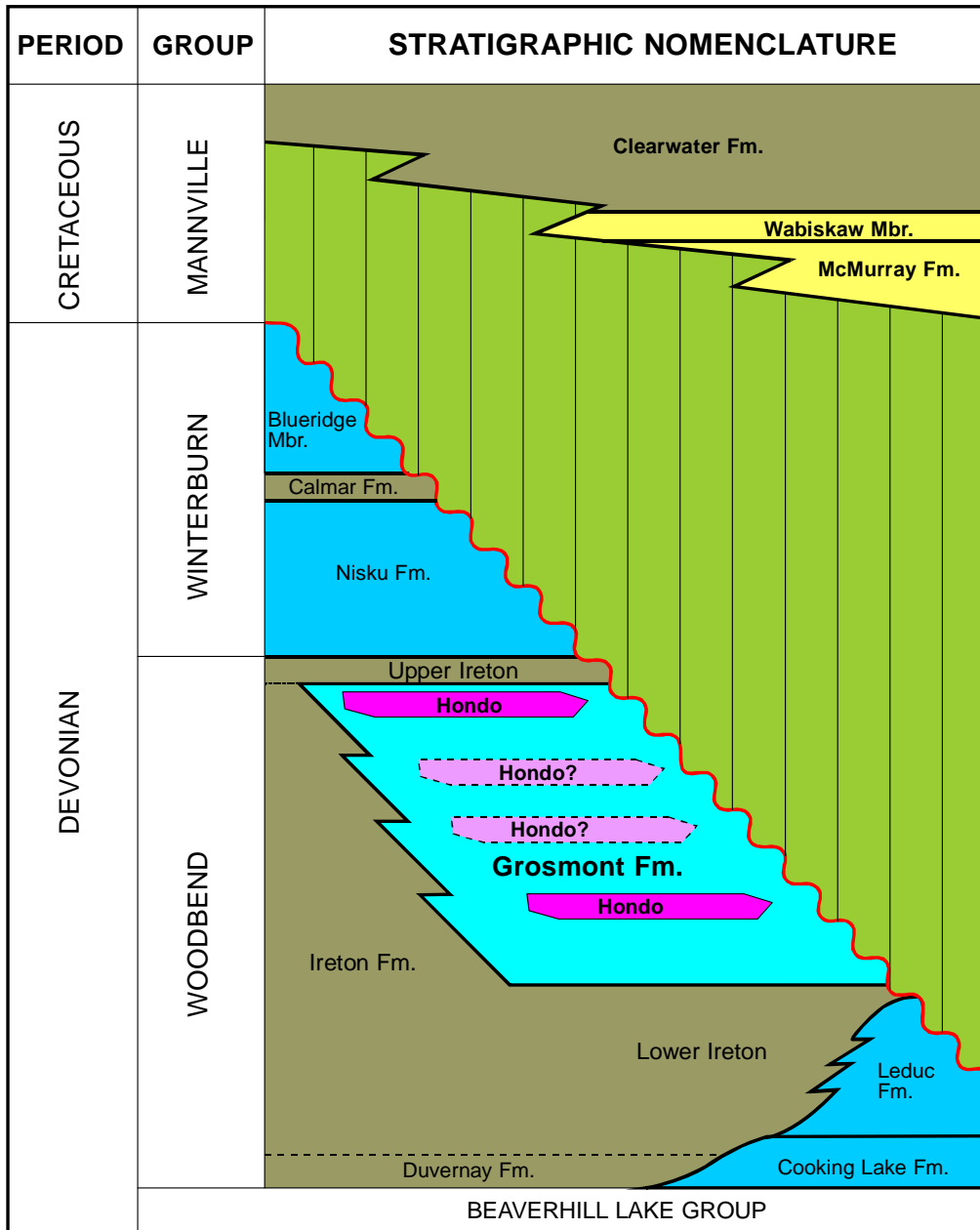
Figure 2.2 Stratigraphic chart for the Alberta Basin in the study area (modified from Switzer et al., 1994 and Dembicki, 1994).

16

2.3.1 Cooking Lake Formation

The Cooking Lake Formation forms a widespread carbonate platform in the eastern part of the Alberta Basin and extends east of the Rimbey-Meadowbrook reef trend (Andrichuk 1958) (Figure, 2.3). These carbonates are mostly peloidal and skeletal limestones (with brachiopods, crinoids, stromatoporoids, bryozoans). Dolomitization has affected this formation especially in the areas beneath the Leduc reefs, and other diagenetic processes have also altered the limestones mainly to vuggy dolostones or dolostones (Amthor et al., 1993, 1994).

2.3.2 Leduc Formation

The Rimbey-Meadowbrook trend follows the direction of the Cooking Lake platform margin (Figure 2.3). Most of the reefs are surrounded by basin-filling shales and marls of the Duvernay and Ireton Formations. The Upper Ireton Formation was deposited in response to a rise in sea level that caused the termination and submersion of the Leduc reefs. These reefs can be subdivided into a reef margin or fore-reef, stromatoporoid building reef, and a reef interior, composed of subtidal skeletal sands flats, peritidal algal laminites, and small patch reefs (Gillivray and Mountjouy, 1975; Burrowes, 1977).

The Leduc Formation has been extensively studied throughout the Western Canada Sedimentary Basin (WCSB) because it contains numerous

17

conventional oil and natural gas reservoirs. The Leduc Formation forms solitary

reefs or composite reef complexes along the western margin of the Cooking Lake

platform, dividing the basin into eastern and western parts.
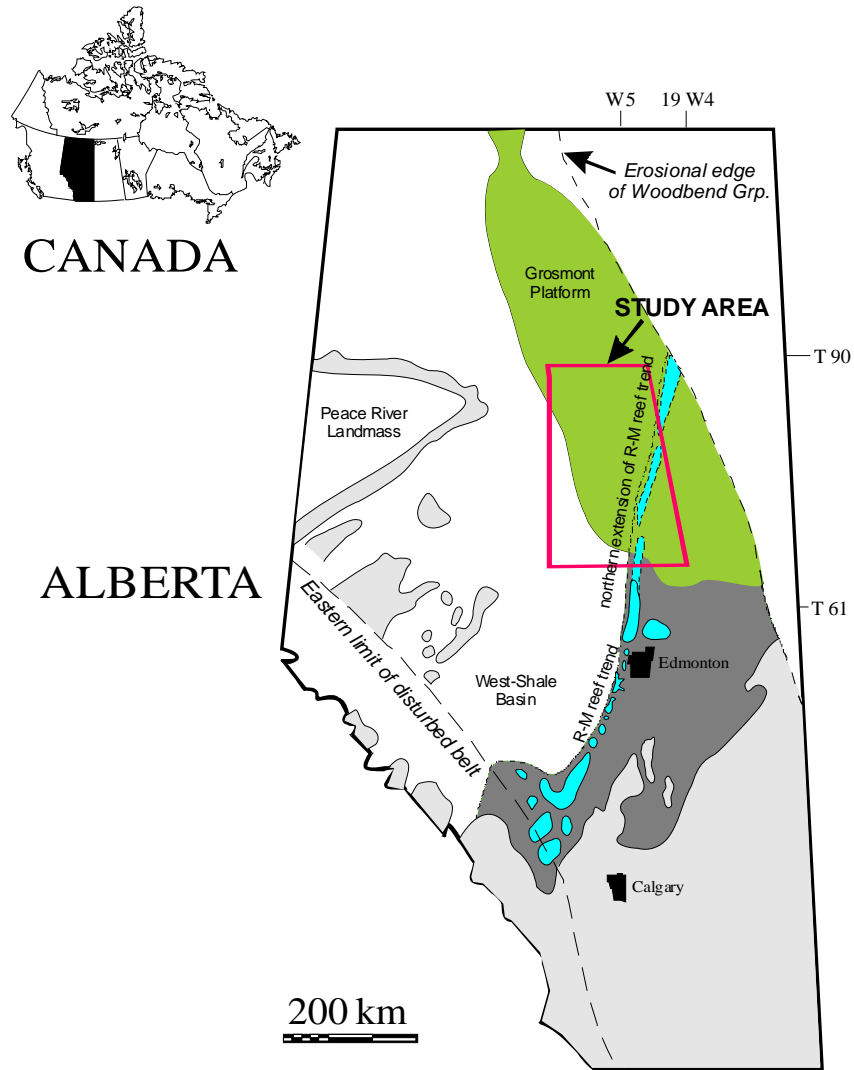
Figure 2.3 Distribution of carbonate platforms and extent of the Rimbey-Meadowbrook reef trend. This reef trend is overlain by the Grosmont platform in its northern part. Location of the study area in red (modified from Huebscher, 1996).

In the study area, the Leduc Formation may have controlled the distribution of the Grosmont sediments. The Cooking Lake and Leduc Formations effectively were covered by the Grosmont platform in their northern parts (Figure 2.3).

2.3.4 Ireton Formation

The Ireton Formation is dominantly composed of shales and marls interfingering with the Leduc and Grosmont Formations. McCrossan (1961) subdivided the Ireton Formation into the Lower, Middle, and Upper Ireton. The lower unit consists of massive, nodular, and banded limestones, with few calcareous shale interbeds. The middle unit is composed of green to gray shales, and the upper unit is mostly fossiliferous marls with some argillaceous limestones. In this study, the Ireton Formation is subdivided into Lower and Upper Ireton. The middle unit, described by McCrossan (1961), is merged with the Lower Ireton (Figure 2.1), and corresponds to the so called "*shale breaks*" (Theriault, 1988; Dembicki, 1994) that separate the Grosmont Formation into its units. The Ireton is conformable with the Beaverhill Lake Group (Figure 2.1). The Upper Ireton is conformable to gradational with the Upper Grosmont Formation, and conformable with the Upper Nisku Formation. In the north-central part of the study area, the shale is predominantly dolomitic. The lower part of the Upper Ireton in the northeast is silty-argillaceous carbonate, and is considered to be part of the Grosmont Formation based on the relatively high carbonate content

19

(Harrison and McIntyre, 1981; Harrison 1982, 1984). The top of the Upper Ireton Formation is a good log marker and is used as the datum for the majority of the stratigraphic cross sections.

2.3.5 Grosmont Formation

The Grosmont Formation represents deposits on a shallow marine carbonate platform. The first description of the Grosmont was made by Belyea (1952) using core data from the well 13-17-67-23W4. The Upper Grosmont was described as a *"widespread biostromal coquinoid limestone and dolomitized limestone and associated reef with coarse vuggy porosity.*" Cutler (1983), Machel and Hunter (1994), and Dembicki (1994), studied the Grosmont Formation in four units: the Lower Grosmont (LGM), the Upper Grosmont 1 (UGM1), the Upper Grosmont 2 (UGM2), and the Upper Grosmont 3 (UGM3). These units are separated by Lower Ireton *"shale breaks",* named consecutively SB1, SB2, and SB3, as identified in well logs (Figure 2.4). Each Grosmont unit represents a shallowing-upward cycle (aggradation of shelf and reef sediments), followed by progradation and infilling of marlstones (Harrison and McIntyre, 1981; Harrison, 1982; Cutler, 1983; Machel and Hawlader, 1990). Depositional lithofacies, as identified by Machel and Hawlader (1990) and Machel and Hunter (1994), include: a) fossiliferous mudstone and wackestone, representing the shales breaks deposited in relatively deep and quiescent water; b) nodular mudstone to wackestone, representing shallower, slightly more agitated waters than facies a; c)

stromatoporoid-coral floatstone, deposited in relatively shallow and quiescent water conditions; d) *Amphipora* floatstone; e) massive, poorly fossiliferous mudstone to grainstone; f) laminated mudstone (dolomite), deposited in a shallow subtidal to intertidal environment; and g) brecciated mudstone (dolomite) containing clasts of facies f (Figure 2.5).
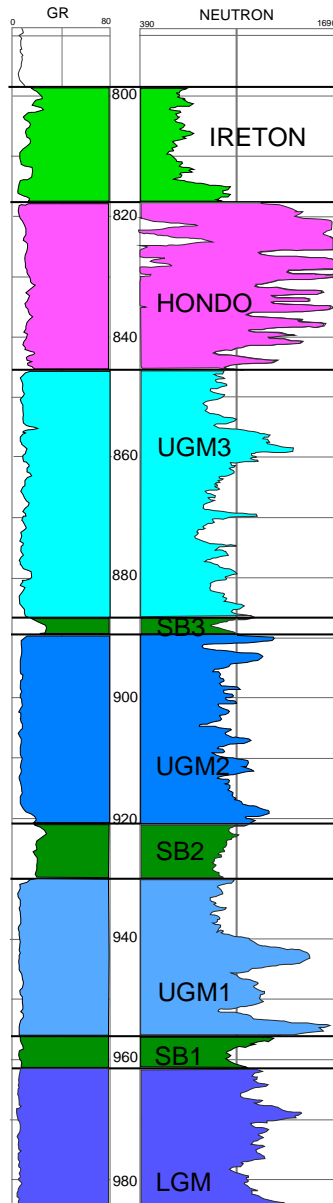
Figure 2.4 Grosmont units in well logs; well 11-29-86-03W5.

UNCONFORMITY   FACIES

g
f
e
d
c
b
a

HARDGROUND

= laminated breccia clast
= laminated carbonate mudstone
= vugs in fine-grained carbonate
= carbonate nodules
= massive and bulbous stromatoporoids
= tabular stromatoporoids
= *Amphipora*
= corals
= brachiopods
= gastropods
= crinoids
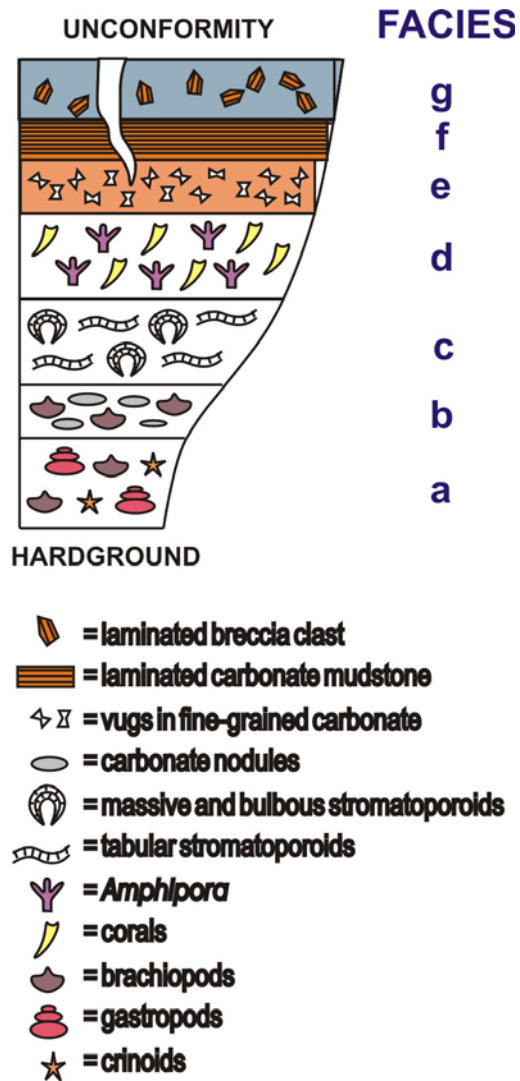
Figure 2.5 Grosmont lithofacies (from Machel and Hunter, 1994).

The Grosmont carbonates have a complex diagenetic history with variable degrees of dolomitization, especially in the northeastern part of the platform. In addition, karstification and brecciation occurred during the Late Jurassic and Early Cretaceous (Huebscher, 1996).

The stratigraphic thickness of the Grosmont is variable on a regional scale, mainly due to erosion along the sub-Cretaceous unconformity (Figure 2.1). Along

its western edge, the Grosmont Formation is overlain by green shales of the Upper Ireton. In the study area, the thickness of the Grosmont Formation ranges from 44 m to 150 m at depths of 250 m to 1435 m. The southwestern edge of the Grosmont Formation appears to be a relatively abrupt and steep margin, where the facies change from platformal carbonates into basinal shales and marls. A map distribution of the Grosmont platform as published in Mossop and Shetsen (1994) has been used in many studies (Figure 2.1). However, the western limit of the platform is poorly defined.

2.3.6 Hondo Evaporites

The first study of the Hondo evaporites was by Belyea (1952). She defined the Hondo evaporites as anhydritic beds in the upper portions of the Grosmont Formation from a 318 feet thick section in well 11-17-78-02W5. Unfortunately, this section could not be reinvestigated for the current study because of the original Hondo section is not available for viewing at the EUB core lab in Calgary. Belyea (1956) later considered the Hondo evaporites as a facies equivalent to the Grosmont Formation, and showed the transition between the Ireton, Grosmont, and Hondo as facies changes from shale to dolostone to interbedded dolostone and anhydrite. Belyea (1964) then suggested that the Hondo represents evaporitic deposits within the Grosmont Formation (see also Meijer Drees, 1986). Cutler (1983) suggested that the Hondo is largely restricted to the upper part of the Grosmont, UGM3, with minor anhydrite present near the top of the UGM2 and locally also in the LGM.

These considerations imply that stratigraphically the term "formation" is misused when referring to the Hondo. Rather the Hondo appears to be merely an evaporitic facies within the Grosmont Formation. According to the International Stratigraphic Guide (1994), a formation is defined as:

> …the primary formal unit of lithostratigraphy classification used to map, describe, and interpret the geology of a region; it is a body of rocks of intermediate rank in the hierarchy of lithostratigraphic units and is identified by its lithologic character and stratigraphic position". (p 35).

The Hondo can be mapped, described, and interpreted, but only within a restricted area. Thus, following the Stratigraphic Guide, the Hondo can be considered a member of the Grosmont Formation.

Regarding the spatial distribution of the Hondo, Mossop and Shetsen (1994) showed a rough outline of the Hondo area, but there is no information about the source of data (Figure 2.1). No isopach maps of the Hondo have been published. Sedimentological characteristics of the Hondo evaporites are poorly understood.

2.4 Stratigraphy of the Winterburn Group

The Upper Grosmont and/or Hondo and/or Upper Ireton are overlain by the Nisku Formation which is part of the Winterburn Group (Switzer et al., 1994). Accumulation of the Nisku probably started with an increase in eustatic sea level, which allowed the development of a new carbonate platform with isolated pinnacle reefs and reef trends (Switzer et al., 1994). The Nisku Formation was

24

affected by pervasive dolomitization, and most of the original textures have been destroyed. In the Grosmont region, the Nisku Formation has been described as vuggy dolomites, with minor limestones (Machel and Hawlader, 1990). Nisku sediments are overlain by the Calmar Formation, which represents a eustatic sea level drop that resulted in an increase of siliciclastic sediment influx (Switzer et al., 1994), represented by argillaceous-silty deposits with thicknesses from 3 m to 10 m. In the eastern part of the study area, the Nisku and Calmar Formations are eroded and truncated by the pre-Cretaceous unconformity (Figure 2.1).

2.5 Paleo-geography and Basin Evolution

The study area is located in the eastern part of the Western Canada Sedimentary Basin (WCSB). The WCSB can be subdivided into the Williston Basin and the Alberta Basin along a structural high dating to the Silurian, the so-called Bow Island Arch that straddles the Alberta-Saskatchewan border (Root, 2001) (Figure 2.6). The WCSB comprises an older pre-Antler passive margin and a younger Laramide to post-Laramide foreland basin.

During the Late Cretaceous-Early Tertiary, the Laramide Orogeny effected a westward tilting of the WCSB, deep burial and concomitant thermal maturation of Devonian source rocks, causing fluids to migrate up-dip toward the east and northeast (Wendte, 1992; Root, 2001).

At the time of Grosmont deposition, during the Middle and early Late Devonian (Givetian-Frasnian), the Grosmont region was located south of the paleoequator within a subtropical setting (Whalen et al., 2000; Potma et al., 2001).
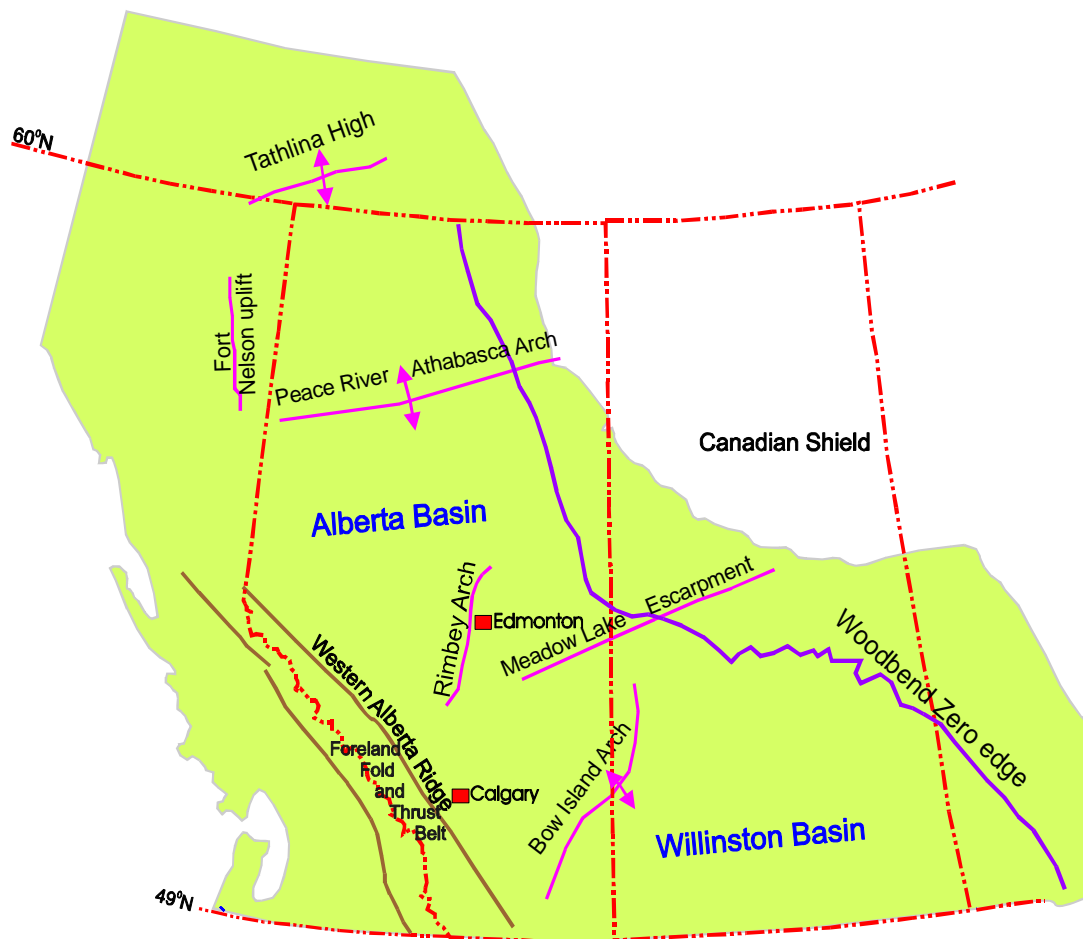
Figure 2.6 Western Canada Sedimentary basin, division and structural elements during the Devonian; they influenced the Woodbend group deposition (modified from Switzer et al., 1994).

This setting and probable trade winds from what is now the northeast caused prime conditions for evaporation in what was part of an intra-cratonic sea within the North America craton (Figure 2.7). At the end of the Frasnian stage, there was a eustatic sea level rise, resulting in basin shales of the Upper Ireton Formation covering the region (Switzer et al., 1994).

Figure 2.7 Paleogeography during the Middle Devonian (~385 Ma). Red outline represents the Alberta Province (modified from Blakey, 2010, http://jan.ucc.nau.edu/~rcb7/namD385.jpg)

Structural elements include the Peace River Arch, the West Alberta Ridge, the Tathlina High, the Ft. Nelson Uplift, and the Meadow Lake Escarpment (Figure 2.6). The Peace River Arch and the West Alberta Ridge effectively separated the ancestral Pacific Ocean from the WCSB (Potma et al., 2001). The Rimbey Arch Trend, another large basement structure also influenced the deposition of the Grosmont sediments (Switzer et al., 1994).

CHAPTER 3

HONDO FACIES

3.1 Introduction

The facies distribution within the study area is based on data from thirty two wells, which were logged and sampled at the EUB Core Research Centre in Calgary. Carbonate facies types were described following the facies model proposed for Late Devonian carbonates by Machel and Hunter (1994). These facies types are widely accepted for the Grosmont Formation. Five out of thirty two cores that penetrate the Grosmont contain Hondo facies (Table 1.1); sampling was focused on these wells. Well 15-17-71-25W4, which is herein informally considered as the "type well" for the Hondo, contains most of the Hondo facies. A total of 89 samples and 75 thin sections were analyzed. Drill cuttings were not used to identify facies. Classification of textures of primary sulphates is based on Maiklem et al. (1969).

3.2 Definitions

The term evaporite is used herein to denote chemical sediments originally precipitated from a saturated surface or near surface brine as a result of solar evaporation (Kendall, 1992; Hardie, 2003; Warren, 2006). Evaporite deposition occurs when the evaporation rate is higher than the total water inflow (Schreiber and Tabakh, 2000). During evaporation seawater transforms becoming more and more saline. A range of evaporite minerals is formed as the result of the

increasing concentration, and the mineralogy is controlled by the ionic composition and degree of evaporation (Warren, 2006).

3.2.1 Gypsum

Gypsum, $CaSO_4 \cdot 2H_2O$, is the principal marine sulphate mineral during primary deposition from evaporated marine water. It precipitates during evaporation after calcium carbonate and dolomite. Gypsum commonly precipitates at and above a concentration of about 3X that of seawater TDS (total dissolved solids, approximately 100 g/l). The rate of precipitation can be quite high, and if there is sufficient accommodation the thickness of rapidly forming gypsum deposits can be considerable. For example, modern gypsum in the Mediterranean Sea and in California ponds precipitates at a rate of 1.25cm per year (Schreiber and Kinsman, 1975).

Gypsum easily dewaters to anhydrite (anhydrite replacing gypsum) at temperatures of >40 to 50° C, corresponding to depths of 600-1000 m, as implied by experimental data, the temperature and depth of the gypsum-anhydrite transformation also depending on fluid composition (Cruft and Chao, 1970). Conversely, anhydrite may get rehydrated to gypsum in response to a decrease in temperature during uplift. However, the rehydration of anhydrite is often inhibited in natural environments by two factors: 1) anhydrite is metastable at shallow depths and commensurate low temperatures, 2) lack of water.

3.2.2 Anhydrite

Anhydrite, $CaSO_4$, is primarily produced by dehydration of gypsum in the subsurface (Sonnenfeld, 1984). Field observation by Picha (1978) in the Persian Gulf off the coast of Kuwait revealed that an increased amount of organic matter decreases the stability of gypsum and facilitates its dehydration during and immediately after precipitation, so that anhydrite formation is synsedimentary in this environment (Buttler et al., 1982). Anhydrite can also be formed by primary precipitation of brines as shown by experimental data (Cody and Hull, 1980), but this is rare and the brine concentration has to reach 4.8 times that of seawater (Sonnenfeld, 1984).

Another mechanism for anhydrite precipitation is known from areas where seawater circulates actively and there is a mixture of different brines. The temperature dependence for the formation of anhydrite versus gypsum was determined experimentally by Blount and Dickson (1969). They concluded that when two gypsum-saturated brines of different temperatures mix, the resulting solution is under-saturated and gypsum tends to dissolve. Additionally, gypsum was the stable $CaSO_4$ phase when the temperature was less than 40° C; at higher temperatures anhydrite is stable. In the case of mixing two anhydrite-saturated brines of different temperatures, the result is a supersaturated brine prone to anhydrite precipitation. This is in line with an early study by Ponsnjak (1940), who demonstrated that the stability of gypsum and anhydrite is a function of temperature. Furthermore, the most common way in which anhydrite forms in

sedimentary environments is by dewatering of gypsum deposits (see section 3.2.1).

3.3 Terminology for Grosmont and Hondo

In this study the term "Hondo sulphates" includes both anhydrite and gypsum. To avoid the term "primary evaporites" (gypsum or anhydrite), the terms "Hondo primary sulphates", "Hondo secondary sulphates" and "diagenetic anhydrite" are proposed, as described below.

"Hondo primary sulphates" corresponds to either gypsum or anhydrite, or both. Almost all primary sulphates in the study area probably formed originally as gypsum, but are anhydrite today. Thus, most anhydrite formed by dehydration of primary gypsum, often with good to excellent fabric retention.

"Hondo secondary sulphates" corresponds to diagenetically altered sulphates in which syndepositional features have been partially to completely altered.

"Diagenetic anhydrite" is anhydrite that was directly precipitated from a diagenetic solution, most commonly in secondary voids or in fractures.

The remainder of this chapter describes Hondo primary sulphates as defined above. The secondary sulphates and diagenetic anhydrite will be discussed in Chapter 4.

3.4 Hondo Facies - Primary Sulphates

Hondo primary sulphates, with their primary bedding morphologies, were found in four cores in the upper portion of the Grosmont Formation, and in the Lower Grosmont in the Grosmont type section well. Well 15-17-71-25W4 is the most instructive for facies analysis because it has 25 meters of core within the Hondo in the Upper Grosmont 3.

3.4.1 Facies A: Laminated anhydrite and laminated dolomudstone

Description: This facies is characterized by finely laminated (lamina thickness = 2 mm to about 1 cm) grey anhydrite and cream to brownish dolomudstones. Laminae are generally planar to wavy and continuous (Figure 3.1 A, B); they represent the major lithology in the type well. Contacts with underlying laminae are mainly sharp. There is no evidence of fossil biota, and it appears that the laminae have not been affected by bioturbation. In thin section, lenticular-microcrystalline anhydrite is oriented more or less horizontally, and dolomite is very fine-grained (dolomicrite). Some anhydrite shows a corrotopic texture, which results from transformation and possible recrystallization of primary gypsum (Figure 3.2). Disseminated rounded grains of pyrite are observed in the dolomudstone layers (Figure 3.1 D).

Interpretation: The dominance of laminated sulphates implies precipitation and deposition in a water body whose bottom received little or no influence from wave action and currents. Evaporitic laminites commonly form in relatively deep,

quiet waters (Warren, 2006), but also in shallow stratified water bodies, such as solar salt ponds (Schreiber, 1978, Schreiber and El Tabakh, 2000). Generally, laminar carbonates and sulphates, especially the ones formed in deep waters, have a broad lateral continuity. For example, in the modern Black Sea such laminae may be correlated over an approximated distance of 1000 Km (Davies and Ludlam, 1973). In case of the Hondo, due to the relatively wide spacing of core, a correlation between laminated units across the study area is unreasonable. Facies A contains some sporadic wavy parallel laminations that are interpreted to be formed by slight currents. Depth of sulphate formation has to be interpreted from others facies. Although, the main mineral in this lithofacies is currently anhydrite, gypsum probably was the first mineral precipitated. Gypsum then dehydrated when temperatures reached > 50° Centigrade, mainly during burial (Hardie, 1967), or under mixing of seawater with different salinity concentrations.

Gypsum crystals have been observed growing in salina ponds in two forms: the mineral forms on the floor of the brine pond as grass-like "meadows" with the crystal axes perpendicular to bedding; and as acicular crystals formed at the air-water interface or at the pycnocline, if there is one (Schreiber, 1978; Schreiber and El Tabakh, 2000). When such crystals become too heavy to float, they sink and align horizontally, creating laminae. Interlamination of sulphates and dolomudstones probably forms from episodic variations in temperature or changes in evaporation rates. Episodes of rainfall or seasonal refreshment could also influence the formation of dolomudstone layers.
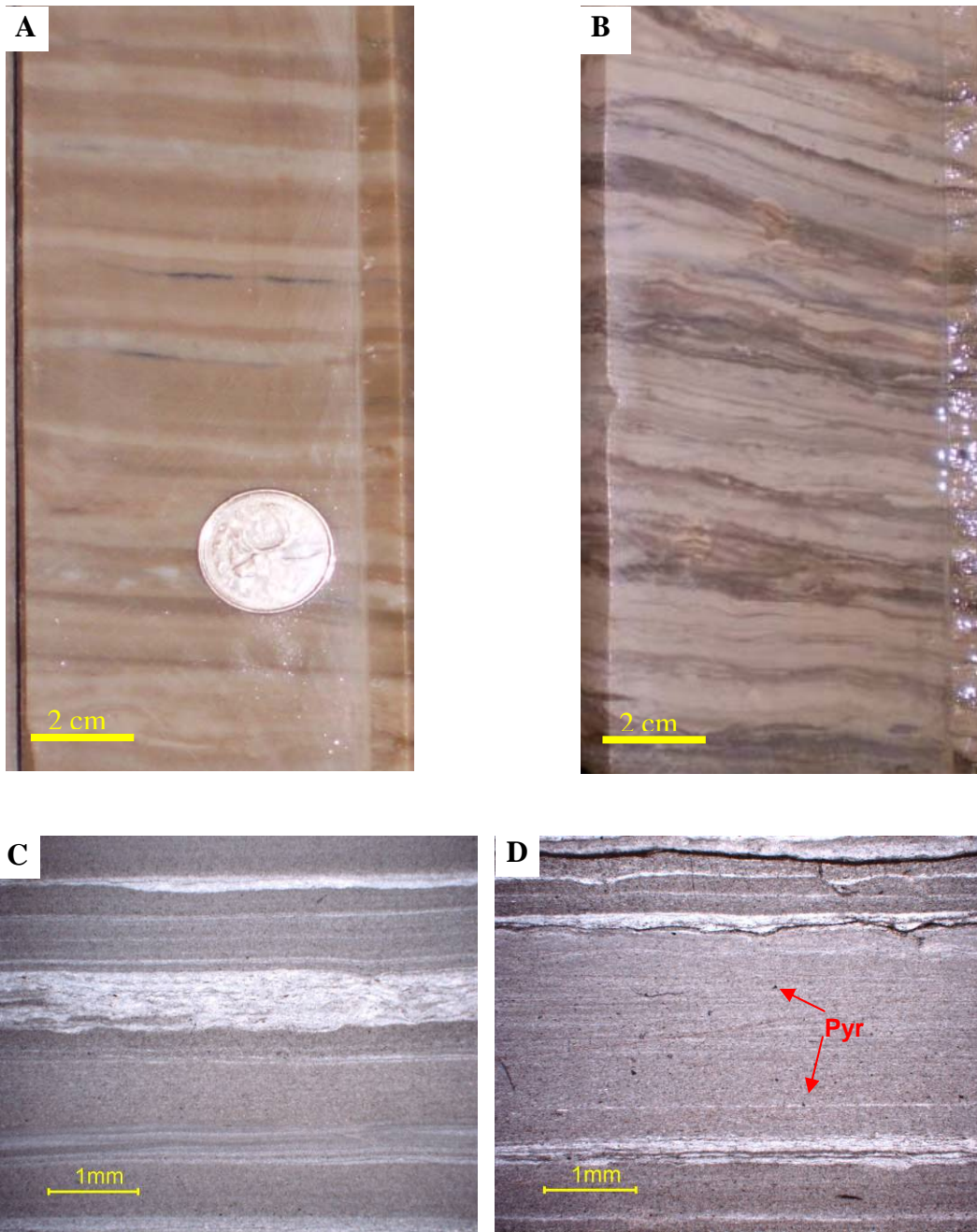
Figure 3.1 Facies A. A Core and C Photomicrograph of thin section (plane polarized light) of parallel lamination of cream dolomudstone interbedded with white anhydrite, well 15-17-71-24W4 (912.45 m). B Core and D photomicrograph of thin section (cross polarized light) of wavy parallel lamination of cream dolomudstone and light grey anhydrite, with some synsedimentary/compactional deformation, well 15-17-71-24W4 (908.90 m). Coin diameter is 1.85 cm.

Dolomudstones in the Hondo are thus interpreted as having formed syndepositionally (further explain in Chapter 4). Salinities in gypsum forming ponds commonly have salinities of 150-320 g/l (Schreiber and El Tabakh, 2000).

The lack of bioturbation is attributed to the relatively high salinity of the brine. In modern evaporitic environments, marine fauna lives in salinities up to 55 g/l, and as soon as salinity increases >35 g/l fauna becomes restricted (Schreiber and El Tabakh, 2000).
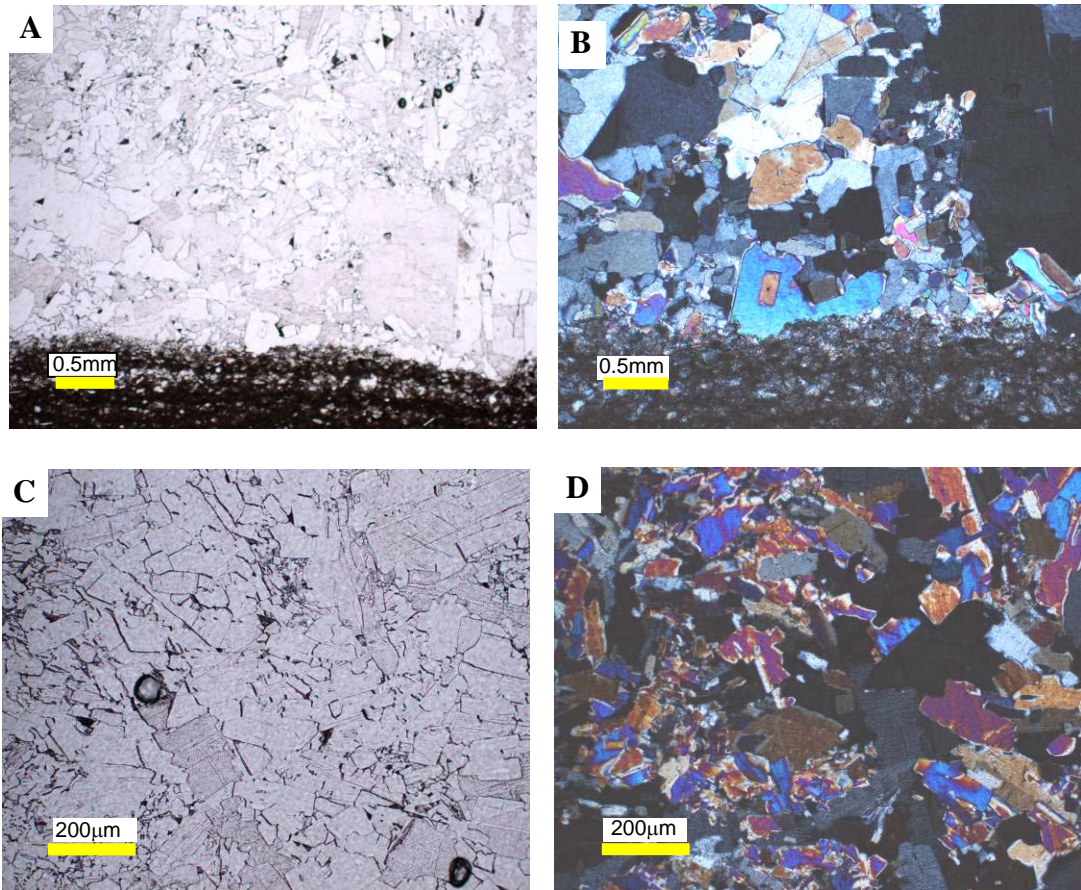
Figure 3.2 Facies A. Photomicrographs of thin sections. A (plane polarized light), B (cross polarized light) of anhydrite, well 15-17-71-25W4 (913.50 m). C (plane polarized light) and D (cross polarized light), well 03-28-70-24W4 (931.60 m). Corrotopic anhydrite (*sensu* Machel, 1985): texture resulting from gypsum-anhydrite transformation (replacement) with possible subsequent anhydrite recrystallization.

Low energy at the bottom of the water body also promotes anoxic conditions that inhibit development of benthic fauna. Taking all evidence together, Facies A is interpreted as deposits formed predominantly in low energy and high salinity shallow-pools.

3.4.2 Facies B: Mosaic anhydrite with microbial mats

Description: This facies, as found in type well 15-17-71-24W4 from 910.15m to 911.4m, contains centimetre sized "nodules" of white anhydrite that are aligned sub-horizontally within a thin-bedded cream-coloured dolomite matrix (Figures 3.3, 3.4) and classified as a mosaic anhydrite. Dolomicritic laminae have sharp contacts with the mosaic areas. These commonly are very thin (few centimetres) in comparison with the sulphate layers. Under the microscope, the nodules are composed of felted anhydrite laths with the long axes diverging into radial sprays or with crystals parallel to each other. The microbial laminae consist of clusters of a granular dolomite-anhydrite mix in the nucleus, surrounded by dolomicrite and micrite.

Interpretation: This type of anhydrite nodules was probably formed displacively by nucleation within carbonate mud, and they coalesced to the mosaic texture with continued growth. It is likely that gypsum crystals originally precipitated and then transformed to a mass of tiny laths plus liquid water ("crystal mush"), which, by weight of the overlying sediments, dewatered and compacted further to spherical or ovoid nodules (Hardie, 2003). Mosaic anhydrite
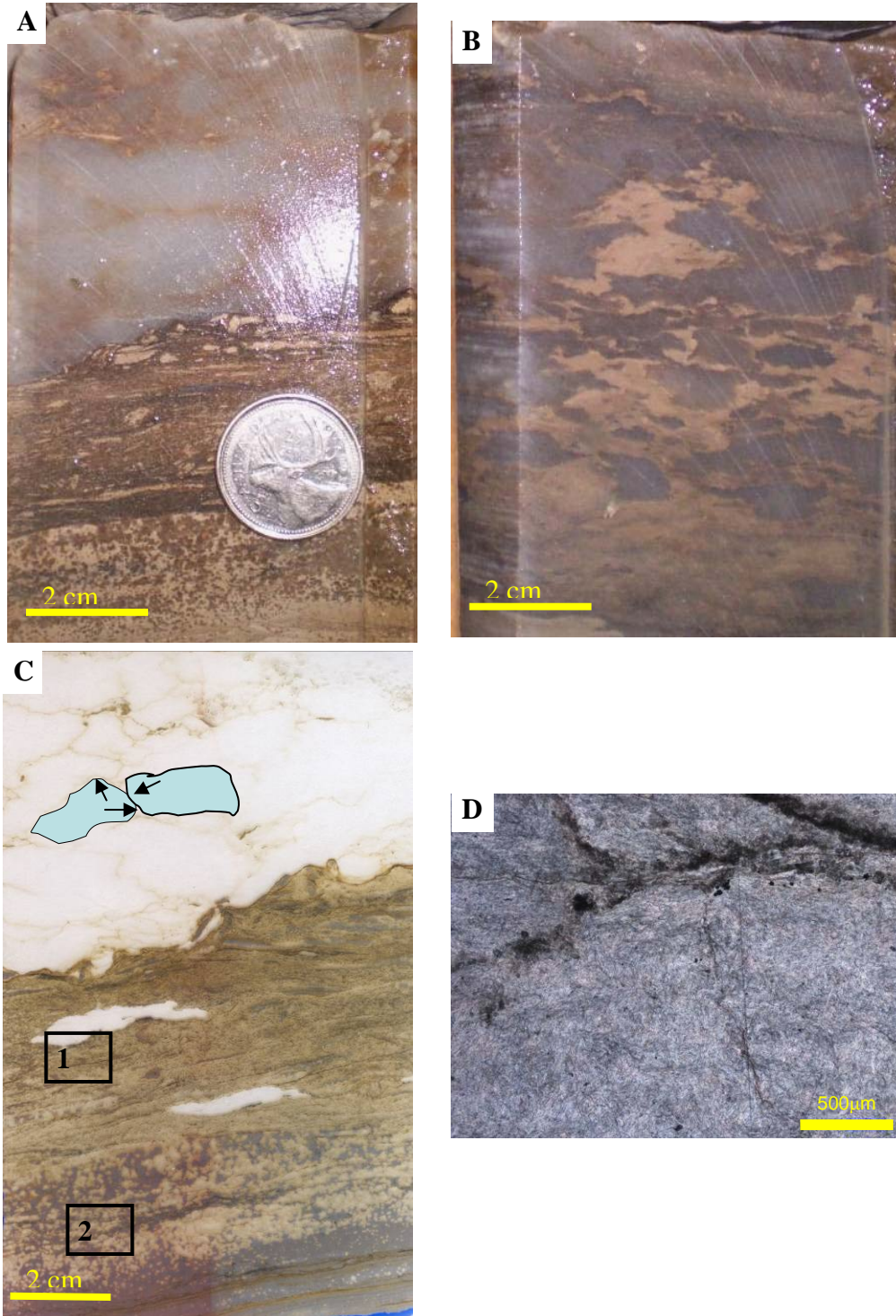
Figure 3.3 Facies B. A, B, C Core, D photomicrograph of thin section. A, and C mosaic anhydrite and microbial mats, well 15-17-71-25W4 (910.70 m). Coin diameter is 2.3 cm. In C, arrows indicate growing directions of anhydrite nodules that are displacing the dolomudstone matrix, detail in D. Black outlined regions are explained in Figure 3.5. B Mosaic anhydrite within cream dolomudstone matrix, well 15-17-71-25W4 (910.30 m). D shows felted anhydrite nodules pushing the dolomite mud and clay particles aside.

is also considered a transitional texture between laminar and nodular anhydrite (Friedman, 1973).
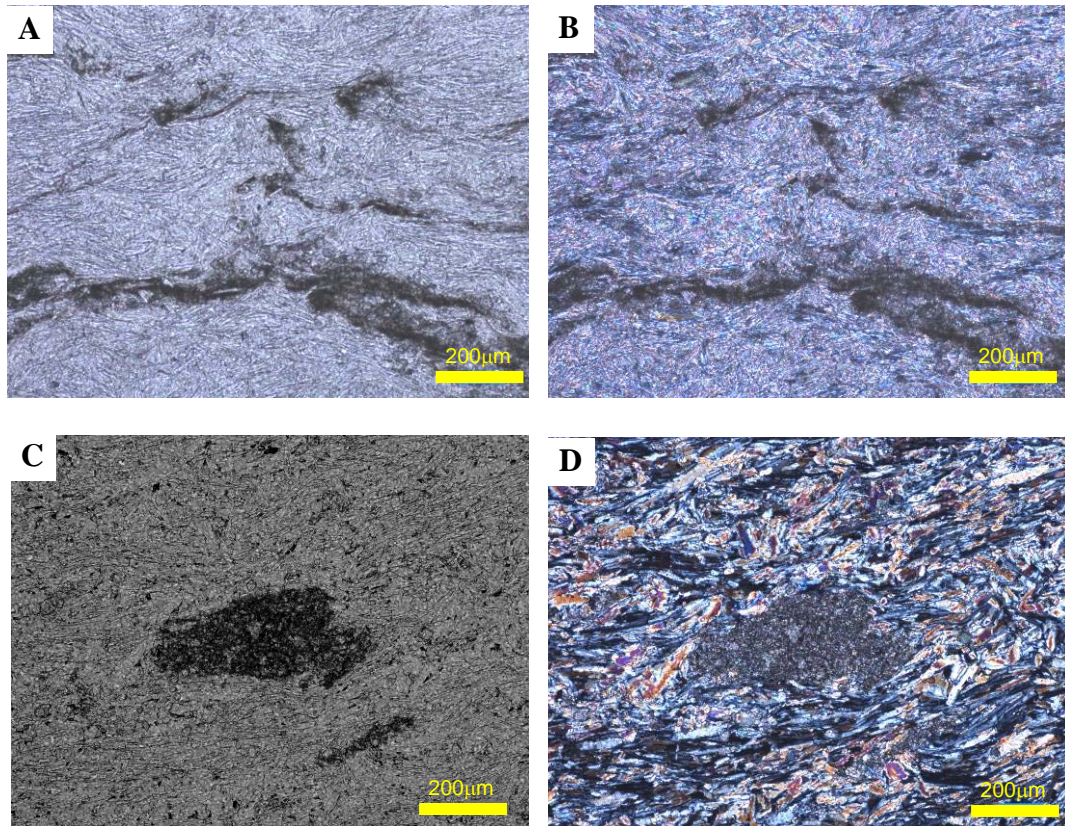
Figure 3.4 Felted anhydrite. Photomicrographs of thin sections A and C (plane polarized light), B and D (cross polarized light) felted anhydrite displacing dolomicrite. As anhydrite nodules grow and coalesce, the sediment is compressed into thin "wisps" among the nodules, well 15-17-71-25W4 (910.55 m).

Facies B is herein interpreted as formed under subaqueous to intertidal conditions within shallow hypersaline lagoons/pools in arid conditions. The microbial laminae mats represent deposition in a hypersaline intertidal environment.
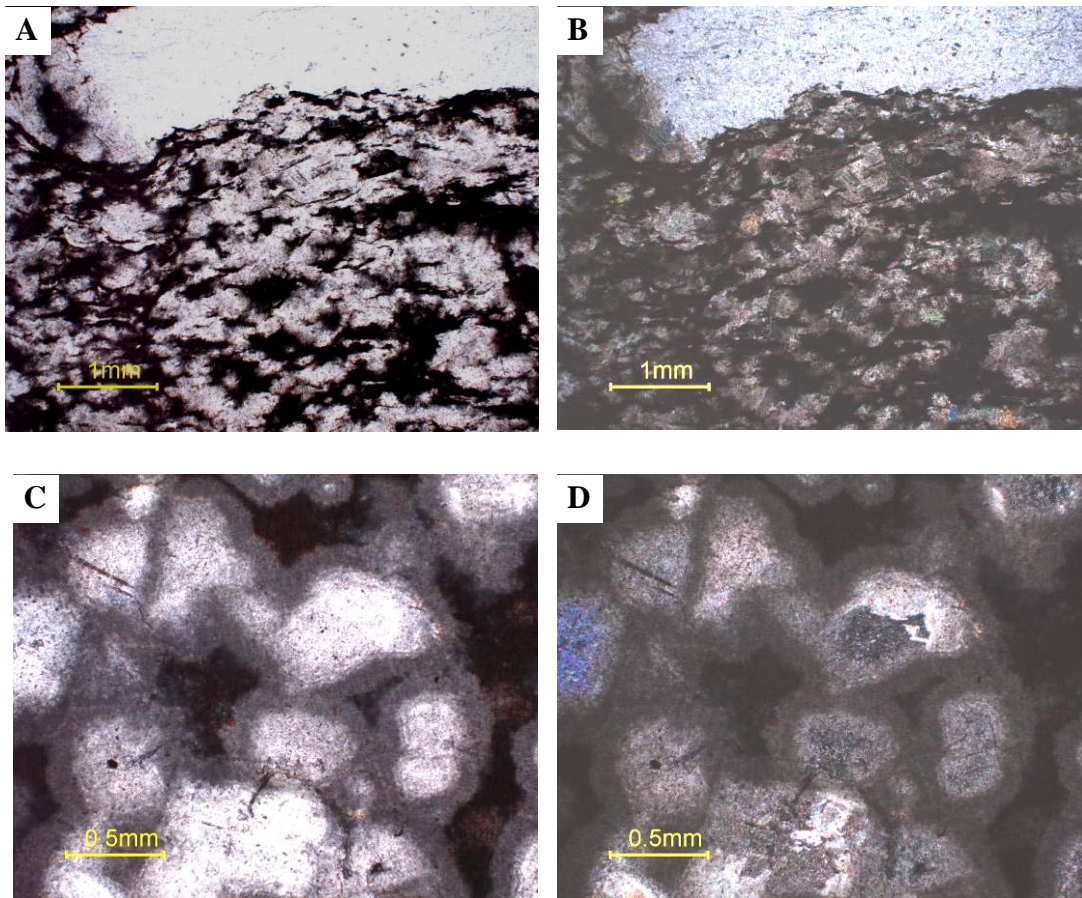
Figure 3.5 Photomicrographs of thin sections. A and B from outlined region 1 from figure 3.3. A (plane polarized light), B (cross polarized light) of microbial laminae. C, D, E and F from outlined region 2 from Figure 3.3. C and E (plane polarized light), D and F (cross polarized light) of anhydrite clusters surrounded by dolomicrite and micrite, well 15-17-71-25W4 (910.30 m).

3.4.3. Facies C: enterolithic anhydrite/contorted bedded anhydrite

Description: This facies is made up of cream-coloured dolomudstone and grey anhydrite layers. There are deformed beds with a ropey structure (Figure 3.6). The anhydrite displaces the sediment around it, causing deformation of the horizontal layers (Figure 3.6).

39

Interpretation: the contorted layers are interpreted as a product of deformation caused by differences in density of semi-fluid gypsum and consolidated or semi- consolidated non-evaporitic sediments formed during

or shortly after deposition (Maiklem et al., 1969). When the sediments are still unlithified, brines may sink into the underlying sediments and facilitate the reaction and alteration of evaporite beds (Warren, 2006). Thus, nodules grow by displacement in the soft sediment within the dolomudstone matrix as the first stage to form enterolithic, contorted fold and mosaic anhydrite (Loucks and Longman, 1982; Rouchy et al., 1985; Shearman, 1985).

3.4.4. Facies D: Displacive-nodular Anhydrite

Description: This facies is characterized by nodular anhydrite. Nodules of this facies are 2mm to 5 mm in size and are embedded in brown dolomudstone. They form displacively within the matrix (Figure 3.7) and can coalesce to layers. In thin section, anhydrite is blocky to lath-shaped.

Interpretation: Nodular anhydrite of this type has been interpreted as formed in a sabkha setting under subaerial exposure (e.g., Dean and Anderson, 1982). However, in the Hondo, such nodules of anhydrite are interpreted to be primary and secondary sulphates formed in a subaqueous setting or during burial. As explained in section 3.4.3 nodules can grow by displacement in soft sediment. The geometry of the layers can also be attributed to the growth of anhydrite within dolomitic sediments, or due to the replacement of gypsum crusts

40

(Shearman, 1970). Sporadic currents could also have deformed the laminae horizontally.
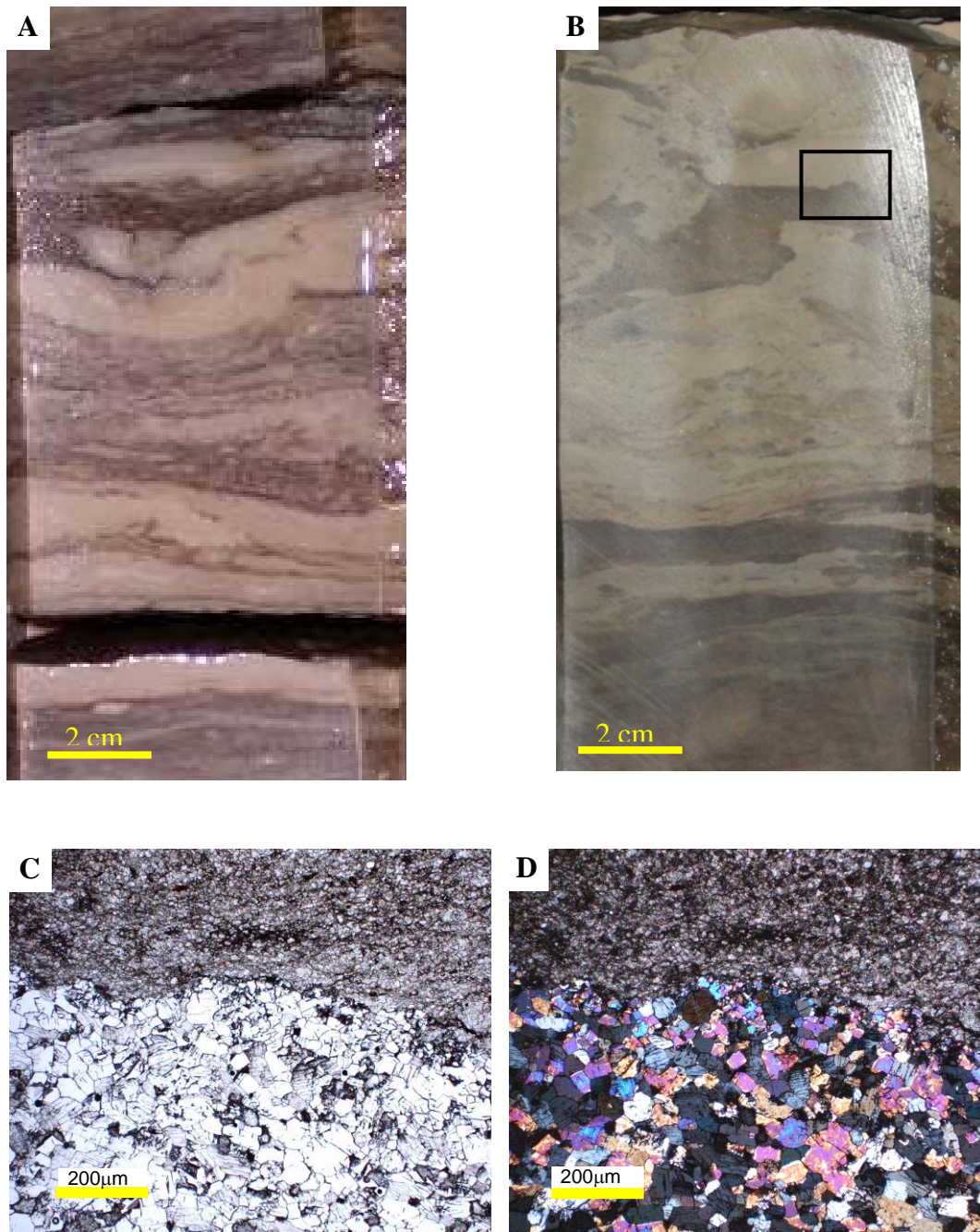
Figure 3.6 Facies C. A Core of light brown to cream-coloured ropy anhydrite and dolomudstone, well 15-17-71-25W4 (889.10 m). B Core of displacive anhydrite within cream dolomudstone (black outlined region in detail in C and D. C and D photomicrographs of thin sections; C (plane polarized light) D (cross polarized light), well 15-17-71-25W4 (904.80 m).
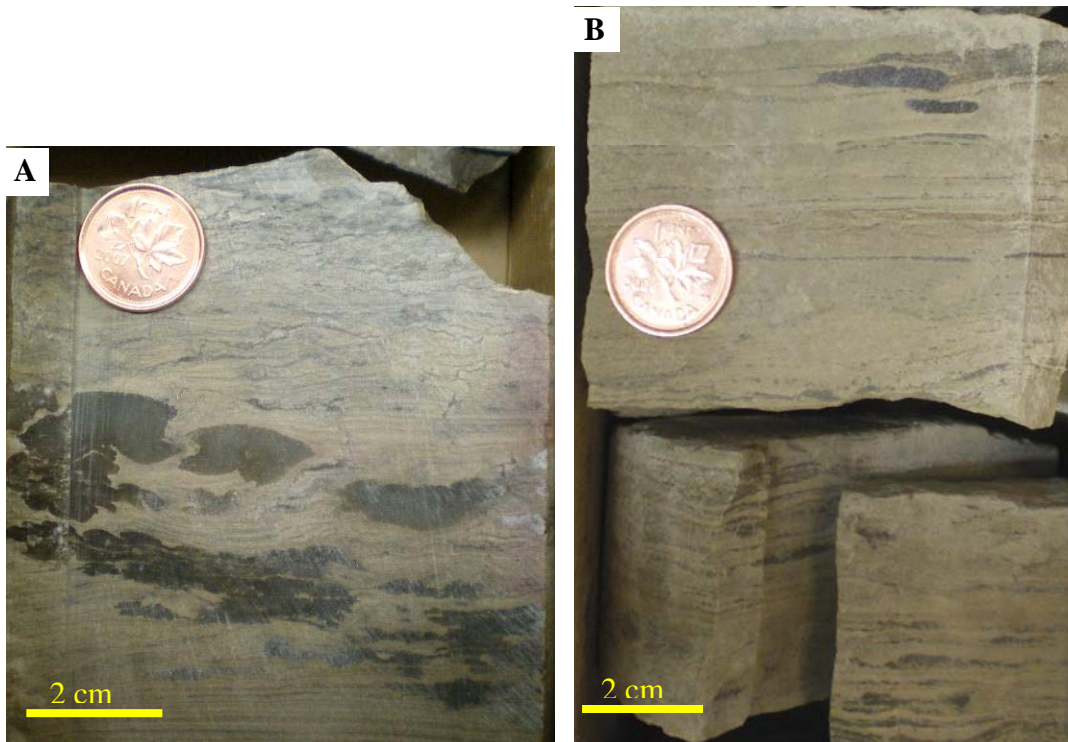
Figure 3.7 Facies D. A Core of displacive anhydrite nodules within cream dolomudstone, well 10-01-71-26W4 (977.4 m). B core with nodules of anhydrite within lamination of dolomudstone and anhydrite, they were probably lenticular gypsum crystals or clusters, well 10-01-71-26W4 (928.30 m). Coin diameter is 1.85 cm.

3.4.5 Facies E: Disrupted bedding and breccias

Description: This facies is made up of breccias with subangular to subrounded intraclasts of brown dolomudstones and small anhydrite nodules less than 1mm in size in a green-coloured mud matrix. Some of the dolomudstone lithoclasts show internal lamination, which correspond to Facies A (Figure 3.8).

Interpretation: This facies is interpreted as synsedimentary breccias, being the product of reworking during storms or minor transgressions with concomitant plastic deformation.

42
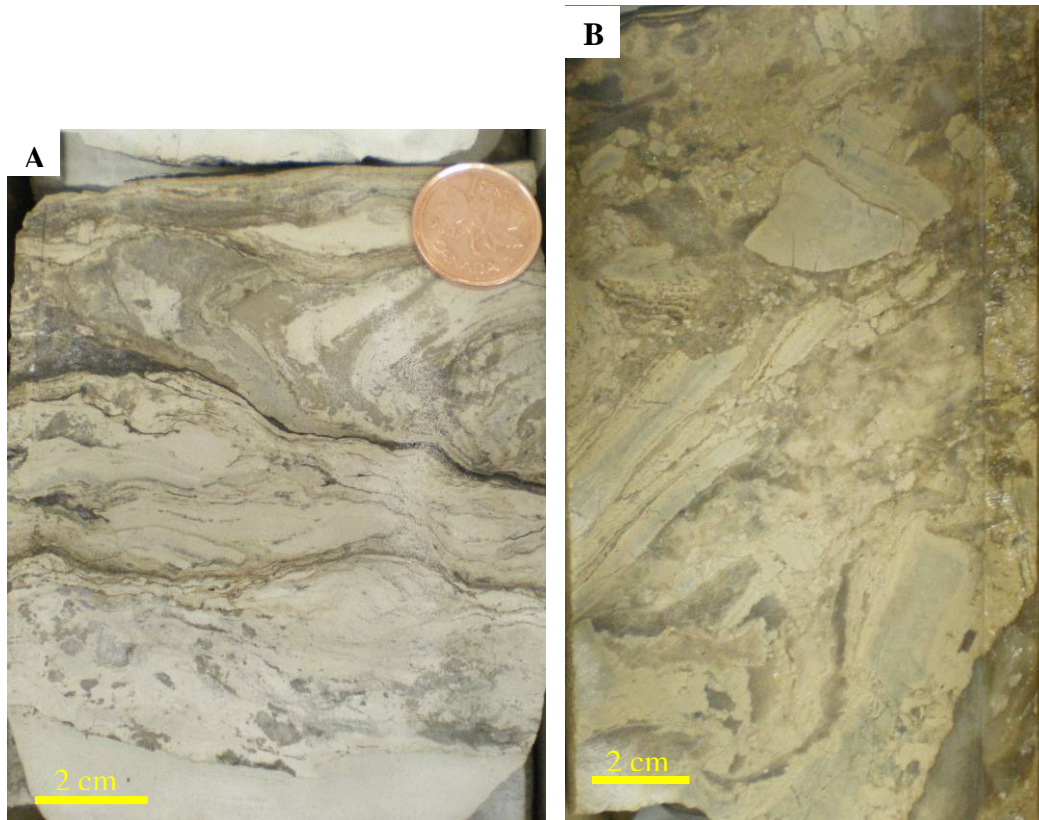
Figure 3.8 Facies E. A Core of laminated dolomudstone and anhydrite deformed as a result of one or several of the following processes: reworking by wave action, synsedimentary/plastic deformation as a result of compactional dewatering, well 03-28-70-24W4 (861.20 m.). Coin diameter 1.85 cm. B Core of breccia, probably formed after subaerial exposure with desiccation, probably small scale teepee formation followed by subaqueous reworking, well 15-17-71-25W4 (912.20 m).

A summary of the core observations is presented in Table 3.1. Most of the Hondo primary sulphates, if interpreted individually, point to a semi-arid to arid shallow marine to coastal (sabkha) setting. Most of the micro-textures suggest formation of sulphates originally as gypsum. To infer a depositional model one has to further consider the stratigraphic and facies relationships on a large scale (Schreiber, 1978 and Schreiber and El Tabakh, 2000). A depositional model for the Hondo is proposed in Chapter 6, after incorporating the geochemistry of the sulphates, and integrating regional and stratigraphic information.

43

Facies Type	Description	Interpretation	Observation	Photograph	Example
A. Laminated anhydrite and laminated dolomudstone	Laminated white to grey anhydrite and yellow to brownish dolomudstones. Lamina thicknesses range from less than 2 mm to about 1 cm. Laminae are generally planar to wavy.	Physical process, low energy and high salinity pools.	Slightly affected by seasonal currents		15-17-71-25W4 912.45 m
B. Mosaic anhydrite with microbial mats.	Mosaic anhydrite and microbial mats. Centimetre scale nodules of white anhydrite aligned sub-horizontally within a cream dolomite matrix. Microbial mats with sharp contact with the dolomite area.	Shallow hypersaline waters, sabkha environment.	Interpretation is made individually for this facies		15-17-71-25W4 910.30 910.70 m.
C. Enterolithic anhydrite / contorted bedded anhydrite	Cream dolomudstone and grey anhydrite layers with deformed beds forming rope structures in some intervals.	Low energy, but deformed syndepositionally due to differences in density.	Vertical deformation of the horizontal layers. Possible seasonal currents.		15-17-71-25W4 904.80 m

Table 3.1 Hondo lithofacies

Facies Type	Description	Interpretation	Observation	Photograph	Example
D. Displacive-Nodular anhydrite	Isolated and coalesced ovoids to irregular shape of white anhydrite with size average of 2mm to 5mm embedded in brown dolomudstone. Displacive layers and nodules of anhydrite.	Formed in a subaqueous setting, by displacement in the soft sediment (currents), or displaced during burial.	It can be associated to early diagenesis.		10-01-71-26W4 928.30 m
E. Disrupted bedding and breccias	Deformed dolomudstone and anhydrite. Breccias with subangular to subrounded intraclasts of brown dolomudstones and small anhydrite nodules less than 1mm. Some of the dolomudstone lithoclasts show internal lamination of Facies A.	Deformation as a result of plastic deformation (synsedimentary), reworking, or compactional dewatering displacement due to wave action/ high energy events.	Possible seasonal storms. Wave action or compactional dewatering.		Well 15-17-71-25W4 912.20 m

Table 3.1 Hondo Lithofacies.

CHAPTER 4

DIAGENESIS

4.1 Introduction

In this chapter the diagenetic features of the Hondo sulphates within the Grosmont Formation are described and interpreted based on core analyses and petrography. Although the main focus of this thesis is the Hondo sulphates, other aspects of the Grosmont Formation, especially from the Upper Grosmont 3, are also examined. The Grosmont Formation shows a complex diagenetic history with features formed from near-surface to burial settings. Diagenetic processes such as dolomitization and dissolution have masked most of the primary features in the Grosmont Formation and the Hondo, and they have modified the reservoir quality. Interpretations of timing are somewhat uncertain due to the complex diagenetic history.

4.2 Diagenetic Settings

Diagenesis effects various changes in sediments after deposition and carries through to incipient metamorphism (Tucker and Wright, 1990). These changes include the volume, carbonate content, and textural features of the rock. Diagenetic processes include dissolution, cementation, compaction, dolomitization, and recrystallization. Diagenetic settings have been defined as marine, meteoric, and burial (Tucker and Wright, 1990). However, Machel (1999) proposed a somewhat different classification that includes near-surface, shallow-

burial, intermediate burial and deep burial settings (Figure 4.1). Near-surface diagenetic settings are those defined to occur within a few meters of burial, where the pore fluids are surface-derived meteoric, brackish, marine, or evaporitic. Shallow-burial diagenetic settings are similar to the near-surface diagenetic settings but physical compaction is or has taken place. A depth of 600-1000m is considered the lower boundary of shallow-burial diagenesis. Intermediate and deep burial diagenetic settings are located below shallow burial settings. Rocks in the intermediate-burial settings experience chemical compaction, subsurface cementation, and dissolution. Stylolites and sutured seams commonly develop. The lower limit of intermediate-burial diagenetic settings and thereby the upper limit of deep-burial diagenetic settings is defined by the top of the liquid oil window in hydrocarbon source rocks (Machel, 1999). This depth has been used also to define the boundary between "diagenesis" and "catagenesis" in terms of petroleum geology and varies depending on the kerogen type and geothermal history (Hunt, 1996). Deep-burial diagenetic settings merge into the metamorphic realm at temperatures around 200°C and commensurate depths and pressures which depend on the regional geothermal gradient (Machel, 1999).

4.3 Grosmont and Hondo Diagenesis

The diagenesis of the Grosmont/Hondo can be represented by a paragenetic sequence (Figure 4.2, modified from Huebscher, 1996). The various diagenetic features in the Grosmont Formation formed over a considerable span of geological time and with several occurrences of overlap between them. The

maximum burial depth in the study area is estimated to have been about 1000 m at the eastern margin of the Grosmont platform, increasing to about 1800 m along the western margin of the platform. The exact timing and duration of subaerial exposure in this region is not known but interpreted to be Late Jurassic to Early Cretaceous. During this time, the eastern but not the western part of the platform was subaerially exposed. All the diagenetic events that affected the Grosmont/Hondo took place between near-surface to intermediate-burial depths (*sensu* Machel, 1999) (Figure 4.1). The remainder of this chapter will discuss only those diagenetic features that are of interest in the present context.
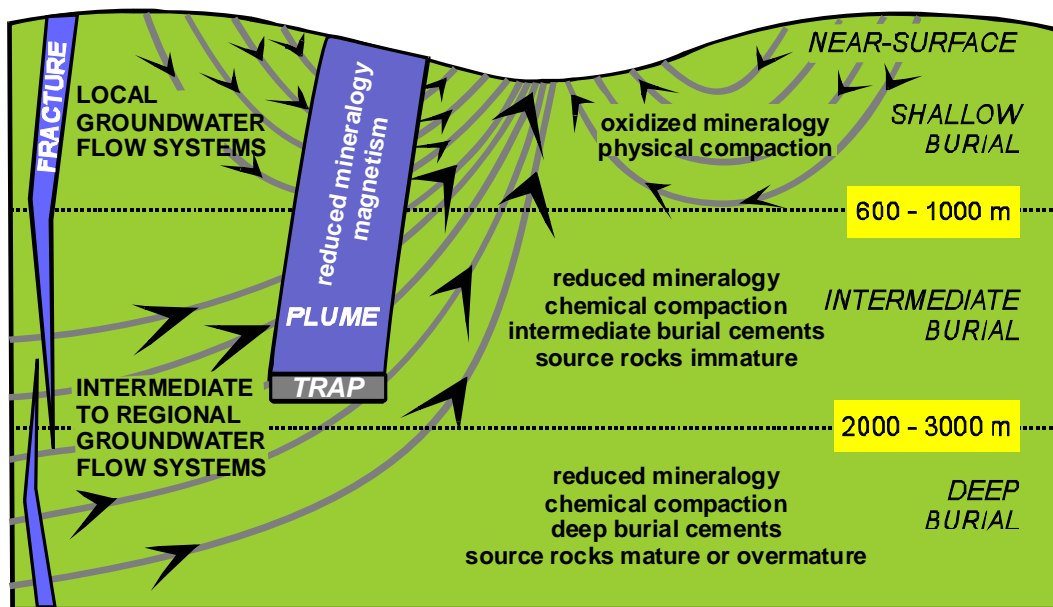
Figure 4.1 Classification of diagenetic settings on the basis of mineralogy, petroleum, hydrogeochemistry, and hydrogeology. Arched lines represent idealized groundwater flow lines. Depth limits separating the burial diagenetic settings are based on geologic phenomena that are easily recognized. Near-surface and shallow-burial settings may be meteoric, brackish, marine, or hypersaline (from Machel, 1999).

Figure 4.2 Generalized burial curve and paragenetic sequence of the Grosmont Platform illustrating the relative timing of the major diagenetic processes and resulting diagenetic phases. Red burial curve represents the eastern part of the Grosmont platform, whereas the blue curve represents the western part of the platform. Dashed lines indicate uncertainties of duration or timing. "+" denotes enhancement, "-"represents degradation of porosity or permeability. The estimated burial history of the Grosmont Formation was constructed by Hubscher (1996), assuming a thermal gradient of 30°C km^{-1} and a surface temperature of 25°C. (Burial curve modified from Huebscher, 1996).

49

4.3.1 Dolomitization

During dolomitization the mineral dolomite, $CaMg(CO_3)_2$, replaces the original limestones consisting of aragonite and/or calcite. Dolomites are considered to form in two categories: syndepositionally and postdepositionally (Budd, 1997). Syndepositional dolostones form in the original environment under "normal" geochemical conditions where the carbonate sediments are deposited; they are also called "primary" and/or "early diagenetic dolomites." Postdepositional dolomites are formed after the sediments are deposited and removed from the initial zone of sedimentation. Formation of dolomite is favoured chemically by the following conditions: low Ca^{2+}/Mg^{2+} ratios, low Ca^{2+}/CO_3^{2-} ratios, high temperature, salinity above seawater salinity, and the sudden release of CO_2 by fluids in certain areas (Carpenter, 1980; Morrow, 1990; Machel and Mountjoy, 1986; Leach et al., 1991; Arvidson and Mackenzie, 1999; Machel, 2004). Under the above conditions, there are several natural settings conducive to dolomitization (Machel and Mountjoy, 1986):

1.   marginal marine environments, including fresh water/sea water mixing zones and normal marine-to-hypersaline subtidal environments;

2.   alkaline environments that are under the influence of bacterial reduction and/or fermentation processes;

3.   burial environments with temperatures greater than $50^{\circ}C$.

Petrographic descriptions follow the textural classification of dolomites modified from Sibley and Gregg (1987) (Figure 4.3).

50
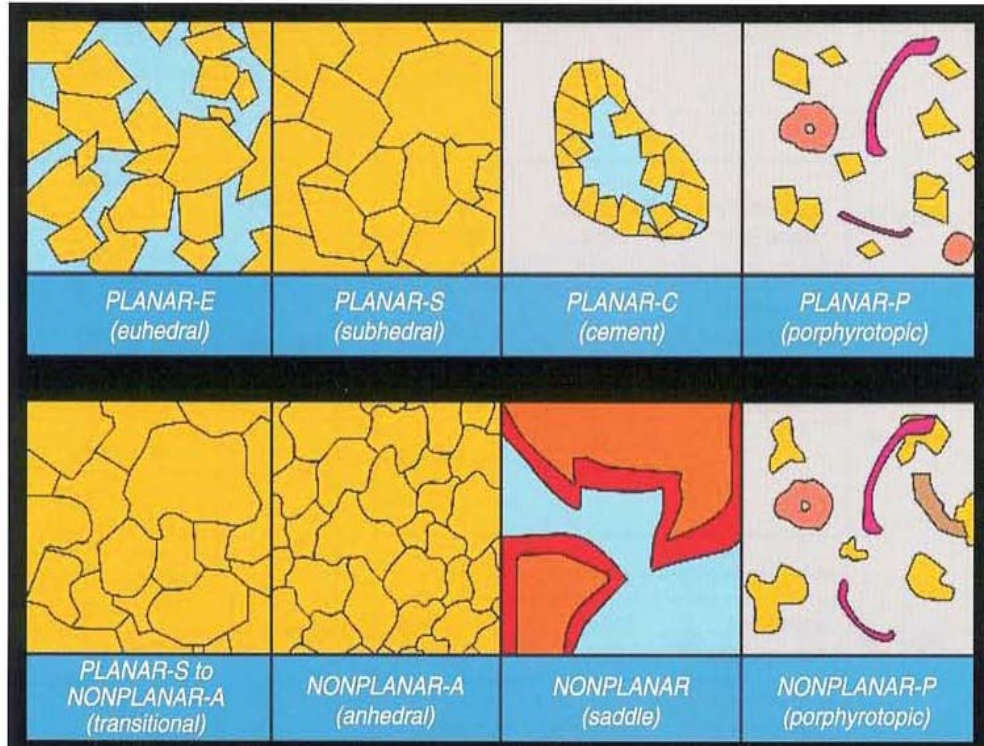
Figure 4.3 Dolomite textural classification combined from Gregg and Sibley (1984) and Sibley and Gregg (1987) (from Machel, 2004).

In deposits formed by evaporation, early diagenesis and compaction are likely to strongly modify and/or destroy textural features in evaporitic beds (Choquette and James, 1990; Warren, 2006). The Hondo sulphates have undergone diagenetic processes of different magnitudes, such as anhydritization, gypsification, and dissolution (brecciation and karstification).

4.3.1.1 Replacement Dolomites

Description: Huebscher (1996) and Huebscher and Machel (2004) discriminated between two major types of dolomite in the Grosmont Formation (Figures 4.4). Type 1 replacement dolomite (R1) is present in all depositional facies of the Grosmont but is most common in the upper members in the

51

northeastern part of the platform. In cores from this area, this type of dolomite is usually light grey to light brown. R1 dolomite preferentially replaced matrix of the original limestones and primary fabrics are preserved as shown in figures 3.1, 3.3, 3.6, 3.7 and 4.4 (see also plate 36, Machel and Hunter, 1994). In thin section, dolomite crystals are planar-E to planar-S and crystals are very small without or with very little textural evidence of recrystallization (Figure 4.5). Type 2 replacement dolomite (R2) was recognized in the southern part of the study area where the Grosmont Formation overlies reefs of the Leduc and Cooking Lake formations. R2 dolomite shows clear evidence of recrystallization (Huebscher and Machel, 2004). In core, this type of dolomite is grey or light brown; it occurs as a pervasive replacement phase including calcitic fossils and commonly has visible intercrystal porosity (Figure 4.4). In thin section, it is coarser than R1 dolomite and the crystals are planar-S to nonplanar-A.

Dolomite types R1 and R2 were also recognized in this study, both in the Grosmont as well as in the Hondo. Dolomite type R1 is matrix selective showing recrystallization in coarser crystal mosaics, with textures ranging from planar-S to nonplanar-A, but most are too small for identification. In cores of the Lower Grosmont and Upper Grosmont 1 (examples are shown in Figures 4.6 and 4.8), replacement dolomite type R1 is characterized by good to excellent preservation of primary fabric. There are intervals with large bioclasts such as coral fragments, stromotoporoids, bivalves, gastropods, and crinoids, which tend to remain as calcite (Figure 4.6). Replacement dolomite type R2 is characterized for coarser crystal mosaics and some dolomite crystals are revealing overgrowth/zoning.
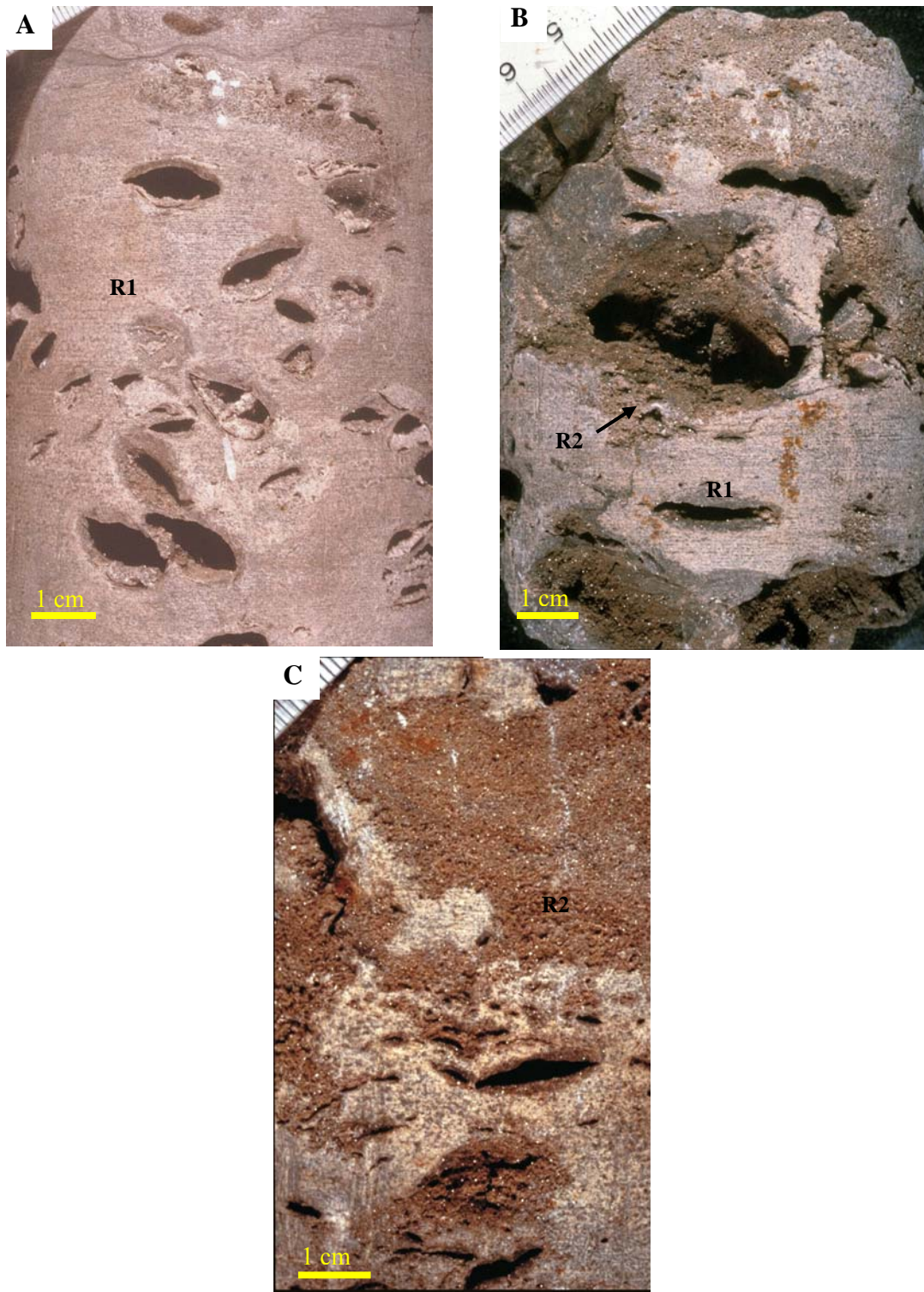
Figure 4.4 Core Samples of dolomite types R1 and R2 and recrystallization of dolomite. Dolomite is formed around moulds and vugs and extends into the matrix. In order A, B, and C show the increasing degree of recrystallization from the outer part of the moulds with increase in crystal size towards the matrix. A well 10-18-76-25W4 (1066.3 m) UGM1. B and C well 11-12-91-24W4 (370.85 m) UGM2. (reproduced from Huebscher, 1996)
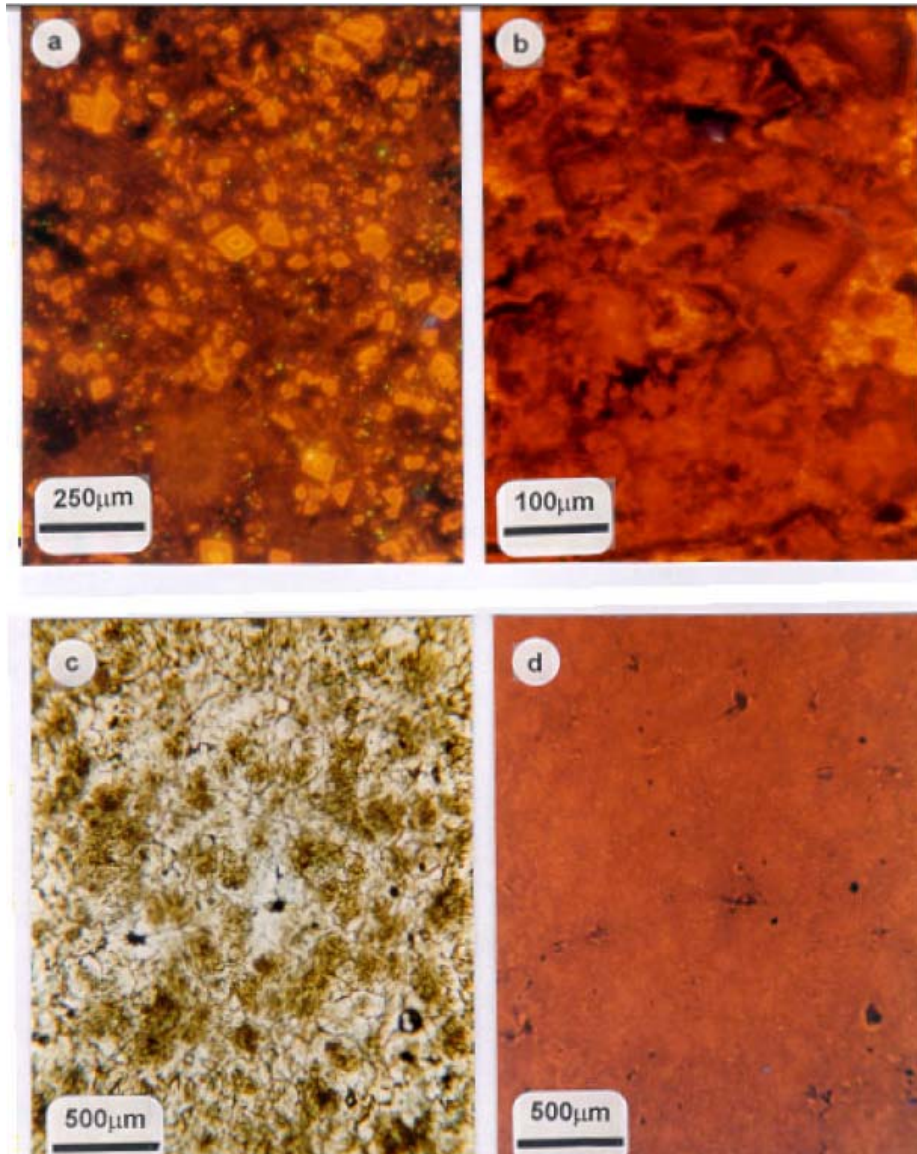
Figure 4.5 Photomicrographs of thin sections of dolomite types. a and b type R1 dolomite, well 10-17-83-18W4, 455.0 m - LGM and 388.5m - UGM2. Thin sections observed under cathodoluminiscence (CL). Dolomite in a dull red luminescent limestone matrix. c and d type R2 dolomite, well 03-34-88-20W4 (466.3 m). Leduc Fm. Planar-E and Planar-S dolomite textures are referred as euhedral and subhedral by Huebscher and Machel, 2004 (reproduced from Huebscher and Machel, 2004).

54
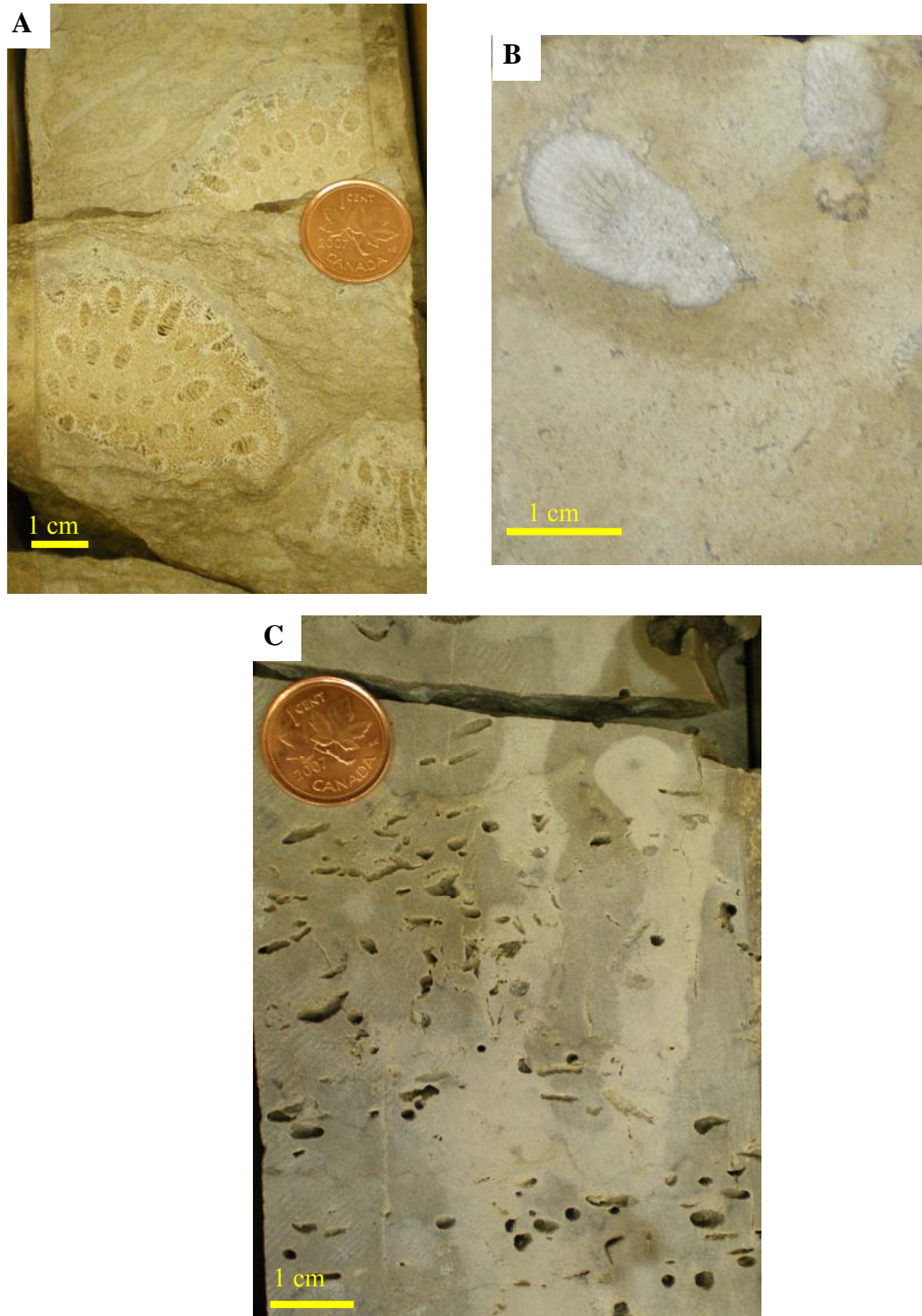
Figure 4.6 Core samples of dolomite type R1. A Coral with preserved residual calcite, calcitic matrix, well 10-17-84-19W4 (516.80 m) LGM. Coin diameter is 1.85 cm. B Coral fragment remain calcitic, but matrix partially dolomitized, 10-17-84-19W4 (506.70 m) UGM1. C Dolomitization affected matrix preferentially with preservation of primary fabrics, preservation of some mouldic porosity from *Amphipora* floatstone, well 03-28-70-24W4 (865.20 m) UGM2. Coin diameter is 1.85 cm
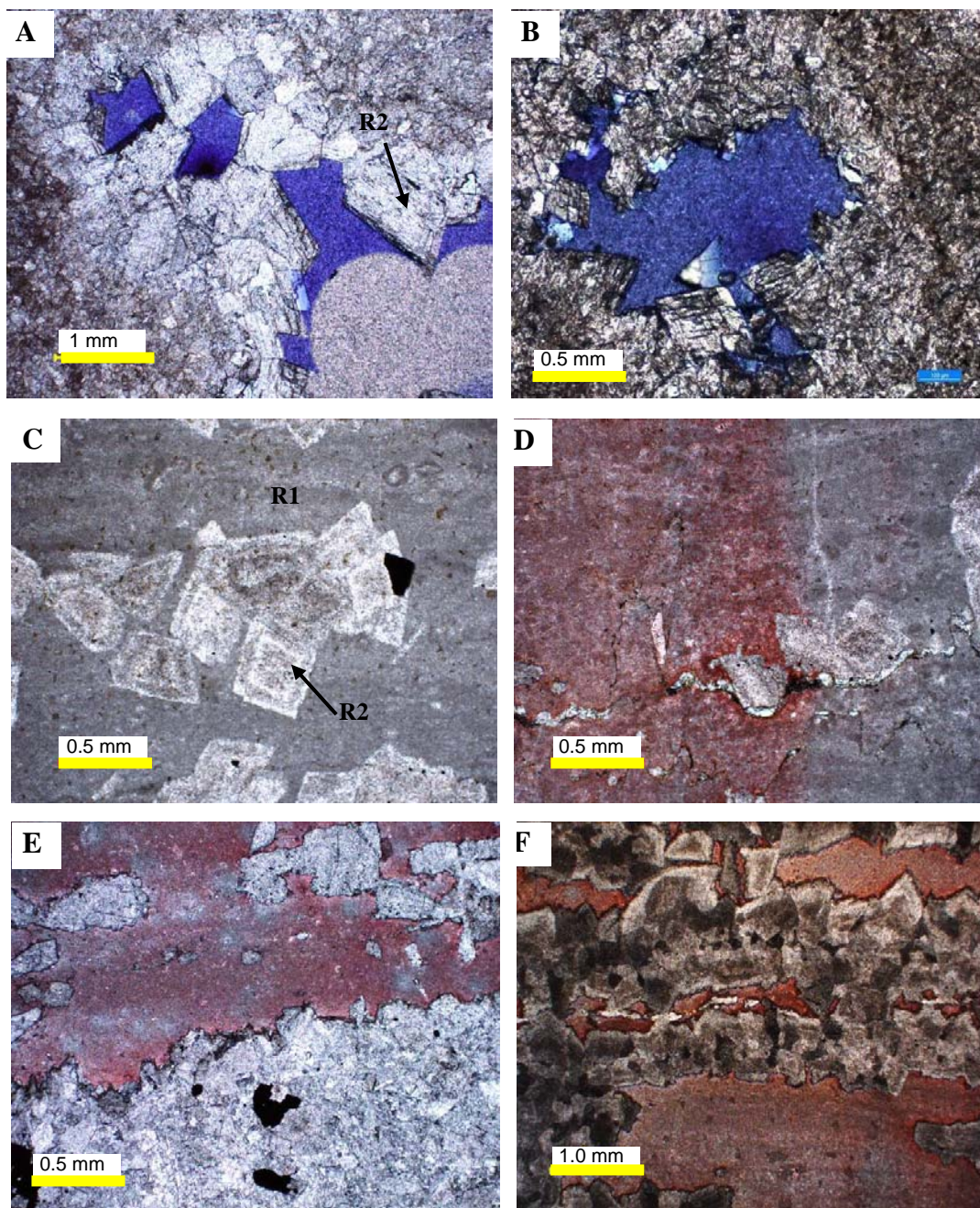
Figure 4.7 Photomicrographs of thin sections showing two types of dolomite. A (plane polarized light), B (cross polarized light) well 02-30-70-01W5 (1066.5 m), UGM1. C, D Dolomite crystals planar-E texture showing zonation (plane polarized light), well 01-09-70-03W5 (1155.8 m). E, F Dolomite R1,bands of clustered dolomite planar-E in limestone matrix (plane polarized light), well 01-09-70-03W5 (1157.3 m) UGM3.
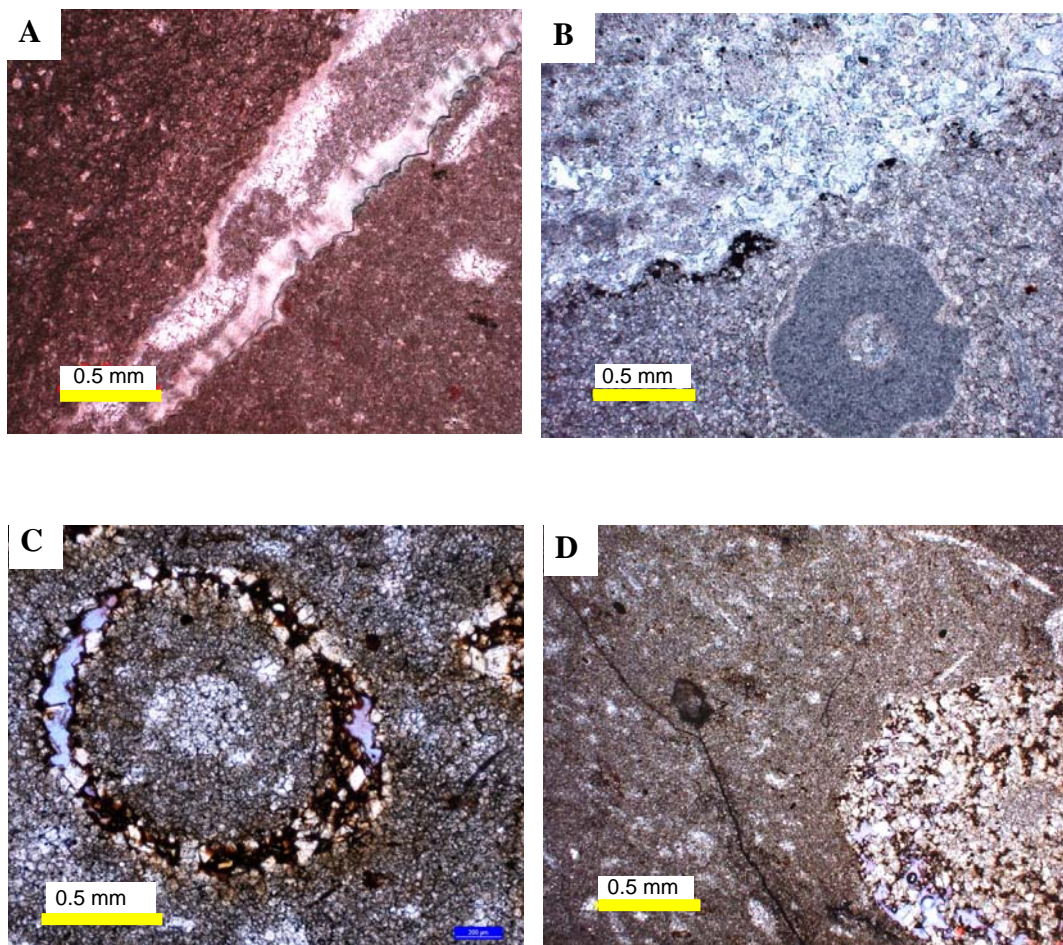
Figure 4.8 Photomicrographs of thin sections of dolomite types. A Well 06-03-70-02W5 (1239.9 m) UGM3. B Mimetic dolomitization, well 06-10-77-25W4 (1059.7 m) LGM. C Fine to medium crystalline dolomite, dissolution around perimeter of crinoid ossicle partially cemented with relatively coarse planar-A dolomite. D Relatively coarse crystalline dolomite. C and D thin sections of well 13-28-93-02W5 (534.5 m) UGM3.

Texturally, matrix dolomitization in the Hondo is essentially identical to type R1 in the Grosmont Formation. In core, dolomite associated with the Hondo primary sulphates is generally cream to light grey in colour as present in the Hondo type well 15-17-71-25W4. Under the microscope, dolomite is cryptocrystalline to fine-crystalline (up to about 50 μm) and is mainly planar-S to

57

nonplanar-A (Figure 4.9). This type of dolomite is observed in all the wells that penetrated the Hondo.
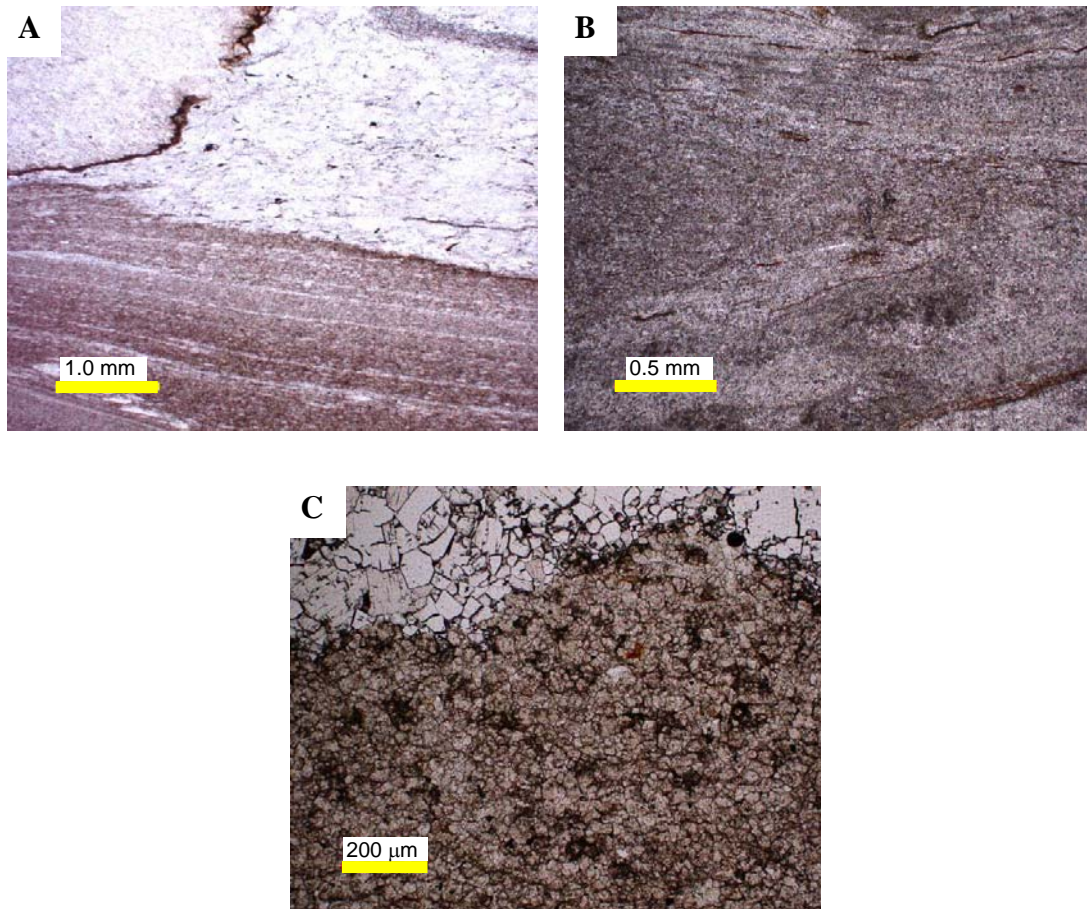
Figure 4.9 Photomicrographs of thin sections of syndepositional dolomite. A Laminae of dolomite and anhydrite (plane polarized light). B Dolomudstone, very fine grained showing some bioturbation (cross polarized light). A and B well 15-17-71-25W4 (913.5 m). C Planar-S dolomite crystals (plane polarized light), well 10-01-71-26W4 (931.6 m)

Interpretation: Type replacement dolomite type R1 is thought to have formed syndepositionally or during shallow burial. Reflux of sulphate-saturated brines could have formed the majority of the dolomite in the Grosmont Formation (Jones et al., 2003; Huebscher and Machel, 2004). In this type of dolomitization,

58

the seawater that evaporates at or beyond the gypsum saturation level and flows seaward within the topmost few metres of the carbonate sediments via density-drive. These fluids form finely crystalline and geochemically distinct dolomite, either as cement or replacement. Dolomite type R2 occurred post-depositionally and according to Huebscher and Machel (2004), this type of dolomite is interpreted to have been formed by burial and warm fluids that migrated from the reef aquifers into the Grosmont.

Dolomitization increases toward the eastern part of the Grosmont platform and toward the upper members of the Grosmont Formation, especially in the Upper Grosmont 2 and 3. This process destroyed most of the original depositional fabric, although some features are still preserved.

4.3.1.2 Recrystallization of Replacement Dolomites

Recrystallization is a process in which the original components of a rock go into solution and then reprecipitate during burial, over time. Significant changes in rock texture and chemical composition are common during this process. The terminology, used in dolostone studies, has been adapted from that used in limestone studies; however, some terms in dolostone analysis are improperly used. The term neomorphism, defined by Folk (1965) in the context of limestones, describes the processes of: 1) inversion (aragonite to calcite), 2) recrystallization (calcite to calcite), and 3) strain-recrystallization (strained calcite to unstrained calcite). In this definition, the gross composition remains constant. Neomorphism has also been used by Gregg and Sibley (1984) and Sibley and

Gregg (1987) to describe dolomites and dolostones, as it includes the transformation of poorly ordered (nonstoichiometric) to ordered (stoichiometric) dolomite. In dolomites, some properties change during recrystallization, yet these properties are not included in the term neomorphism, leading to misuse of the term. Due to this confusion, Machel (1987) redefined the term recrystallization by combining the initial definitions for neomorphism and recrystallization. As a result, the term recrystallization includes: textural, structural-ordering, and geochemical compositional changes, and changes in paleomagnetic properties. Machel (1997) recommended the term "significant recrystallization" to minimize the problem of having to recognize whether a dolomite or dolostone has undergone any dissolution-reprecipitation on a submicroscopic scale. In highly recrystallized rocks, inherent properties may represent the event of dolomitization, whereas other properties represent recrystallization.

Description: In hand specimens, recrystallization of dolomite is observed at the borders of vugs or moulds; recrystallized dolomite shows a different crystal size and colour than the matrix (Figure 4.4). Under a microscope, recrystallized dolomite shows increasing crystal size from 200 μm to 5mm; textures are mainly planar-S to nonplanar-A (Figure 4.10).
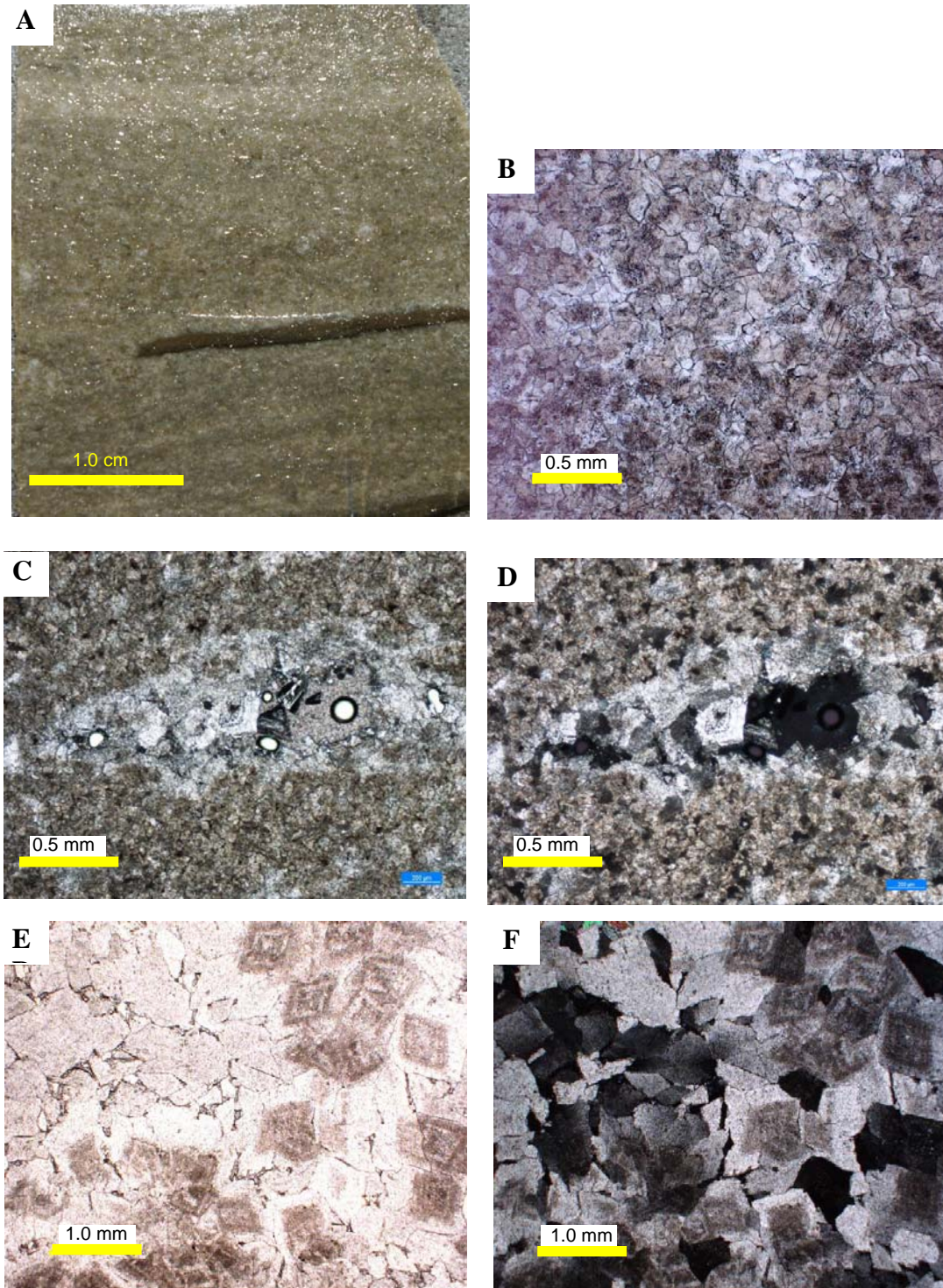
Figure 4.10 Tight recrystallized dolostone. A on hand specimen. B to F photomicrographs of thin sections. A Recrystallized dolostone; larger crystals have planar-S to nonplanar-A texture, well 08-16-87-01W5 (891.0 m) UGM3. C (plane polarized light). D (cross polarized light), well 10-35-73-04W5 (1120.7 m) UGM2. E (plane polarized light). F (cross polarized light), zoned dolomite crystals are replaced by coarser dolomite, well 01-09-70-03W5 (1157.3 m) UGM3.

61

Interpretation: Recrystallization of dolomite is ambiguous. It is not clear if dolomite R2 is the result of recrystallization of dolomite R1 or is the result of a mix of recrystallization and dissolution processes. Huebscher (1996) stated:

> … replacement dolomite type R1 was converted (recrystallized) to replacement dolomite R2 in the upper members of the Grosmont Formation by ascending fluids that migrated from the Cooking Lake/Leduc aquifer into the Grosmont aquifer. This implies that ascending fluids were also responsible for the formation of replacement dolomite R2 in the LGM. (p 176)

If type R2 dolomite was formed by recrystallization and dissolution, it probably occurred when the Grosmont Formation was subaerially exposed and karstification took place. Mattes and Mountjoy (1980), Machel (1997), and Machel et al. (1999) suggested that no matter where in the burial environment it is formed, burial dolomite is more stable than marine and evaporitic dolomite, and it is also less likely to be recrystallized.

4.3.2 Dissolution-1

Dissolution is the leaching of unstable minerals to form secondary porosity in the host rock (Scholle and Scholle, 2003). Dissolution is common in sulphates and lithified dolostones that have an unstable mineralogy, and is favoured by cold temperatures, changes in fluid composition, and the presence of acidic fluids (Tucker and Wright, 1990) for carbonates and sulphates.

Description: Dissolution in the Grosmont is observed as: (1) bioclast-selective dissolution that created mouldic porosity (Figures 4.11and 4.13); (2) vugs and cavities formed without specific shape(s) (Figure 4.12); (3) intercrystal porosity commonly filled with bitumen (Figure 4.13); (4) halite dissolution as suggested by isolated moulds of halite hoppers (Figure 4.14).
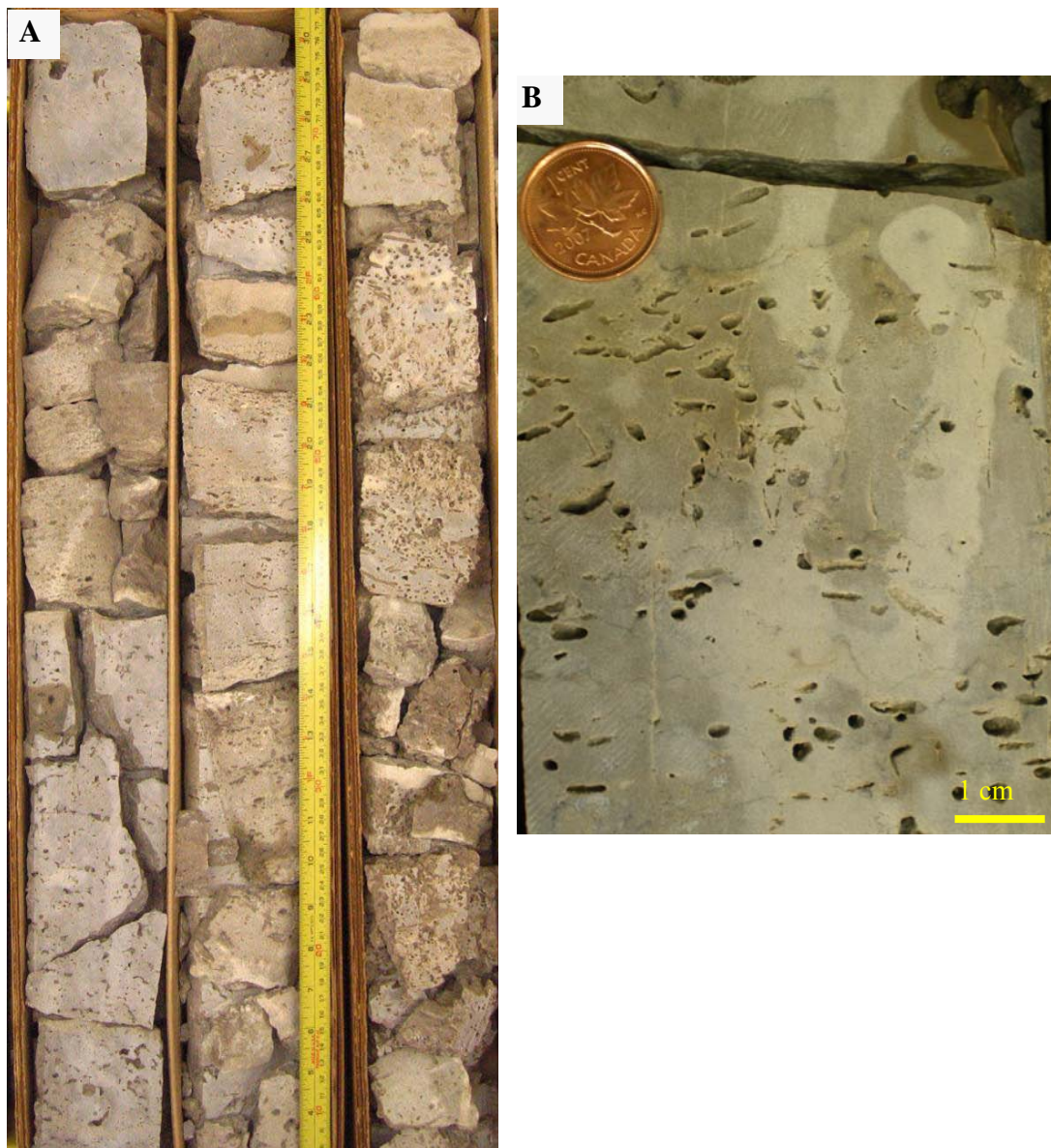
Figure 4.11. Mouldic porosity in core samples, *Amphipora* floatstone. A and B: well 03-28-70-24W4 (751.90 m), Nisku. B (865.20 m) UGM3. Coin diameter is 1.85 cm.
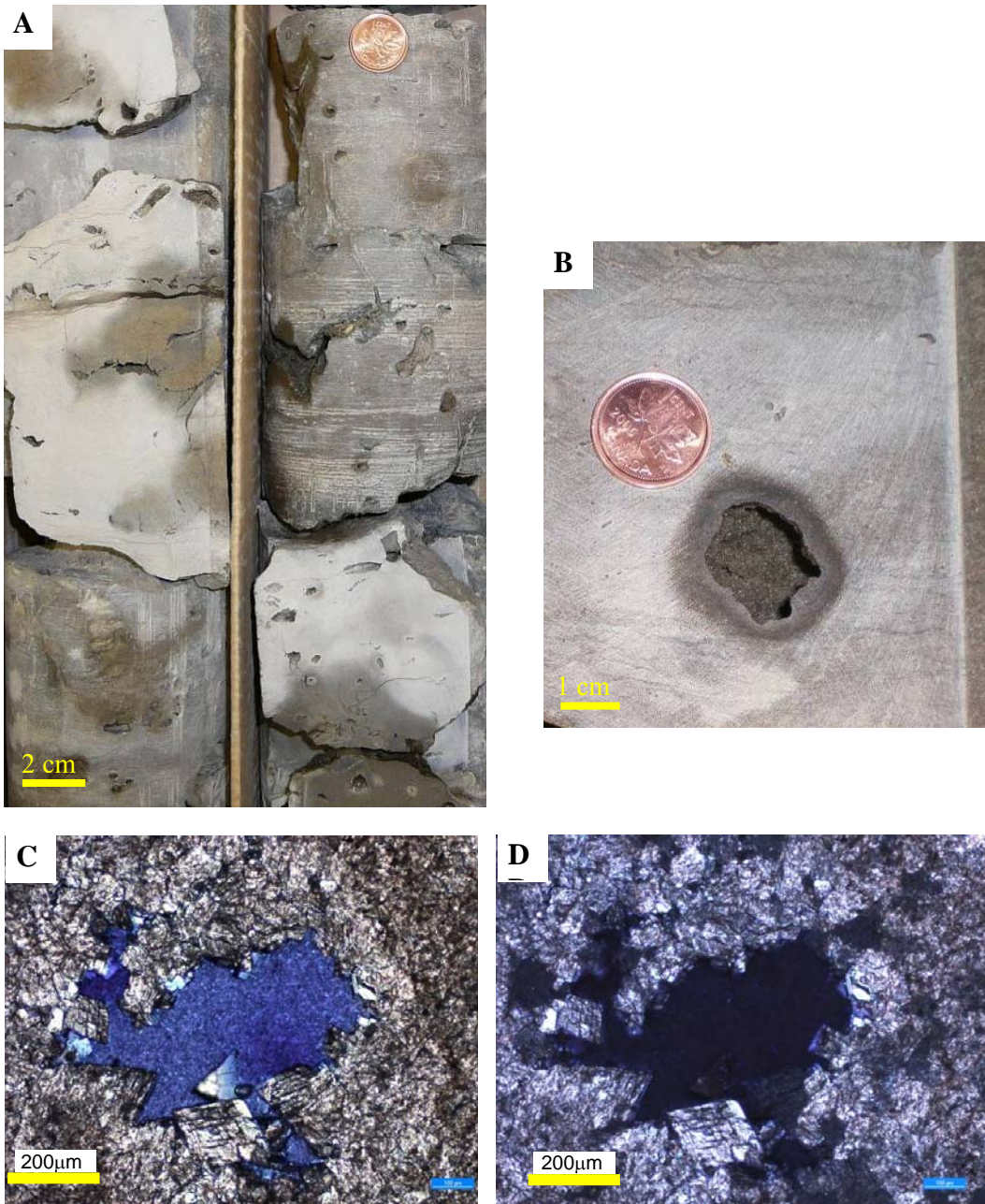
Figure 4.12 Vuggy and cavity porosity in dolostones of the Grosmont Formation. A Core sample, well 06-10-77-25W4 (1053.0 m) UGM1. B Core showing a vug probably previously filled with anhydrite, well 10-35-73-04W5 (1116.8 m) UGM2. Coin diameter is 1.85 cm. C and D Photomicrographs of thin sections, C (plane polarized light) D (cross polarized light), well 01-09-70-03W5 (1158.5 m) UGM3.
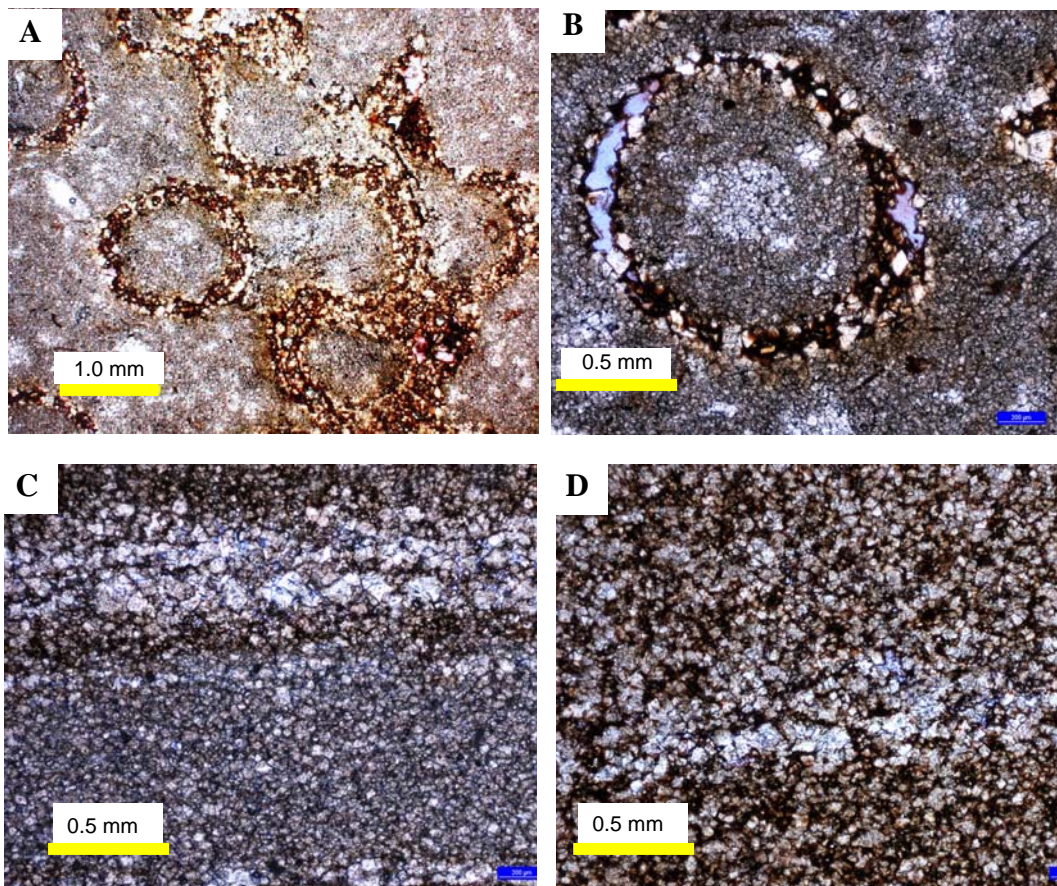
Figure 4.13 Photomicrographs of thin sections of secondary porosity. A, B Mouldic porosity in thin section (plane polarized light). There are bitumen and crystals of dolomite within the outline of the moulds, well 13-28-93-02W5 (534.5 m) UGM3. C, D Intercrystal porosity in thin section A (plane polarized light) B (cross polarized light), bitumen in pores, well 13-28-93-02W5 (574.5 m) UGM1? (this well does not have logs and core is incomplete).

Interpretation: Dissolution-1 occurred in the near-surface to shallow settings. Creation of secondary porosity may be attributed to meteoric waters that penetrated partially lithified sediments. Moulds, vugs, and small cavities are interpreted to have formed as a result of calcite/dolomite and sulphate dissolution. Dissolution of halite apparently occurred during physical compaction but after partial cementation, as shown by the curved faces of halite hoppers (Figure 4.14).
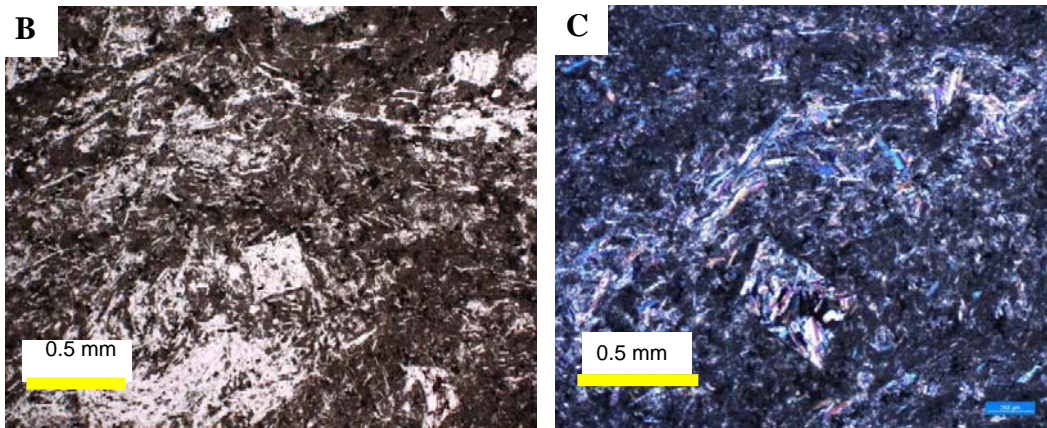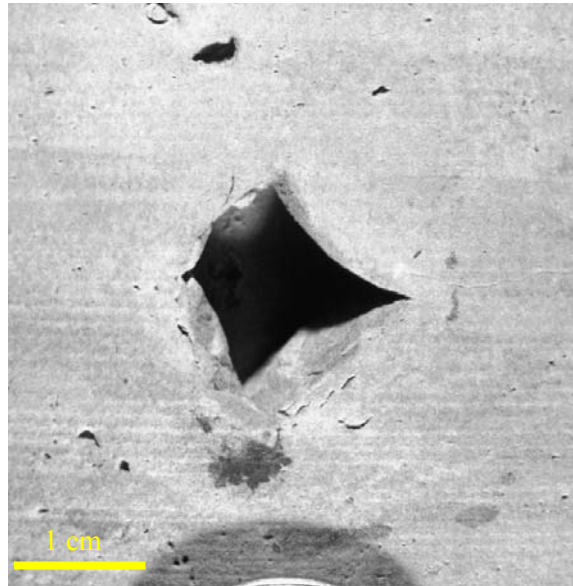
Figure 4.14 Halite hopper moulds. A Slabbed core surface showing probable pseudomorph of a halite hopper in dolomudstsone, well 11-35-85-18W4 (278 m) UGM3. B and C photomicrographs of thin sections; left under plane polarized light, right under cross polarized light; replacement of the halite crystal by gypsum, well 10-01-71-26W4 (978.20 m) UGM3.

4.3.3 Anhydritization

Description: Anhydrite is the main mineral recognized as a secondary sulphate in the Hondo and Grosmont. Some samples contain a mixture of anhydrite and gypsum, with anhydrite as the main component.

66

Anhydritization affected the Grosmont and Hondo in three different ways: (1) replacement (transformation) of primary gypsum by anhydrite via dewatering; (2) replacement of remnant calcite or dolomite; and (3) cementation/infill of moulds or vugs.

4.3.3.1 Replacement (transformation) of primary gypsum by anhydrite

The gypsum to anhydrite replacement (transformation) occurred during relatively rapid burial in the Late Devonian and Early Mississippian (Figure 4.2). This transformation preserved some of the primary textures as found in core (see Chapter 3). However, at the microscale the primary textures have been almost obliterated. The former gypsum mineralogy of the primary sulphates is now present as felted and corrotopic anhydrite, the latter to be the result of the replacement of gypsum by anhydrite with possible subsequent anhydrite recrystallization (Figure 4.15). Some anhydrite crystals show a porphyrotopic texture (larger crystals), see Figure 3.2, Chapter 3.

4.3.3.2 Replacement of remnant calcite or dolomite

Some core intervals contain large (up to several centimetres) nodules/domains of milky-white anhydrite that appear to be replacive (see Figure 4.16).

The anhydrite in the samples shown in Figure 4.16 was probably formed originally as gypsum and later transformed to anhydrite during intermediate burial (Machel, 2004, Figure 7), as indicated by corrotopic microfabrics.
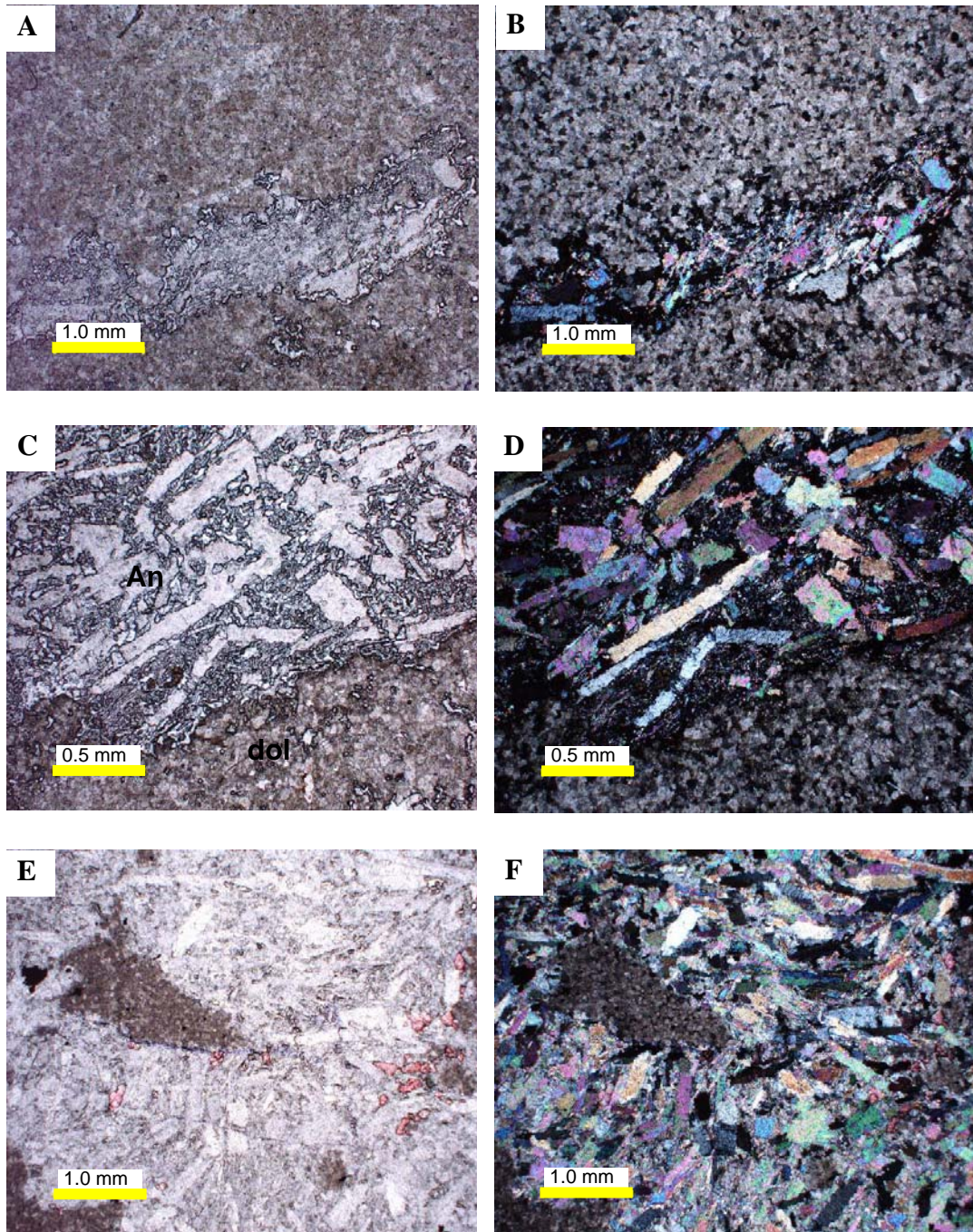
Figure 4.15 Anhydritization. Photomicrographs of thin sections: left side (plane polarized light), right side (cross polarized light). Corrotopic anhydrite, anhydrite consists of porphyrotopic crystals in a fine crystalline matrix. A, B, C and D anhydrite crystals are corroded, well 02-30-79-04W5 (1066.5 m) UGM3. E and F Dolomite "island"floating within the anhydrite, well 01-09-70-03W5 (1159.4 m) UGM3.
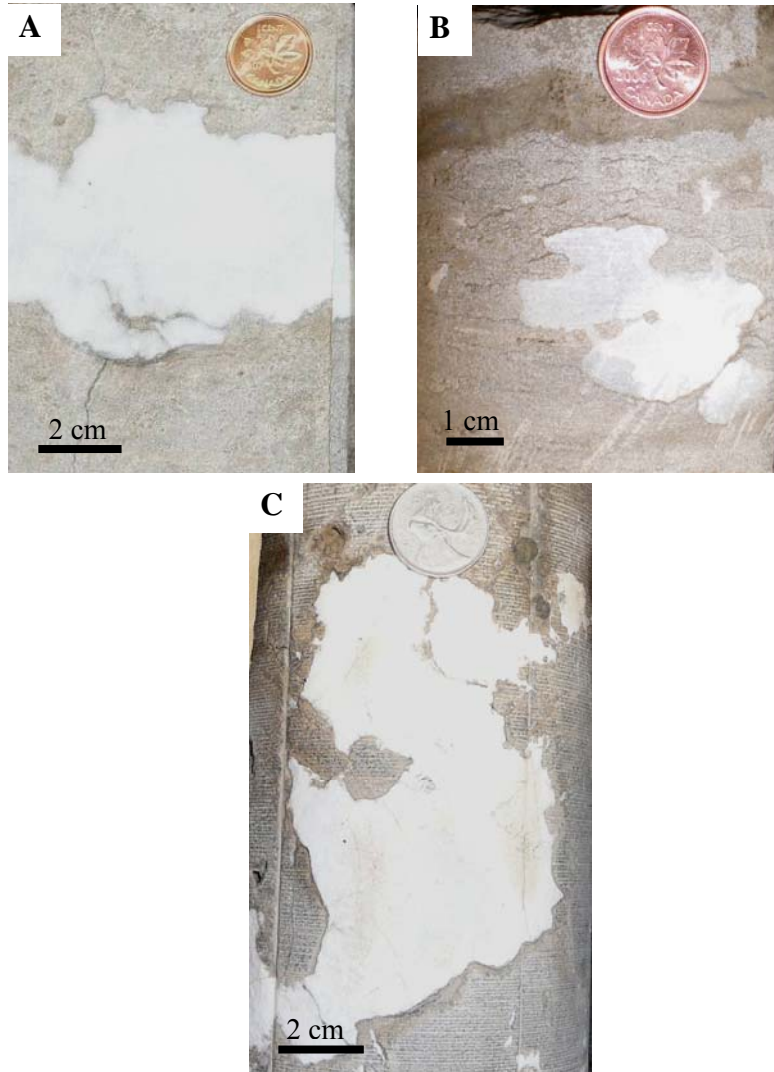
Figure 4.16 Core samples showing anhydrite replacing remnant calcite or dolomite. A Well 02-15-17-71-25W4 (1068.50 m) UGM2. B Well 01-09-70-03W5 (1159.5 m). A and B, coin diameter is 1.85 cm. C Well 10-18-76-25W4 (1064.6 m) LGM. The jagged and lobate interface between anhydrite and dolomite, as well as "islands" of dolomite "floating" in the anhydrite, suggest that this type of anhydrite formed during an advanced stage of matrix dolomitization or after matrix dolomitization (*sensu* Machel, 2004). However, it is also possible that this type of anhydrite replaced limestone matrix as opposed to dolomitized matrix; coin diameter in C is 2.3 cm.

4.3.3.3 Cementation of moulds and/or vugs

In some intervals within the Grosmont units, especially in UGM3, UGM1 and LGM, moulds like *Amphipora* floatstones are cemented by anhydrite (Figure 4.17).
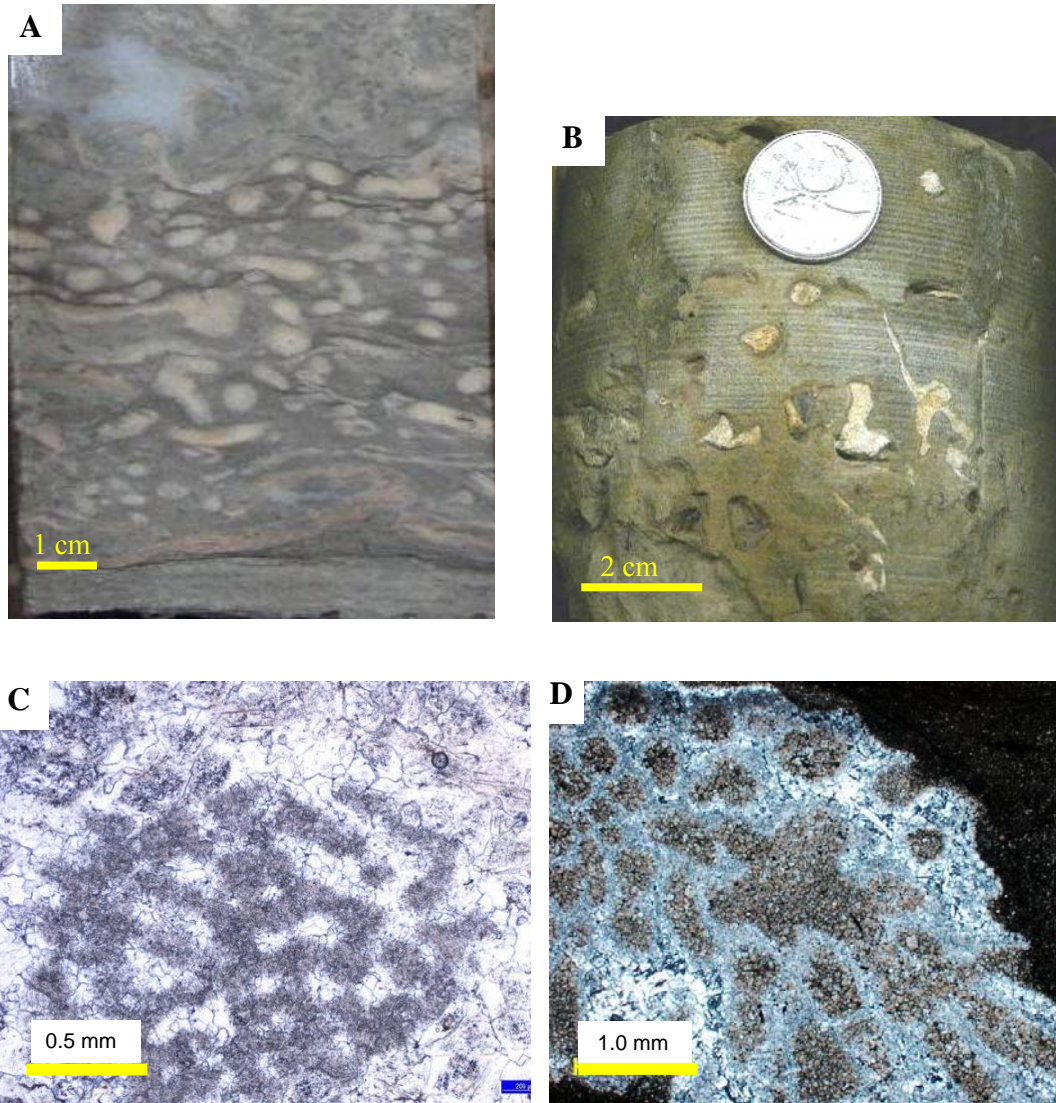
Figure 4.17 A Core with anhydrite in coral framework, well 04-15-69-24W4 (1010.4 m) LGM. B Core with anhydrite in vugs, well 02-30-79-24W4 (1068.4 m) UGM3. Coin diameter is 2.3 cm. C and D photomicrographs of thin sections. C (plane polarized light) well 08-16-87-01W5 (875.7 m) UGM3, D (crossed polarized light) well 15-17-71-25W4 (1013.45 m) LGM.

Interpretation: The transformation of gypsum to anhydrite probably occurred in three ways:

1.   solar heating of gypsum in surface conditions occurs when gypsum is exposed in a dry climate. Such climate-induced transformation commonly

70

forms milky aggregates of microcrystalline anhydrite, which is considered an early alteration of the gypsum matrix (Shearman, 1963);

2.   in phreatic zones where the pore fluids contain high sodium and chlorine concentrations, the transformation of gypsum to anhydrite is called subaerial desiccation (Amieux, 1980);

3.   Murray (1964) observed the anhydritization of gypsum at depths of 700-800 m. Mossop and Shearman (1973) reported gypsum transformation at depths of 1200 m, suggesting that the conversion is dependent on the geothermal gradient and overburden pressure.

Replacement of gypsum by anhydrite seems to have occurred within the Hondo near-surface to shallow-burial settings. During the deposition of the Grosmont Formation (Frasnian-Givetian stage), climate, latitude, and wind conditions were ideal for the formation of primary Hondo sulphates. Some synsedimentary anhydrite was probably formed by solar heating before lithification. Secondary anhydrite replacing dolomite or calcite or filling moulds or vugs may have taken place in the burial setting. Anhydritization is completed when sediments are buried. Gypsum was not observed in cores below a depth of 1120 m in this study.

4.3.4. Chemical Compaction/Stylolitization, Burial Stress Fractures

Compaction infers a reduction in bulk volume of a sediment; it can be mechanical or chemical and it takes place with increasing temperature and

pressure during burial. The cause of mechanical compaction is sediment overburden. Chemical compaction is caused by pressure-solution during deep burial. This process results in dissolution of particles in contact with each other, development of fissures, formation of stylolites and dissolution seams. Grain size, mineralogy, and texture of the original sediments, as well as contact between beds and presence of organic layers, may also strongly influence the sites of chemical compaction and stylolitization. However, subtle depositional and early diagenetic characteristics often control the location of pressure-solution features (Rittenhouse, 1971). Stylolites, the most common product of chemical compaction, are defined as thin zones of discontinuous surfaces produced by vertical movements and pressure accompanied by dissolution (Shinn and Robbin, 1983). The size of stylolites varies from microscopic (microstylolites) to several meters in length with amplitudes of up to several centimetres, occasionally decimetre-scale. Dissolution seams are mainly formed in fine grained sediments that contain clays, organic matter, or sulphide particles (Wanless, 1979; Tucker and Wright, 1990).

Description: In Hondo primary sulphates there is no clear evidence of stylolites or dissolution seams. However, stylolites and dissolution seams are present in the Upper Grosmont 3, 2 and 1 at depths varying from 520 m to 1180 m; examples are shown in Figures 4.18 and 4.19. Stylolites are nearly horizontal and have a columnar (vertical - rectangular peaks) to wavy geometry in some cases with sharp peaks, tapered and pointed. The amplitudes commonly are less than 20 mm (Figure 4.18). Wispy stylolites and dissolution seams are also

72

common, mostly in the Lower Grosmont and Upper Grosmont 1.
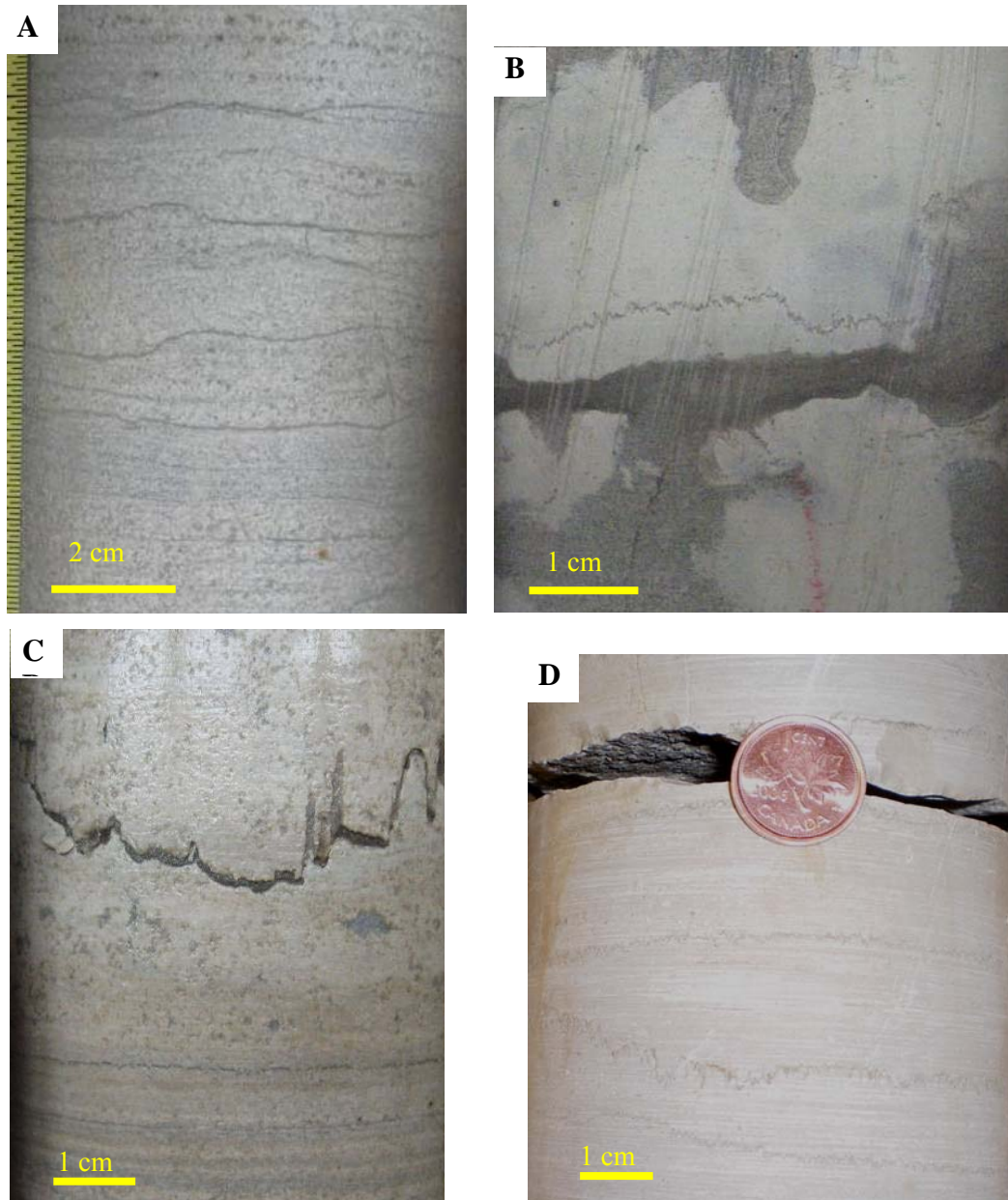
Figure 4.18 Stylolites in the Grosmont Formation. Core samples. A Wispy stylolites with low amplitude, well 15-23-68-01W5 (1127.80 m) UGM2? (well without logs). B Slightly undulous, subhorizontal stylolites, well 06-11-89-25W4 (626.5 m) LGM. C Sharp-peak to rectangular amplitude, well 15-23-68-01W5 (1108.60) UGM2. D Low-amplitude stylolites (seismographic type according to Park and Schot, 1968 classification), well 01-09-70-03W5 (1157.1 m) UGM3. Coin diameter is 1.85 cm.
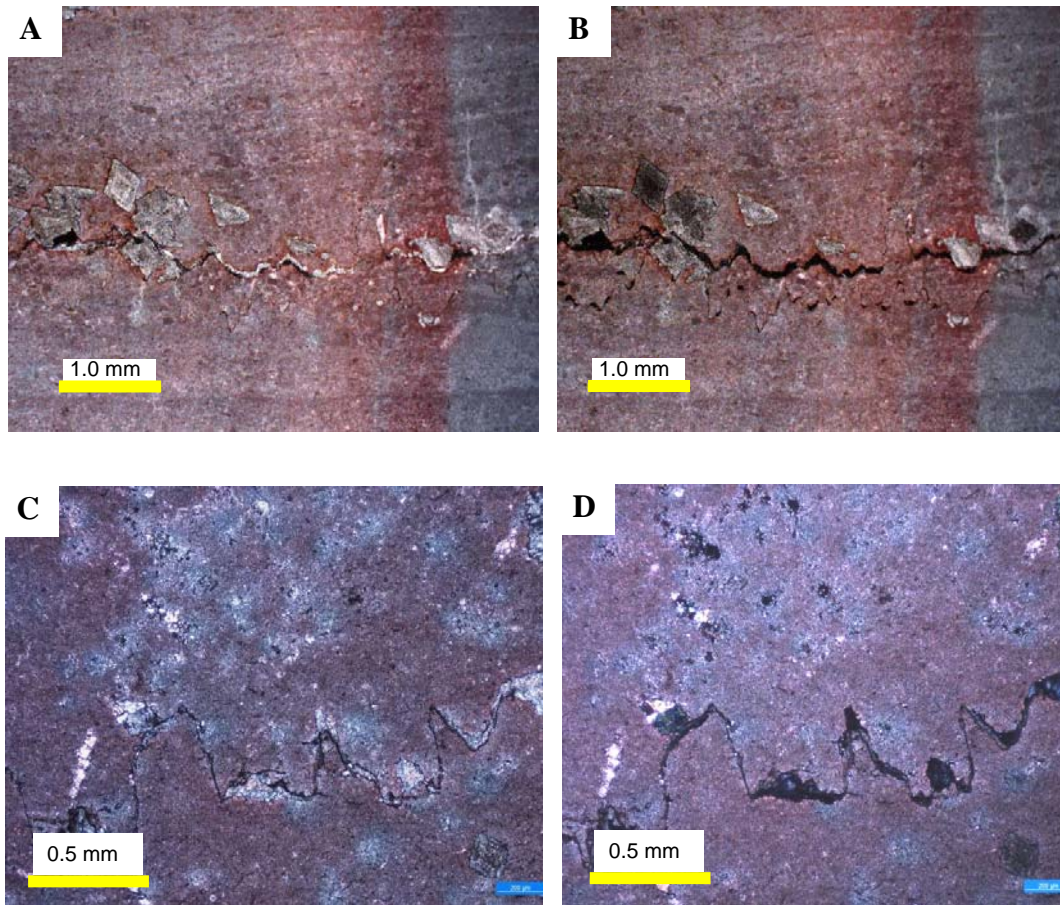
Figure 4.19 Microstylolites. Photomicrographs of thin sections. Stylolites are marked by concentrations of insoluble material along their irregular surfaces. A and C (plane polarized light); B and D (cross polarized light), well 01-09-70-03W5 (1155.8 m) UGM3.

Interpretation: Chemical compaction in the Grosmont occurred within intermediate burial settings. A considerable loss of thickness in the Hondo and the Grosmont Formation was inhibited by early dolomitization. Lucia (2004) demonstrated that dolostones are less susceptible to compaction than limestones, and this has been observed in the Grosmont Formation, where extensive compaction and loss of layer thickness appear to have been prevented by the presence of fairly early, pervasive, matrix dolomitization, which occurred during late Devonian or Mississipian times (Huebscher, 1996). A depth of 500 m for the

74

onset of chemical compaction was proposed by Lind (1993). Development of stylolites in the Grosmont Formation may have started during the Middle Mississippian and lasted until the Permian (Figure 4.2).

4.3.5 Gypsification

Some microfabrics suggest that anhydrite was re-hydrated to gypsum and later dehydrated again to anhydrite (see section 4.3.11). Rehydration to gypsum must have taken place during uplift in the time interval between the Pennsylvania and the Jurassic-Cretaceous, which led up to extensive karstification (Figure 4.2).

4.3.6 Dissolution-2, Karstification

Karstificaton of the Grosmont and Hondo was extensive and pervasive, and resulted in a number of distinctive features.

4.3.6.1 Brecciation:

Description: Brecciated zones and extensive dissolution are typical features in the eastern edge of the Grosmont platform. Karsted intervals are also referred to as "caves" from well logs and are present in townships 85 to 93 and ranges 16W4 to 25W4 (Dembicki, 1994). Dembicki (1994) used the term "caves" to include vugs, collapse breccias, large dissolution cavity zones, or a combination of these features. Huebscher (1996) identified two levels of enhanced "cave" formation that appear to be sub-horizontal and regionally correlatable.

In this study, breccias are identified in the upper members of the Grosmont close to the sub-Cretaceous erosional edge, as shown in Figure 4.20. There are at

least two types of breccias: dolostone matrix-supported breccias, and clasts and/or green shale supported breccias with large (centimetres) clasts, some clasts are oil impregnated.

4.3.6.2 Disintegrated dolomite

Description: Dissolution of dolomite has been observed also on the microscale. Luo and Machel (1995) used SEM-microscopy and concluded that the dolostones of the Grosmont have experienced three types of dissolution: intracrystal, intercrystal and pervasive.

In the cores analyzed, especially in Upper Grosmont 3 and 2 and towards the eastern part of the platform. Some intervals appear to have no mineralic rock matrix (Figure 4.21) but consist of disintegrated dolomite "cemented" by bitumen. In these intervals, bitumen is the supporting material containing disassociated dolomite crystals. Leaching of the bitumen with organic solvents yields a residue of fine-crystalline dolomite powder (Figure 4.21).

Interpretation: Most breccias in the upper units of the Grosmont Formation are interpreted to be postdepositional solution-collapse breccias. Extensive dissolution in the eastern part of the Grosmont platform likely occurred during Jurassic and Cretaceous times, when the Devonian strata were subaerially exposed.
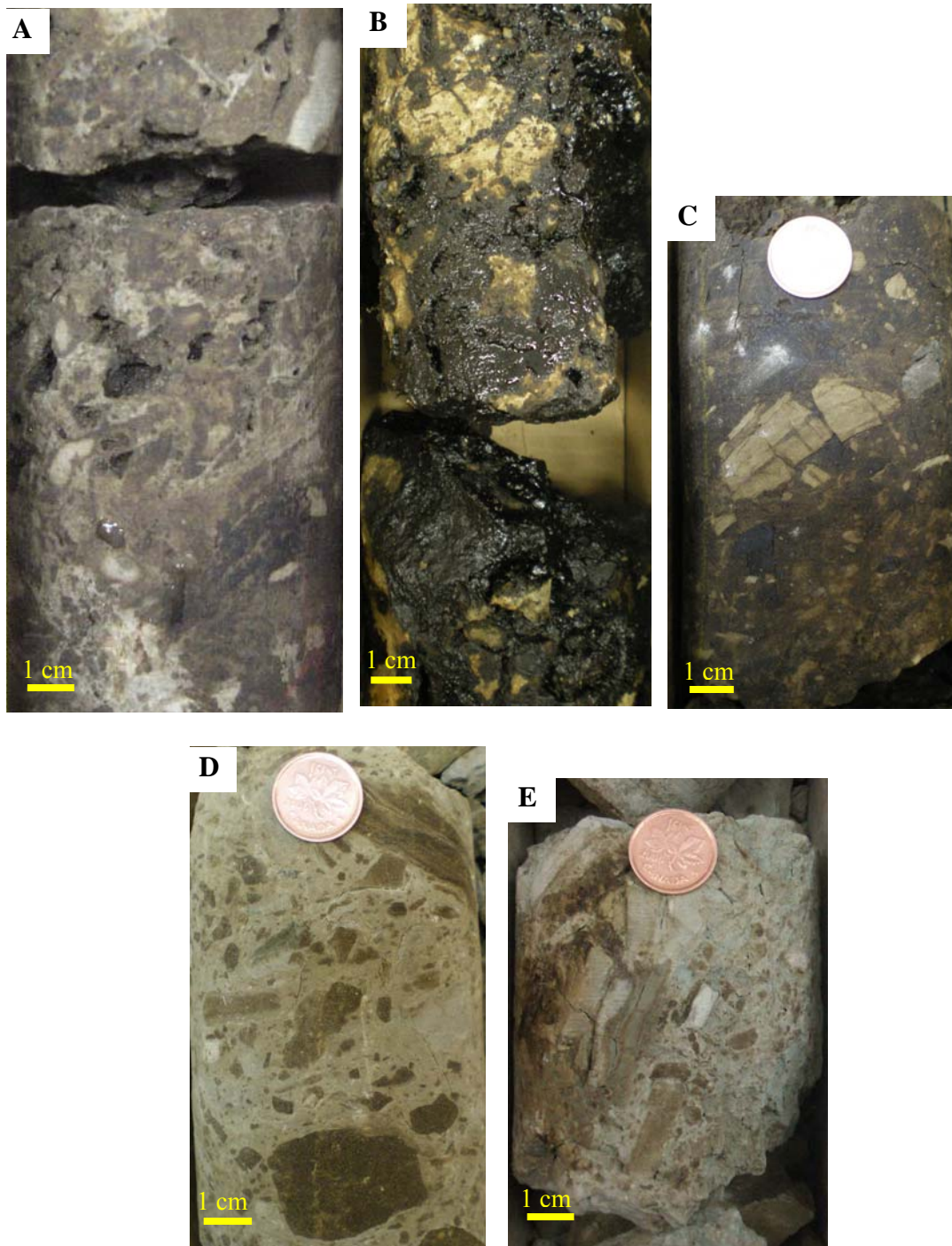
Figure 4.20 Core samples of breccias. A an B Dolostone matrix- supported breccias A well 06-10-77-25W4 (1053 m) B and C well 06-34-85-19W4m (383 m) and (328.5 m). Coin diameter 1.85 cm. D Green shale supported breccia, breccia with intraclasts of different sizes, some of them with oil impregnation, well 10-09-83-19W4 (374.5 m). E Green shale supported breccia, well 10-17-84-19W4 (359 m). Coin diameter 1.85 cm.
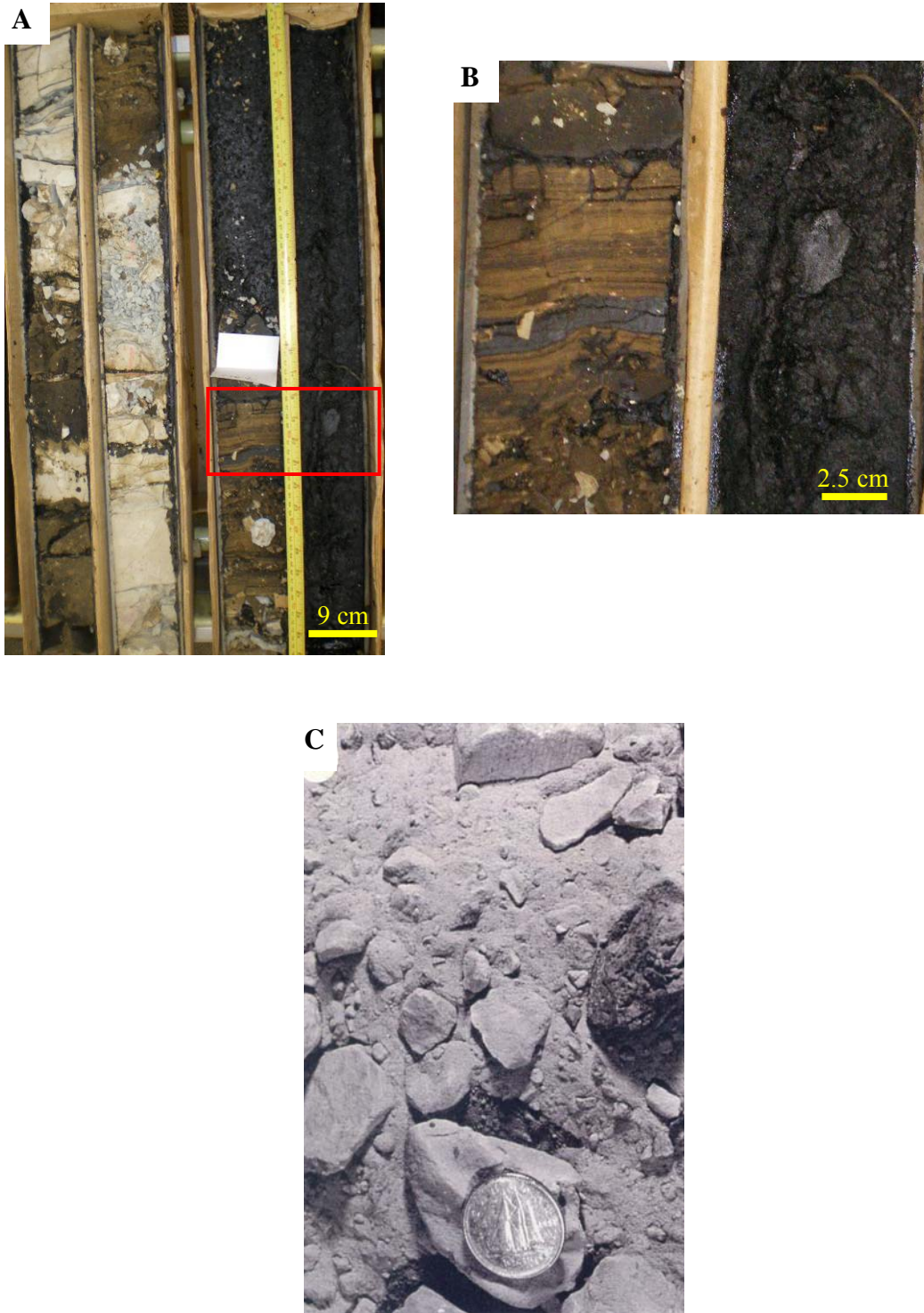
Figure 4.21 Cores samples of bitumen-supported dolomite intervals. A and B well 10-17-83-18W4 (355.4 m). C Dolomite powder, bitumen was leached from the sample, well 07-29-84-18W4 (355.0 m). Photograph C reproduced from Huebscher, 1996. Coin diameter is 2.3 cm.

This interpretation further implies that most of the sulphates in the eastern part of the Grosmont platform were dissolved by circulating meteoric waters. Some bitumen-supported intervals and breccias are present at the same stratigraphic level as the Hondo, however there is no direct physical evidence of Hondo sulphates in the east part of the Grosmont platform.

4.3.7 Dolomite Cementation

Cementation is the process of filling out open space, either of primary or secondary origin, with newly precipitated minerals (Scholle and Scholle, 2003). During burial, precipitation of minerals such as calcite, dolomite, or sulphates, is common when pore fluids are supersaturated with Ca^{2+}, Mg^{2+}, or SO_4^{2-} ions (Tucker and Wright, 1990). Capacity of fluid flow, temperature, and changes in chemistry of the fluids all influence the precipitation of cements.

There are two types of dolomite cementation in the Upper Grosmont 3: late dolomite cement and saddle dolomite.

4.3.7.1 Late dolomite cement

Description: Late dolomite cement was identified only in a thin section of well 08-16-87-01W5 at a depth of 892.2 m. The average size of dolomite crystals is 200 μm but the upper range is 500 μm; textures are planar-E and planar-C with zoned crystals (Figure 4.22). This type of dolomite is associated with saddle dolomite.
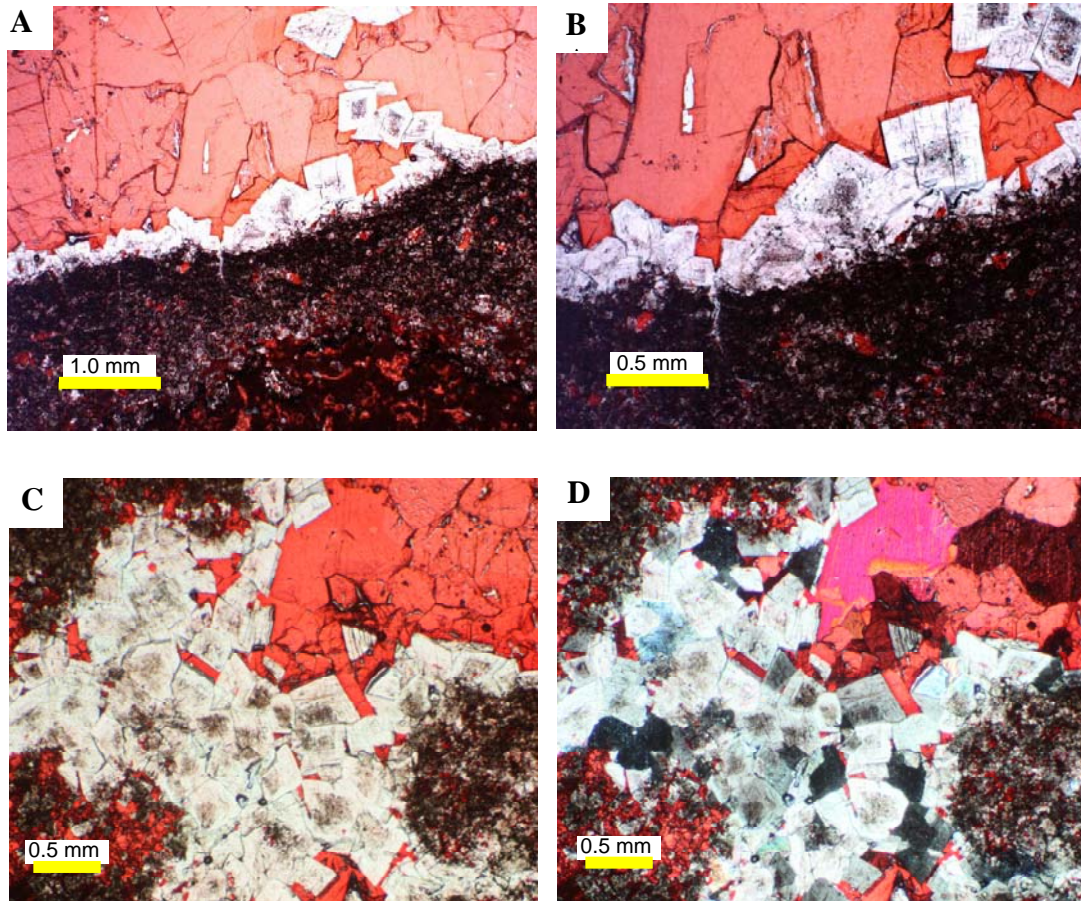
Figure 4.22 Photomicrographs of thin sections of late dolomite cement. Cement is filling secondary pores. A (plane polarized light) and B (cross polarized light) zonation in some dolomite crystals. C (plane polarized light) and D (cross polarized light) Well 08-16-87-01W5 (892.2 m) UGM3.

4.3.7.2 Saddle dolomite

Description: Saddle dolomite was identified in two wells: 08-16-87-01W5 (892.2 m) and 01-09-70-03W5 (1159.4 m) in the Upper Grosmont 3. Saddle dolomite is nonplanar, coarse-grained, curved crystals that display sweeping extinction in cross polarized light (Figure 4.23).

Interpretation: Saddle dolomite commonly precipitates in open pore spaces

at temperatures ranging from 80°C to 150°C by means of one of the following three mechanisms: (1) advection from igneous/metamorphic-basement fluids, (2) from local redistribution of preexisting dolomite during stylolitization and (3) by thermochemical sulphate reduction (TSR) in a closed system (Radke and Mathis, 1980; Machel, 1987; Machel and Lonnee, 2002).

The saddle dolomite found in the UGM3 probably formed by hot fluids passing up through fractures. Lack of core control in the area prevents a more precise interpretation. Fracturing in the basement of the Proterozoic may be have been activated.

4.3.8 Calcite Cementation and Replacement and fractures

4.3.8.1 Calcite cement

Description: Calcite cement is present within dolomudstone as millimetric crystals (<10 mm) filling cavities and vugs within all the Grosmont units (Figures 4.24 D, E and 4.25), as well as in rare narrow fractures that cross-cut saddle dolomite (Figure 4.23).

Interpretation: This type of calcite cementation is generally rare in the Grosmont. Its textures and paragenetic position, especially that it postdates saddle dolomite, suggest that if formed late diagenetically from either meteoric waters related to karstification or from warm burial fluids that ascended from deeper strata. A more precise determination of the nature of this type of cement is beyond the scope of this study.
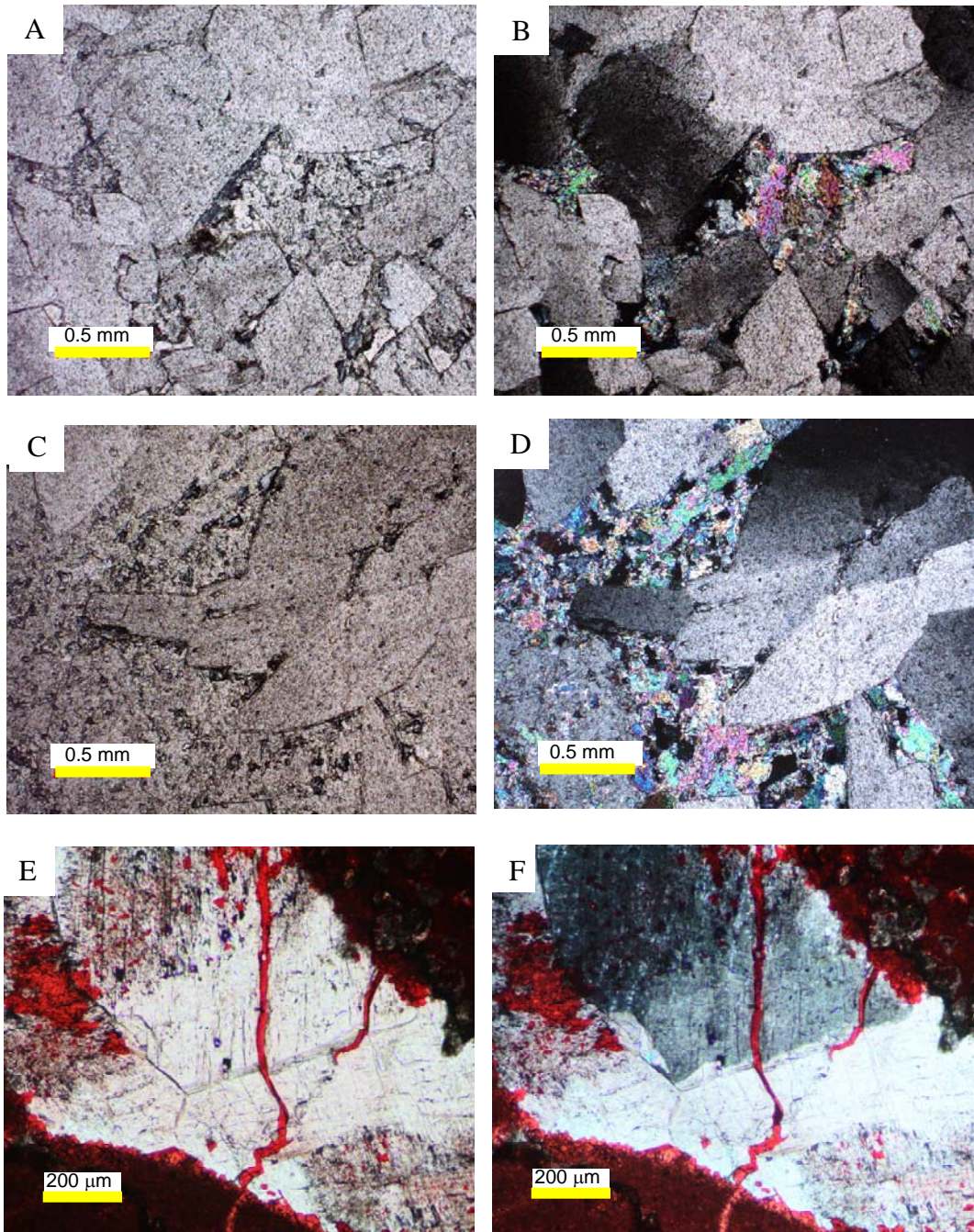
Figure 4.23 Photomicrographs of thin sections of saddle dolomite. A and C (plane polarized light); B and D (cross polarized light), anhydrite is present filling the remaining pore space, well 01-09-70-03W5 (1158.5 m) UGM3. E (plane polarized light) F (cross polarized light), fracture filled with calcite is cutting saddle dolomite crystals, well 08-16-87-01W5 (892.2 m) UGM3.
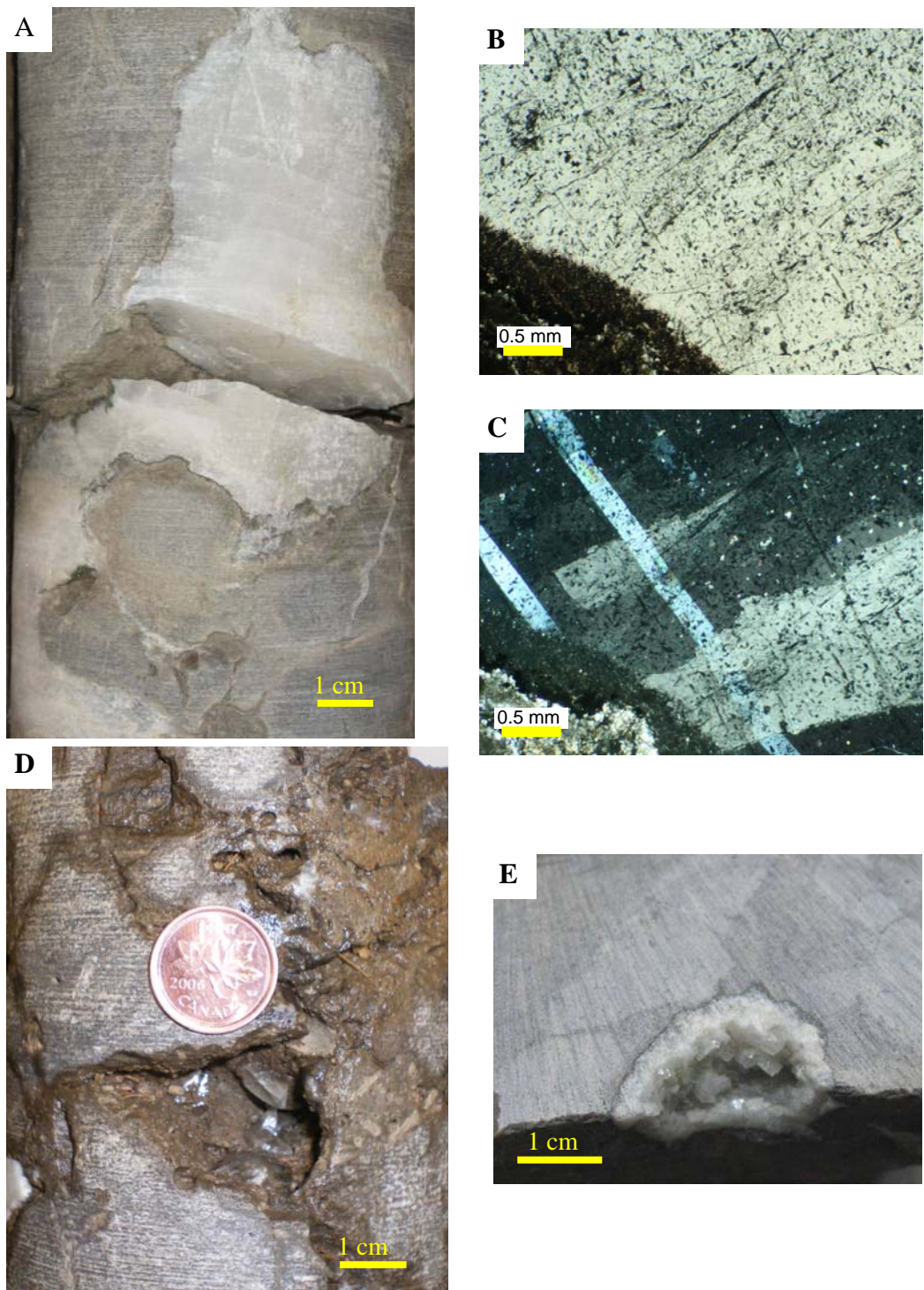
Figure 4.24 Late diagenetic calcite as a cement and as replacement. A Core showing calcite replacing dolomite. B and C photomicrographs of thin sections; A (plane polarized light) and C (cross polarized light), showing twin planes, well 11-35-70-25W4 (896.1m) Nisku-UIRE?. D and E Calcite crystals growing within vugs seen in cut core. D Well 10-35-73-04W5 (1120.55 m) UGM2. Coin diameter is 1.85 cm. E Well 05-25-69-20W4 (730.97 m) UGM1.
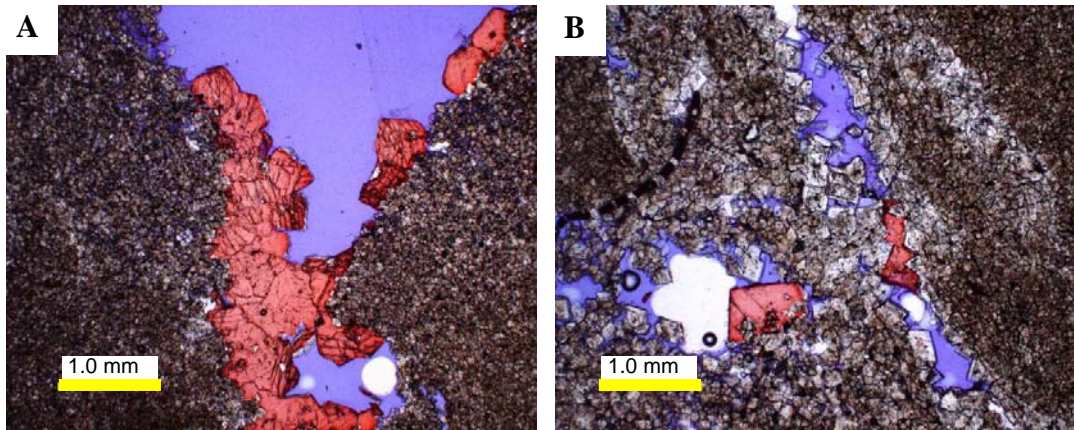
Figure 4.25 Photomicrographs of thin sections of blocky calcite cement growing in pores A and B (plane polarized light), well 13-01-91-05W5 (672.8 m) UGM3.

4.3.8.2 Calcite replacement and dedolomitization

The process of dissolution of dolomite and replacement by calcite is defined as dedolomitization/calcitization (Flügel, 1982).

Description: There is partial dedolomititization in the Grosmont Formation within dolomitized intervals, especially within Upper Grosmont 2 and Upper Grosmont 3 in the central area of the platform. Dolomudstones are the main lithology affected by calcitization. In hand specimen, calcites of this type can appear as massive replacive "blobs" (Figure 4.24 A). Under the microscope, the replacement of dolomite or anhydrite is shown by remnants of the precursor minerals embedded in the calcite (Figure 4.26). In some cases, calcite has corroded dolomite rhombs from the centre to the edge of the crystals.
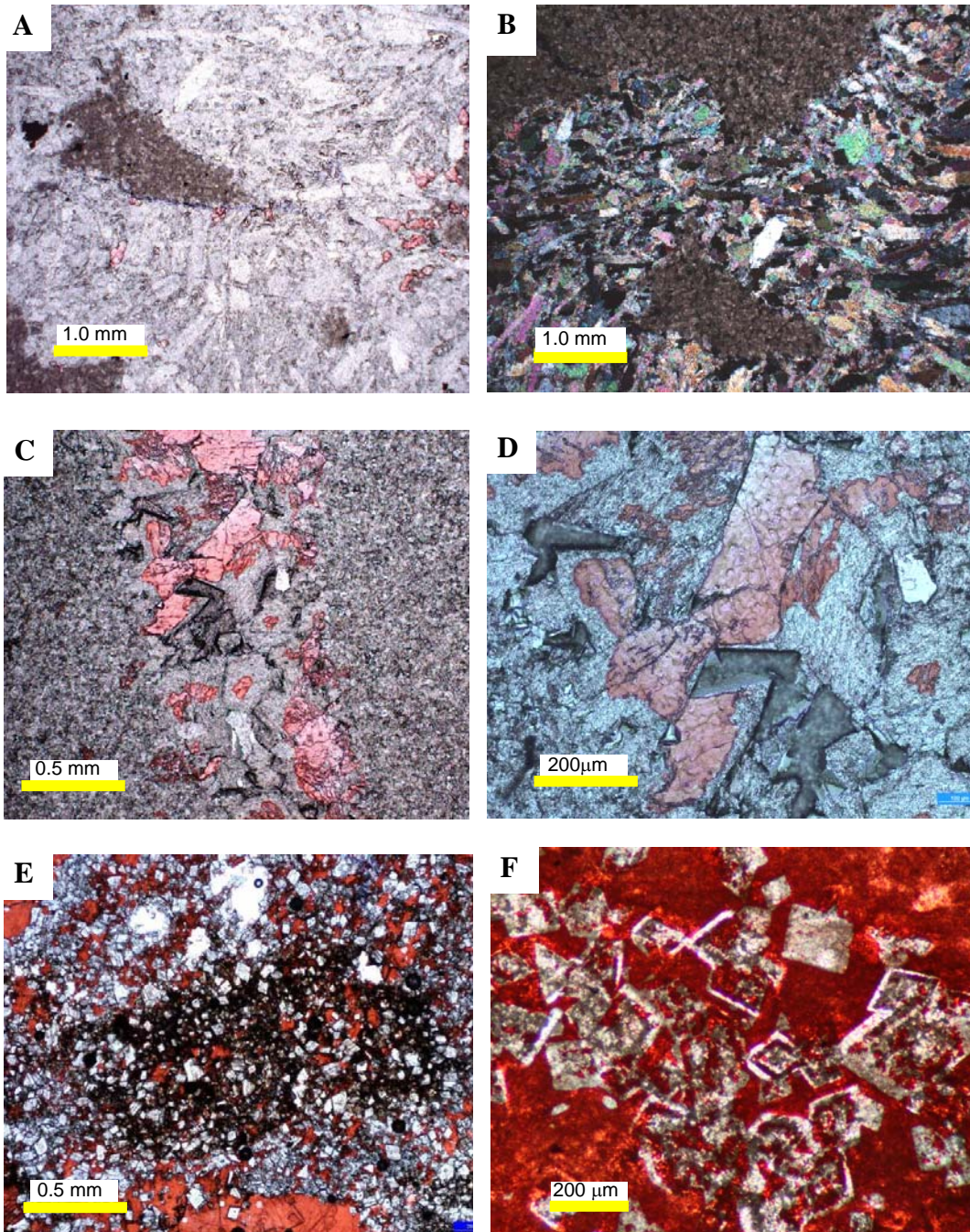
Figure 4.26 Photomicrographs of thin sections showing features of replacive calcite. A (plane polarized light), B (cross polarized light): calcite replacing anhydrite, well 01-09-70-03W5 (1159.4 m) UGM3. C and D (plane polarized light) calcite replacing zoned dolomite crystals, well 03-28-70-24W4 (859.25 m) UGM2. E Dedolomitization, presence of bitumen within intercrystal porosity, well 10-14-88-02W5 (719.5 m) Nisku. F Calcitization along core/rim interface, well 08-16-87-01W5 (892.2 m) UGM3.

Interpretation: Dedolomitization process is associated with the presence of waters enriched with Ca and within near-surface/shallow burial settings (De Groot 1967; Evamy, 1967; Warrak, 1974). In the Grosmont, dissolution of gypsum or anhydrite may have increased the Ca/Mg ratio and the amount of sulphate concentrates in pores. A reaction between sulphates and dolostones produces calcium carbonate which precipitates, and magnesium sulphate which is much more soluble and stays in solution (Sanz-Rubio et al., 2001). Thus, in a sulphate rich water phase, dolomite becomes unstable and dissolves, resulting in the precipitation of calcite. Sanz-Rubio et al. (2001) note that dolomite dissolution can be expressed chemically as:

$$CaMg(CO_3)_2 + CaSO_4 \ (aq) \longrightarrow 2CaCO_3 + Mg^{2+} + SO_4^{2-}$$

dolomite   gypsum   calcite
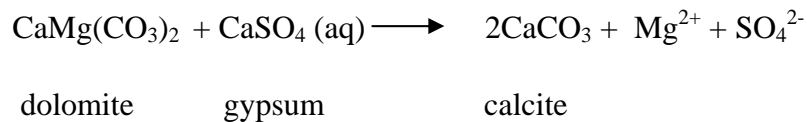
In this study, dedolomitization is interpreted to occur during/after subaerial exposure mediated by meteoric waters (*sensu* Huebscher, 1996).

4.3.8.3 Fracturing

A fracture is a nonsedimentary mechanical discontinuity within a rock produced by brittle failure and created by the stresses of compaction or tension.

Observation: Fractures in the Hondo cores are rare, with main fracture sets being vertical to subvertical and partially-to-totally filled calcite or anhydrite.

Fractures in the other Grosmont units are also linear and parallel, commonly with vertical-to-subvertical orientation, and are filled with calcite, anhydrite, or pyrite (Figures 4.23, 4.27, and 4.28). Dolomudstones and vuggy dolomudstones are the main lithologies that contain a high density of fractures. In the north-eastern part of the study area, close to the erosional edge, fractures in the Upper Grosmont 2 and 3 are filled with bitumen. Some fractures can be traced for 3 metres in core.
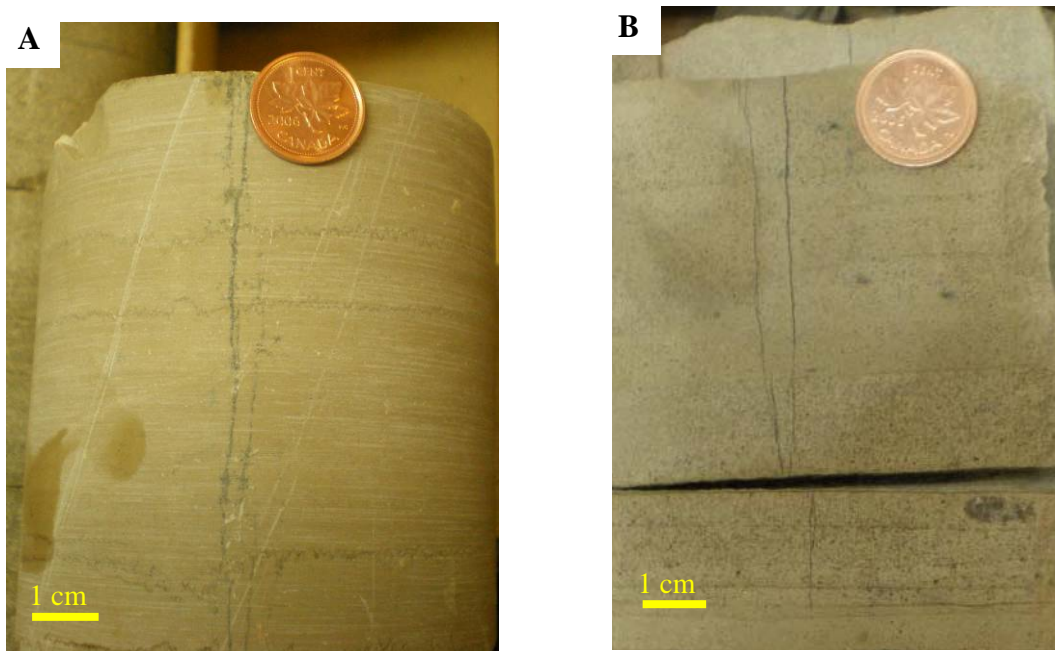
Figure 4.27 Core samples showing narrow vertical fractures within the Grosmont Formation. A Fracture filled with pyrite crossing horizontal low-amplitude stylolites, well 01-09-70-03W5 (1156 m) UGM3. B Vertical fracture partially filled with calcite, well 10-01-71-26W4 (975.80 m) UGM3. Coin diameter is 1.85 cm.
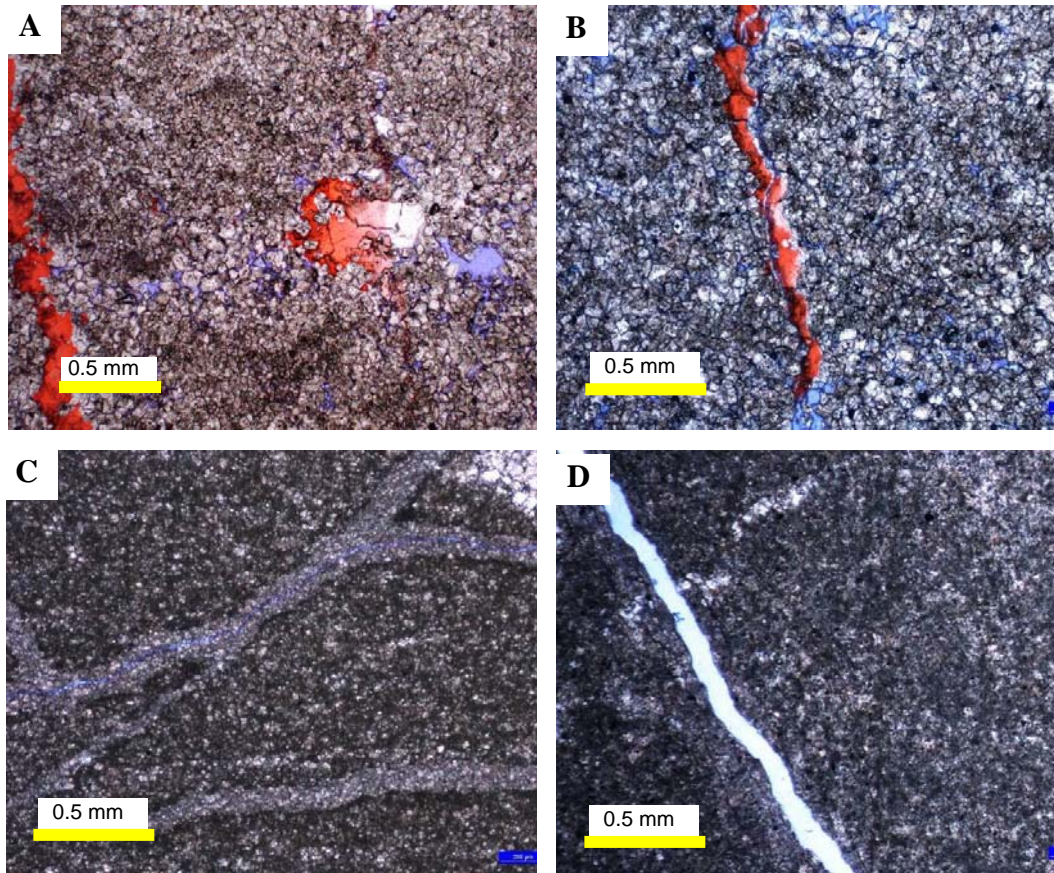
Figure 4.28 Photomicrographs of thin sections of microfractures. A and B Stained thin sections (plane polarized light) of calcite filling micro-fractures, well 03-28-70-24W4 (861.8 m) UGM2. C and D Thin sections (plane polarized light), well 10-14-88-02W5 (719.5 m) UIRE. C Rare anastomosing micro-fractures, partially open. D Open micro-fracture

Interpretation: Close to the sub-Cretaceous unconformity, the genesis of fractures of length > 1 m is most likely related to tectonic movements, a hypothesis supported by their parallel-set arrangement.

4.3.9 Anhydrite Cement

Description: Fractures of the type described in section 4.3.8 are also filled partially or totally with anhydrite. This type of anhydrite is euhedral to subhedral rhombohedral crystals (Figure 4.29).

Interpretation: Anhydrite cement laths formed most likely from re-distribution of primary or secondary anhydrite that had formed elsewhere in the Grosmont/Hondo during earlier diagenetic phases. The crystal habit (Figure 4.29) suggests formation directly as anhydrite (without a gypsum precursor) at depths in excess of 600 -1000 m (*sensu* Machel, 1993).

4.3.10 Oil Migration and Biodegradation

The oil is trapped as high viscosity bitumen in the eastern part of the Grosmont platform, close to the sub-Cretaceous erosional edge. In the cores analyzed in the southwestern part of the platform, encompassing most of the current study area, there is very little or no presence of bitumen within the Grosmont. Where present, bitumen occurs in all Grosmont facies but it is especially prevalent in areas where dissolution was pervasive as in karsted intervals but also in non-karsted intervals (Figure 4.30). The oil was transformed to low API by anaerobic biodegradation (Head et al., 2003; Larter et al., 2006) (most earlier studies had interpreted the biodegradation to be aerobic, e.g, Brooks et al., 1988). Biodegradation appears to affect the reservoir to this day at or near the surface and in the shallow subsurface (Hein et al., 2008). A rare product of biodegradation is elemental sulphur, formed sporadically in core (Figure 4.31).
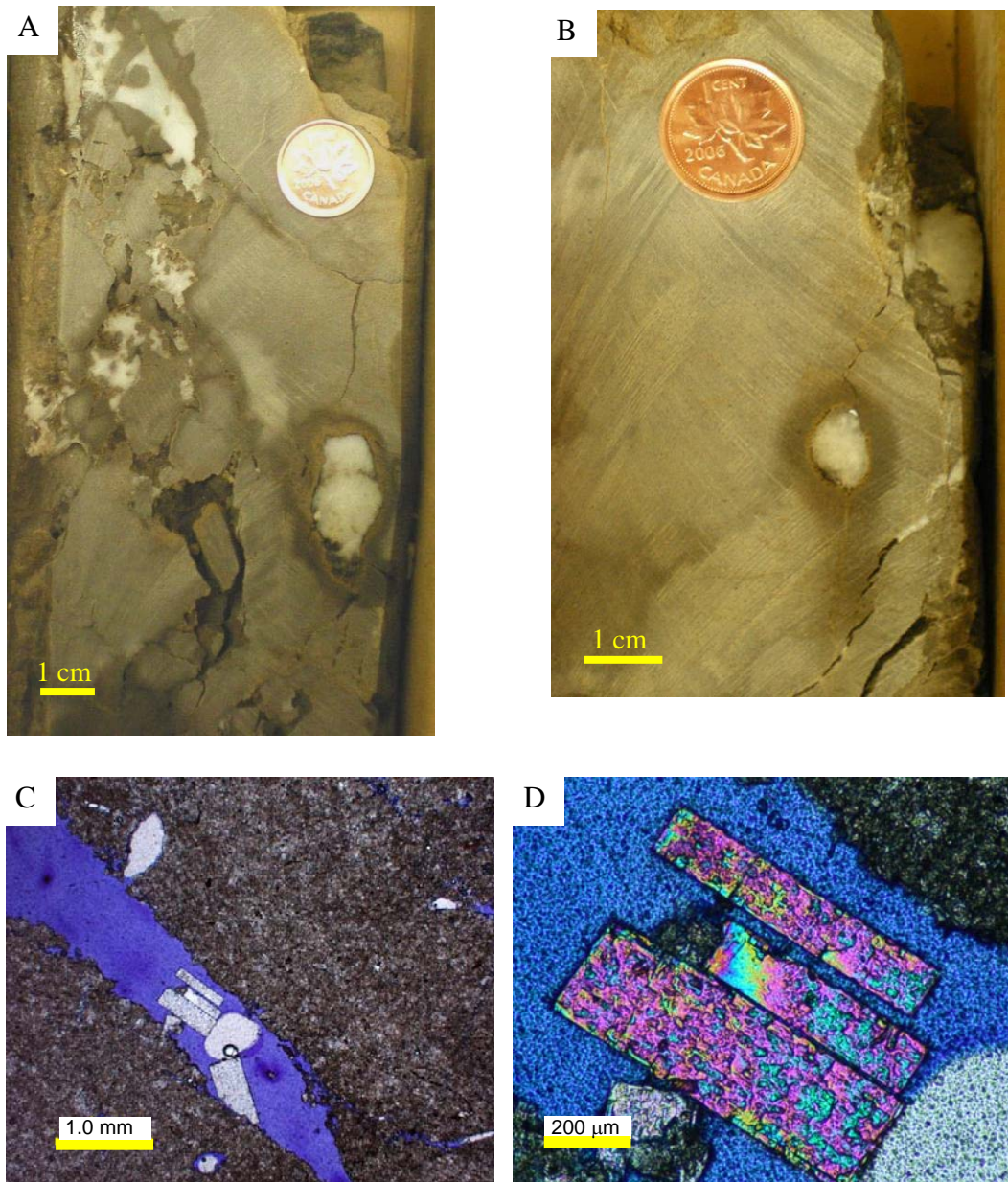
Figure 4.29 Late-diagenetic anhydrite cement. A.and B Core sample of fractures partially filled of anhydrite, well 10-35-73-04W5 (1117.50 m) and (1118.8 m) UGM2; diameter of coin is 1.85 cm. C and D Photomicrographs of thin sections, C (plane polarized light) D (cross polarized light) of anhydrite laths within a fracture, well 10-35-73-04W5 (1118.5 m) UGM2.
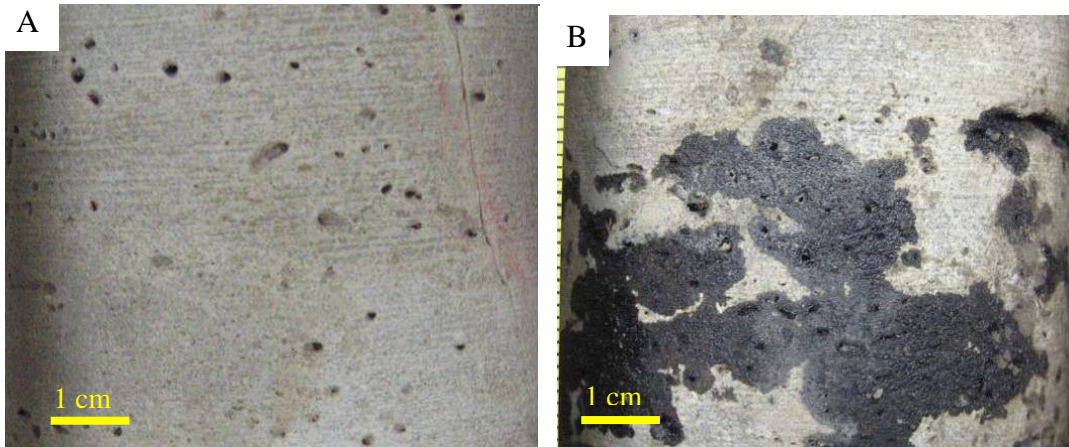
Figure 4.30 Core samples showing vuggy porosity in the Grosmont partially filled with bitumen. A vuggy porosity, B vuggy porosity partially filled with bitumen, well 06-11-89-25W4 (578.20 m) and (584.8 m) UGM2.

Figure 4.31 Sulphur on core surface, well 10-17-84-19W4 (499.6 m) LGM.

4.3.11 Gypsification

Description: Gypsum was positively identified in two wells, as recognized in hand specimen and verified by XRD (Figure 4.32). A few other samples show a mixture of anhydrite and gypsum, with anhydrite as the main component.

Interpretation: Gypsum is interpreted to have formed by rehydration of anhydrite during uplift and exhumation (see section 3.2). Meteoric waters probably penetrated the formation through fractures and partially transformed anhydrite to gypsum. The same process may have occurred after karstification. The presence of gypsum at depths greater than 600 m (see Figure 4.32 and 4.33) may indicate gypsification of previous anhydrite due to the presence of unusually high pressure in that well.

Figure 4.32 Core sample of gypsum nodule and dolomudstone, well 10-18-76-25W4 (1062.10 m) UGM3-UGM2.
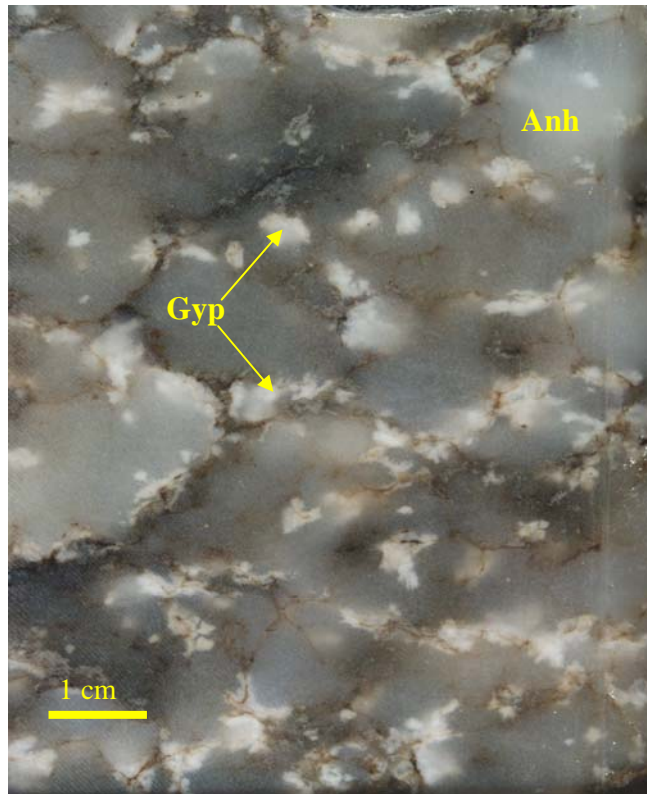
Figure 4.33 Replacive gypsum rosettes in mosaic anhydrite formed during uplift and partial rehydration, well 10-17-84-19W4 (501.00 m) LGM.

4.4 Summary and Conclusions

Diagenetic processes have prominently changed the original fabrics, component compositions, and petrophysical characteristics in the Grosmont and the Hondo. The most important processes that affected the Hondo and Grosmont were dolomitization, dissolution, anhydritization, chemical compaction/stylolitization and fracturing, dolomite dissolution, dolomite cementation, calcite cementation, oil migration, and gypsification.

Dolomitization occurred in more than one phase and had variable effects on porosity and permeability. In some cases dolomitization increased intercrystal

porosity but in some areas the growth of crystals led to the occlusion of pores and decrease of the reservoir quality.

Anhydritization occurred with increasing depth of burial while gypsification may have occurred during uplift and when meteoric waters entered the platform. The primary sulphates originally may have formed widespread seals that were largely removed due to later dissolution. In the central and southwestern parts of the study area, the presence of Hondo sulphates of primary or secondary origin reduces the reservoir quality in the entire Grosmont Formation. In the eastern part of the platform, dissolution appears to be more pervasive than in the southwestern part; consistent with meteoric water input from the east. "Bitumen supported" and brecciated zones are presently widespread in the Upper Grosmont members. These intervals represent areas with high porosity and bitumen saturation and are partly in the same stratigraphic level as the Hondo primary sulphates.

Stylolites are common in the Grosmont Formation, mainly in the Lower Grosmont and Upper Grosmont 3. Molds and vugs, formed by dissolution of calcite or anhydrite, are interconnected by fractures. An increase in permeability caused by fracturing is questionable in the south-central part of the area because of cementation of the fractures. However, in the northeastern part of the study area fractures play an important role in enhancing vertical permeability. These fractures may have formed during the Laramide orogeny, enhancing migration of oil.

CHAPTER 5

GEOCHEMISTRY

5.1 Introduction

Geochemical methods, such as stable isotope analyses of C, O, S, and Sr, were applied to anhydrite, gypsum, dolomite, and calcite samples. The aim of these analyses is to better understand the history of the sediments, the nature, and timing of the various diagenetic fluids. The overall scope of these geochemical investigations is limited, as the main focus of this thesis is on other aspects (see Chapter 1).

5.2 Methods

Samples were chosen following petrographic analysis. Anhydrite, gypsum, and dolomite from the Hondo, dolomite and calcite from the other Grosmont units were sampled for geochemical analysis. Sample extraction was carried out using a low speed micro-drill with tungsten carbide and diamond bits. The resulting fine powder samples, less than 50 μm in size and approximately 15 mg, were used to measure C, O, and S, and approximately 25 mg was used to measure Sr.

5.2.1 Carbon and Oxygen isotopes

A total of eight samples of dolomite and calcite matrix, and calcite (calcite crystals, filling voids and/or in veins) were analyzed for carbon and oxygen isotopes. The analyses were run at the Isotope Science Laboratory at the

University of Calgary. The following description of the carbon and oxygen isotope procedure is taken from Isotope science laboratory-guide, Department of physics and astronomy, university of Calgary (2010). Powdered samples were digested with anhydrous phosphoric acid in a Y tube reaction vessel at 25°C for about 4 hours; samples containing both calcite and dolomite were subjected to chemical separation techniques, as described by Al-Aasm et al. (1990). The evolved CO_2 gas was cryogenically distilled from the reaction vessel. CO_2 was analyzed for the $^{13}C/^{12}C$ ratio using a VG 903 isotope mass spectrometer. O and C isotope data are reported in per mil notation (‰), relative to the international Vienna Peedee Belemnitella (VPDB) standard. Internal laboratory standards were run at the beginning and end of each set of samples and used to normalize the data as well as to correct for instrument drift. Precision and reproducibility were ±0.2 per mil for both $\delta^{18}O$ and $\delta^{13}C$.

5.2.2 Sulphur isotopes

A total of eight samples of primary and secondary sulphates were analyzed for their sulphur isotope composition at the Isotope Science Laboratory at the Department of Physics and Astronomy at the University of Calgary. The following sulphur isotope procedure is taken from the Isotope science laboratory-guide, Department of physics and astronomy, University of Calgary (2010). Sulphur isotope ratios ($^{34}S/^{32}S$) were measured using continuous flow-isotope ratio mass spectrometry (CF-EA-IRMS). Instrumentation was comprised of a Carlo Erba NA 1500 elemental analyzer interfaced with a VG PRISM II mass

spectrometer. Samples were weighed in high purity tin cups, then dropped into the high temperature EA combustion reactor (the combustion furnace of the EA was maintained at a temperature of 1020°C). A carrier gas (UHP He) swept the gaseous pyrolysis products through a gas chromatography (GC) column allowing SO_2 to separate from CO_2. Then, the SO_2 was introduced via an open split/interface to the ion source of the mass spectrometer. Ion currents of masses 64, 65, and 66 were measured simultaneously. The $^{34}S/^{32}S$ ratio of the sample gas was compared to that of a standard SO_2 reference gas (ISL S102). Results are presented in per mil notation relative to the international Vienna Canyon Diablo Troilite (VCDT) standard. Precision of measurements was ±0.25 per mil.

5.2.3 Strontium isotopes

Fiveteen samples from Hondo sulphates and Upper Grosmont units were analyzed for strontium (Sr) isotope ratios. Seven of the samples were anhydrite, one was a mix of anhydrite and gypsum, four were calcite, and three were mixes of calcite and dolomite. The samples were processed on a VG 354 thermal ionization mass spectrometer (TIMS) at the Radiogenic Isotope Laboratory of the University of Alberta. Values for $^{87}Sr/^{86}Sr$ were corrected to the NBS 987 STD and the value for repeated runs was 0.710245. Analytical precision on individual runs had an average of 1.67×10^{-6} (2σ).

5.3 Carbon and Oxygen Isotopes

The carbon and oxygen isotope data of this thesis are interpreted according to generally recognized principles, as summarized in numerous text books and technical reports, e.g. Tucker and Wright (1990), chapter 6.

Carbon isotopic compositions have been determined for various sedimentary reservoirs (Figure 5.1) and these values are commonly applied both in the analysis of secular changes and in the redox condition of ocean chemistry (Land, 1980). Stable isotopic curves for the Paleozoic time have been drawn for the average $\delta^{13}C$ of limestones in a given period of time (Keith and Weber, 1964; Garrels and Perry, 1974; Veizer et al., 1980); however, isotopic curves do not resolve shorter excursions in ocean geochemistry (Arthur et al., 1983).
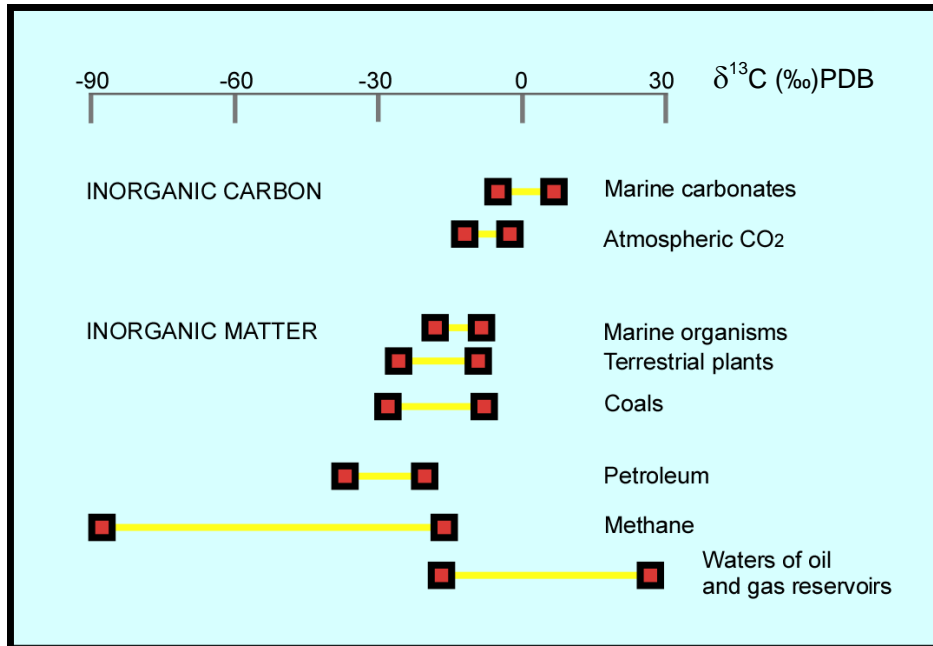
Figure 5.1 $\delta^{13}C$ values in various natural carbon reservoirs (modified from Pierre, 1994).

Reference scales generally correspond to those defined in large natural reservoirs with constant stable isotopes (Pierre, 1994). For ^{18}O and ^{13}C the reference is normally the VPDB (Pee Dee Belemnitella) standard which corresponds to the calcite of the rostrum of a belemnite of the Pee Dee Formation from the Upper Cretaceous in South Carolina (Craig, 1957). Oxygen is reported with reference to the Standard Mean Ocean Water (SMOW) defined by Craig (1957). A relationship between the SMOW and the VPDB standard was established by Craig (1961) for calcite as:

$$\delta^{18}O \text{ (calcite SMOW)} = 1.03086 \ \delta^{18}O \text{ (calcite VPDB)} + 30.86 \qquad (1)$$

According to Hays and Grossman (1991), it is possible to estimate the calcite paleotemperature (T) based on meteoric calcite values using the $\delta^{18}O_c$ ($_c$= Calcite), relative to VPDB and $\delta^{18}O_W$, relative to SMOW, by using the following equations based on O'Neil et al. (1969):

$$T \text{ (°C)} = 15.7 - 4.36 \ (\delta^{18}O_c - \delta^{18}O_w) + 0.12 \ (\delta^{18}O_c - \delta^{18}O_w)^2 \qquad (2)$$

5.3.1 Dolomite Isotopes

Isotopic data from dolomites have proven useful in the interpretation of their geologic history (Land, 1983). Most of the data on recent sedimentary dolomites show that the oxygen isotopic fractionation between dolomite and water is higher by about 3 to 4% than the fractionation of calcium carbonate and

99

water (Clayton et al., 1968; Land, 1980). The most commonly used fractionation equation for the dolomite-water equilibrium according to Land (1983) is:

$$10^3 \ln \alpha_{\text{dolomite-water}} = 3.2 \times 10^6 T^{-2} - 3.3 \qquad (3)$$

During diagenesis, modifications in temperature, chemical composition, pH, and partial pressure of CO_2 in the pore waters cause isotopic reequilibration. Isotopes of carbon are related to the total dissolved inorganic carbon (CO_2, HCO_3, CO_3^{2-}, H_2CO_3). The isotopic composition of ^{13}C in dolomite is strongly influenced by the composition of the precursor. Therefore, the $\delta^{13}C$ value of calcium carbonate being dolomitized is commonly retained by the dolomite (Tucker and Wright., 1990). Dolomite rocks associated with hypersaline environments are sometimes slightly enriched in ^{13}C (Pierre, 1994).

5.4 Sulphur Isotopes

The sulphur isotope values of various natural sulphur reservoirs are shown in Figure 5.2. Seawater sulphates represent one of the main natural reservoirs of dissolved sulphur (Payton et al., 1998). Sulphur has four stable isotopes: ^{32}S (95.02%), ^{33}S (0.75%), ^{34}S (4.21%), and ^{36}S (0.02%). Isotopic compositions are reported as ratios of $^{34}S/^{32}S$ in ‰ relative to the Vienna Canyon Diablo Troilite (VCDT) standard (Coplen and Krouse, 1998). Values of $\delta^{18}O$ and $\delta^{34}S$ for gypsum and anhydrite, precipitated from modern oceanic waters, are close to 13 ‰ and 21.5 ‰, respectively (Pierre, 1994).

These values have varied systematically over geologic times, and there are secular isotope trends for both $\delta^{18}O$ and $\delta^{34}S$ of marine sulphates that serve as reference values for studies of provenance and diagenesis (Holser et al., 1979; Claypool et al., 1980). Late Devonian seawaters sulphate had $\delta^{18}O$ $\approx$+14‰SMOW and $\delta^{34}S$ $\approx$+25‰ VCDT (Claypool et al., 1980).
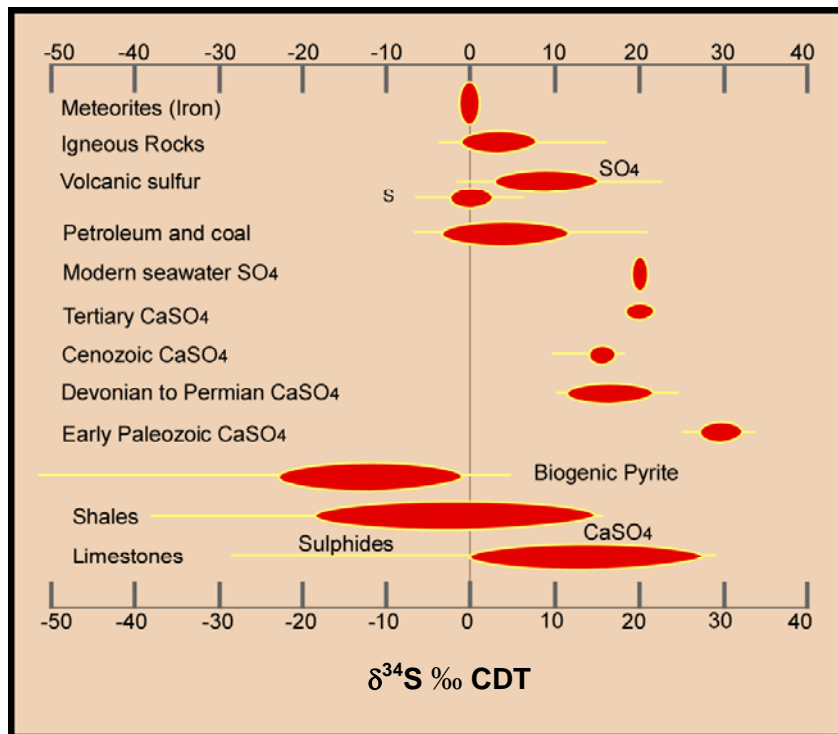
Figure 5.2 $\delta^{34}S$ ranges of various systems and selected water sulphates (modified from Pierre, 1994).

5.5 Radiogenic Strontium Isotopes

Strontium is the most abundant trace element in carbonate sediments and carbonate rocks. Strontium is the ninth most abundant component in seawater (Land, 1983). Strontium has four stable isotopes: ^{88}Sr, ^{87}Sr, ^{86}Sr, and ^{84}Sr. Among them, ^{88}Sr, ^{86}Sr, and ^{84}Sr are not radiogenic, whereas ^{87}Sr is generated by the decay of ^{87}Rb.

The strontium isotope composition of a rock thus depends on the initial Rb/Sr ratio and age, which is the basis of the Rb-Sr method of radiometric dating (Tucker and Wright, 1990). Heavy isotopes like strontium (masses 86, 87, and 88) do not fractionate in the same way as light isotopes such as oxygen and carbon. The mass difference between ^{86}Sr and ^{88}Sr is not high enough to fractionate the two isotopes during mineral precipitation or recrystallization; thus, the minerals (in this case anhydrite, calcite, or dolomite) conserve the same isotopic ratio as the fluid from which they precipitate (Pierre and Fontes, 1978).

The ^{87}Sr/^{86}Sr ratio of seawater has varied during geological time (Veizer et al., 1999; Veizer and Compston, 1974; Brass, 1976; Burke et al., 1982). The constructed curve shows that during the Phanerozoic, the ^{87}Sr/^{86}Sr seawater ratio fluctuated significantly (Figure 5.3). Values of ^{87}Sr/^{86}Sr ranging from 0.7078 to 0.7082 are suggested for Middle Devonian seawater (Veizer et al., 1999). Carbonates that interacted with basinal fluids during burial from the Western Canada Sedimentary Basin are reported to have higher radiogenic ^{87}Sr/^{86}Sr ratios than the coeval marine carbonates in the basin (Mountjoy et al., 1992). Machel and Cavell (1999) introduced the term MASIRBAS (maximum Sr isotope ratio of basinal shales) to define the regional background of strontium isotope values of basinal shales under normal subsurface diagenetic conditions. In the Western Canada Sedimentary Basin, the value calculated for MASIRBAS is 0.7120. Carbonate cements with ^{87}Sr/^{86}Sr ratios > 0.7120 are likely to have been formed from a metamorphic or extrabasinal component, whereas ^{87}Sr/^{86}Sr ratios < 0.7120 are likely to have been formed intrabasinally without fluids that had interactions

with metamorphic rocks. When these values were compared with literature data (Connolly et al., 1990; Armstrong et al., 1998), the MASIRBAS is valid for the entire stratigraphic section from the Pleistocene glacial till to the Middle Devonian, and probably for the Cambrian as well (Machel and Cavell, 1999).
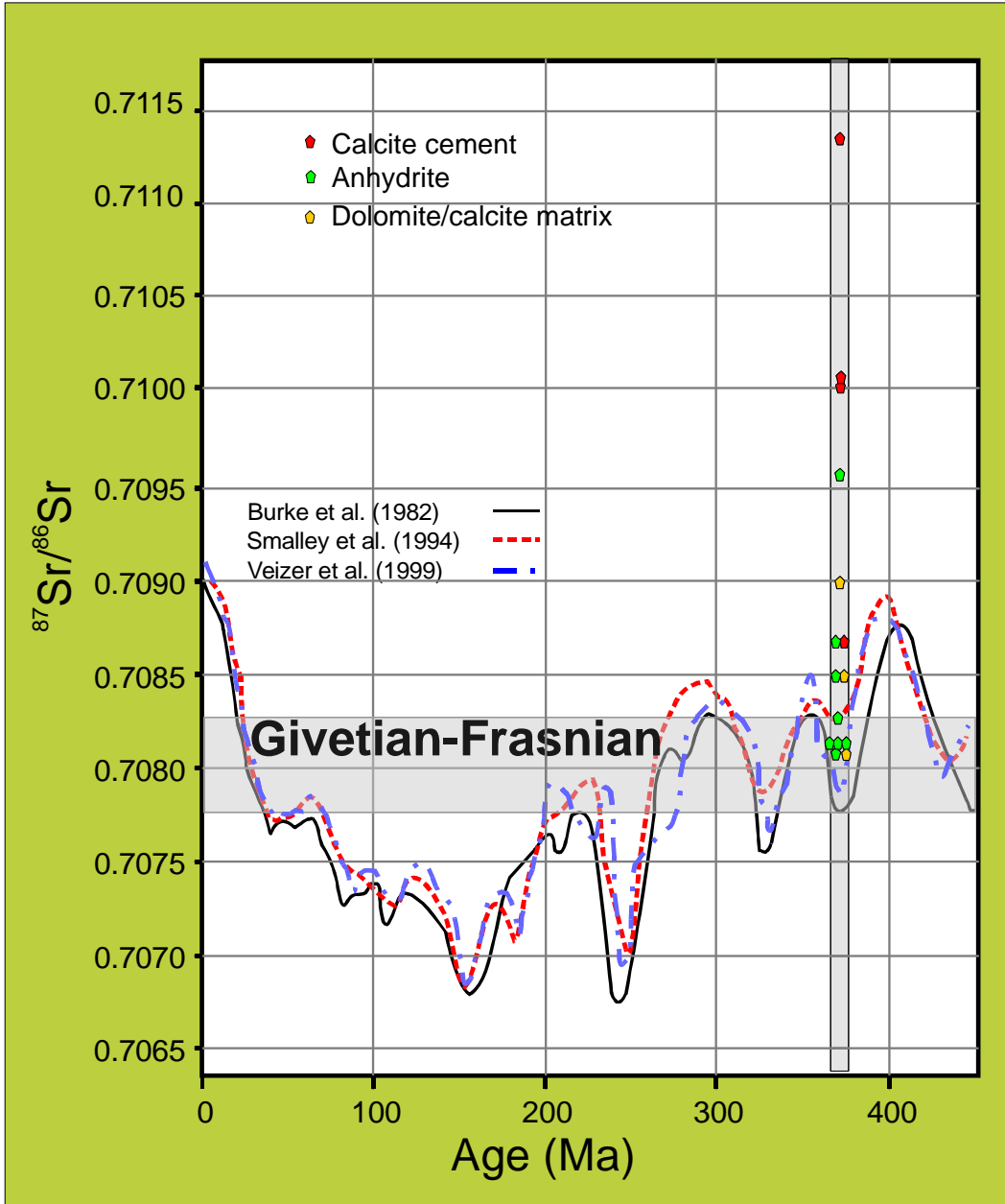
Figure 5.3 Secular variation curve of $^{87}Sr/^{86}Sr$ ratios during the Phanerozoic. Width of bar from ~ 385 to 375 m.y represents stratigraphic range of Grosmont-Hondo deposition. (modified from Veizer et al., 1999).

5.6 Geochemical Results

5.6.1 Carbon and Oxygen

The following is a summary of the carbon and oxygen isotopic compositional findings for the Hondo sulphates and Grosmont Formation in the study area (Table 5.1).

1. Matrix dolomite (n = 4) yielded $\delta^{18}O$ values from -7.2 to -6.2 ‰ VPDB, and $\delta^{13}C$ values from 0.7 to 2.7 ‰ VPDB.

2. Matrix calcite (n = 4) yielded $\delta^{18}O$ values from -8.2 to -5.9 ‰ VPDB, and $\delta^{13}C$ values from 0.07 to 1.18 ‰ VPDB.

3. Calcite cement and calcite crystals (n = 4) yielded $\delta^{18}O$ values from -12.1 to -11.5 ‰ VPDB, and $\delta^{13}C$ values from -13.3 to -2.0 ‰ VPDB.

$\delta^{18}O$ and $\delta^{13}C$ values for the Grosmont samples values are plotted in Figures 5.4, 5.5, and 5.6.

WELL	UNIT	DEPTH (m)	$\delta^{13}C_{cal}$ (‰)	$\delta^{18}O_{cal}$ (‰)	$\delta^{13}C_{dol}$ (‰)	$\delta^{18}O_{dol}$ (‰)	COMMENTS
10-35-73-04W5	UGM2	1120.5	-12.4	-11.5			Calcite crystals in vugs
08-16-87-01W5	UGM3?	892.2	-13.3	-11.6			Calcite filling vugs
03-28-70-24W4	UGM2	855.7	-6.9	-12.0			Calcite crystals
11-35-70-25W4	UIRE	895.05	-2.0	-12.1			Calcite filling (fracture-vein)
15-17-71-25W4	HONDO	890.1	not enough CO2 generated				Dolomite+anhydrite, matrix
01-09-70-03W5	HONDO	1157.3	1.18	-7.7	2.7	-7.2	Dolomite+calcite, matrix
08-16-87-01W5	UGM2	892.2	0.07	-8.2	0.7	-6.2	Dolomite+calcite, matrix
15-23-69-01W5	UGM3	1120	1.51	-5.9	1.3	-6.2	Dolomite+calcite, matrix

Table 5.1 Samples analyzed for carbon and oxygen isotopes. Values of $\delta^{13}C$ and $\delta^{18}O$ for calcite and dolomite. $\delta^{13}C$ and $\delta^{18}O$ in VPDB ‰.
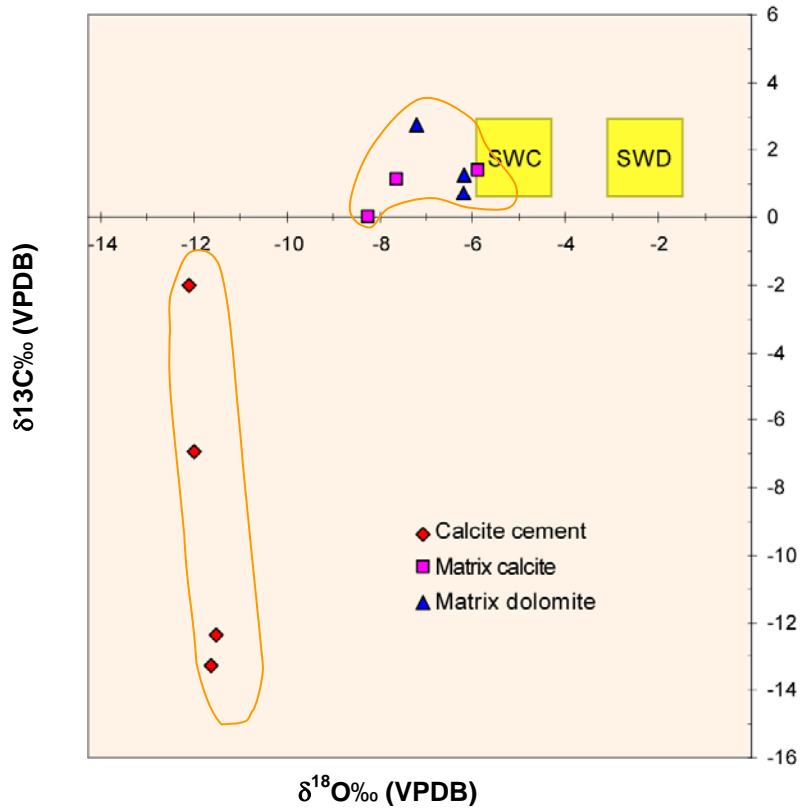
Figure 5.4 Stable isotopes $\delta^{18}O$ versus $\delta^{13}C$ composition of the Hondo, UGM3, and UGM2. Seawater equilibrated calcite (SWC), seawater-equilibrated dolomite (SWD) for the Devonian.
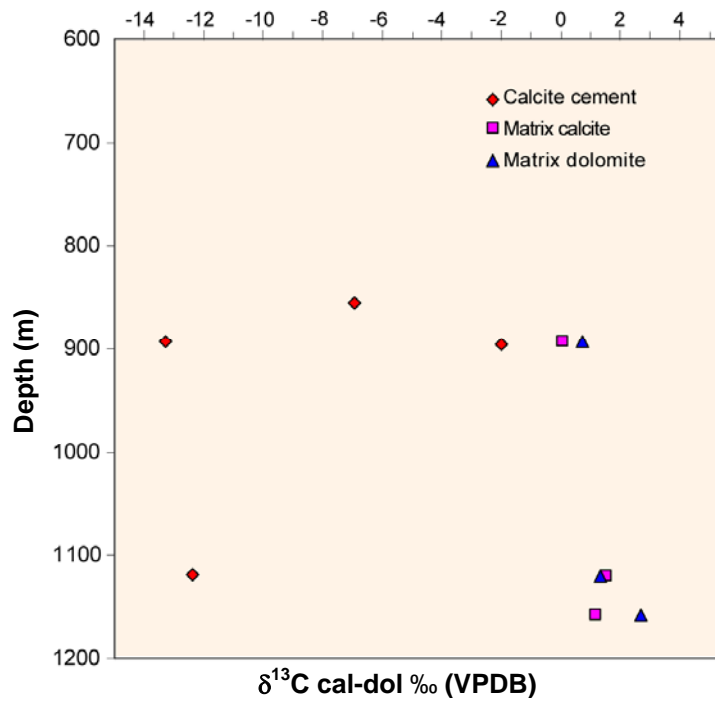
Figure 5.5 $\delta^{13}C$ composition versus depth for samples from the Upper Grosmont 3 and Upper Grosmont 2.
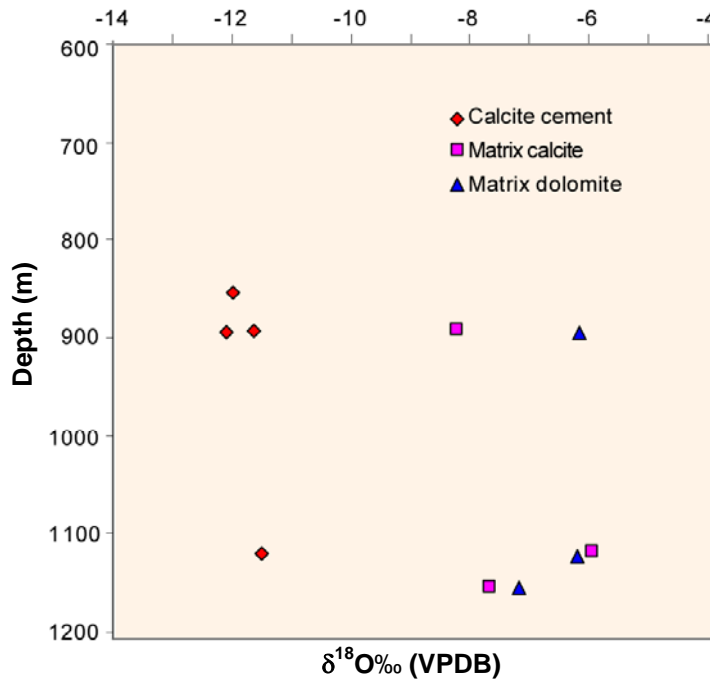
Figure 5.6 δ^{18}O composition versus depth for samples from the Upper Grosmont 3 and Upper Grosmont 2.

5.6.2 Sulphur

Hondo sulphates yielded values from 23.7 to 27.4 2 ‰ VCDT for δ^{34}S and 14.9 to 16.6 ‰ SMOW for δ^{18}O (Table 5.2). Values are plotted in Figures 5.7 and 5.8.

WELL	UNIT	DEPTH (m)	δ^{34}S (‰)	δ^{18}O (‰)	%O	COMMENTS
15-17-71-25W4	HONDO	910.70	27.4	15.0	27	Anhydrite -mosaic
15-17-71-25W4	HONDO	913.5	27.4	16.6	28	Anhydrite-bedded
10-35-73-04W5	UGM2	1118.5	23.7	14.3	26	Anhydrite-nodules
02-30-79-04W5	UGM3	1068.5	26.6	15.9	26	Anhydrite and Gypsum
08-16-87-01W5	UGM3	751.03	27.3	15.0	26	Anhydrite
08-28-69-04W5	UGM2	1314.25	25.0	16.3	27	Anhydrite-nodule
15-23-69-01W5	UGM3	1111.5	27.9	14.9	26	Anhydrite-bedded
15-23-69-01W5	UGM3	1120	26.3	15.5	27	Anhydrite+pyrite-

Table 5.2 δ^{34}S and δ^{18}O of Hondo sulphates. δ^{34}S in VCDT ‰ and δ^{18}O in ‰ SMOW

106
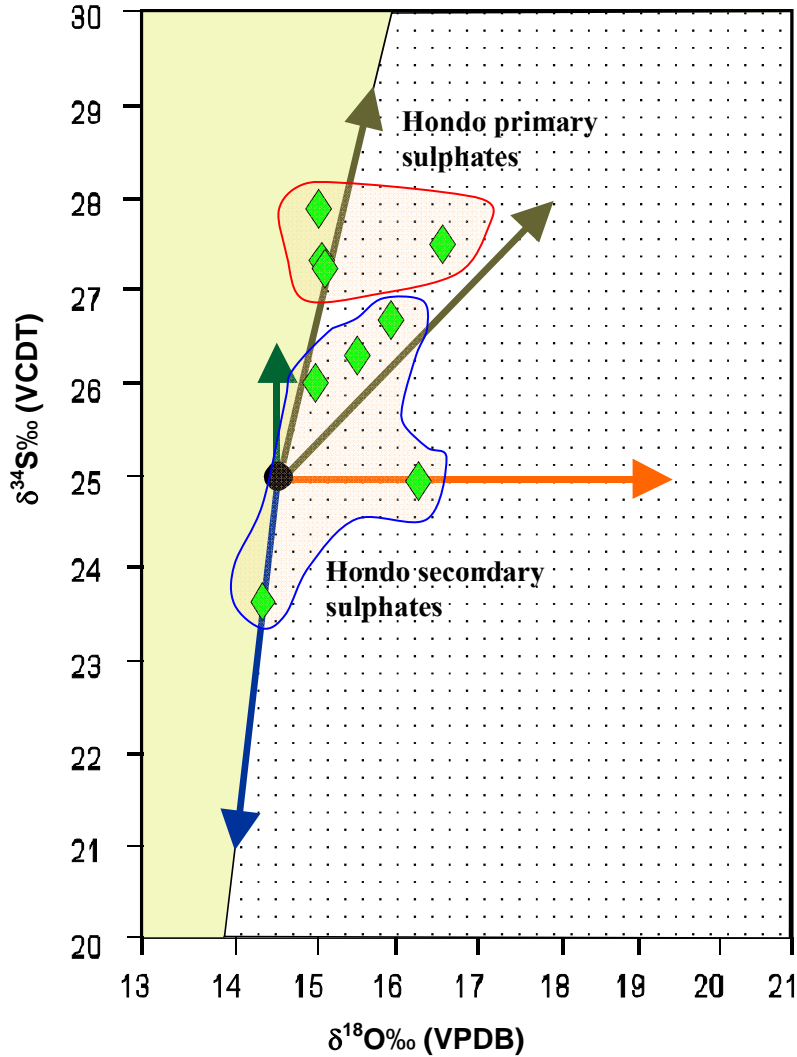
Figure 5.7 Sulphur and oxygen isotopic values for anhydrites of the Grosmont Formation. Direction of sulphur and oxygen isotopes changes for a number of processes. Brown vectors represent isotopic changes due to bacterial sulphate reduction, a red vector represents gypsum-anhydrite transformation and/or oxygen isotope equilibration with carbonate waters, blue vector represents mixing of sulphates from another stratigraphic level; green vector represents thermochemical sulphate reduction (modified from Machel, 1985).
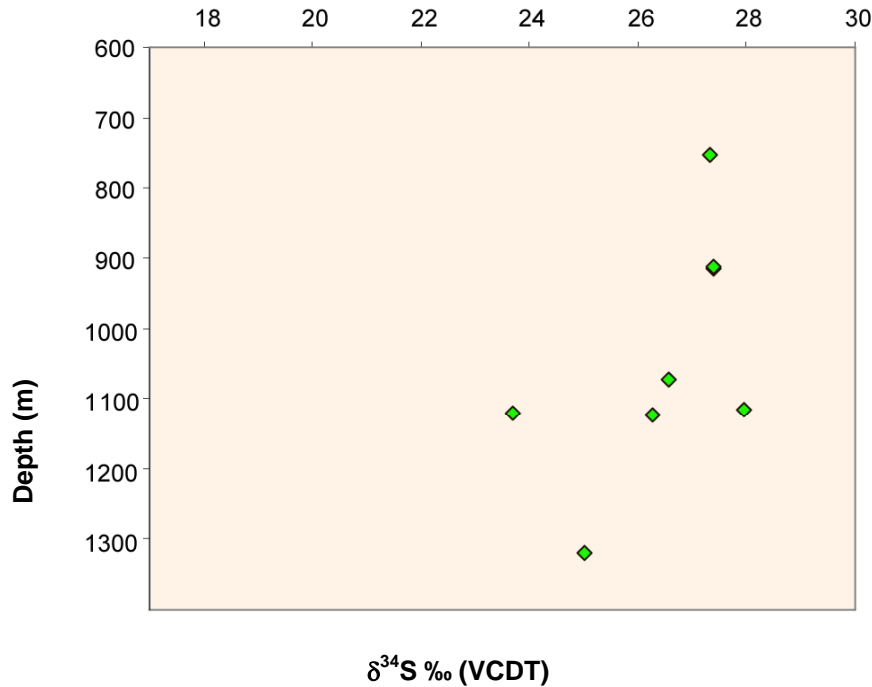
Figure 5.8 δ^{34}S versus depth.

5.6.3 Strontium

^{87}Sr/^{86}Sr ratios for primary and secondary sulphates are shown in Table 5.3.

1. Anhydrite and gypsum samples from the Hondo, the UGM3, two samples from the UGM2, and one from UIRE yielded ^{87}Sr/^{86}Sr values ranging from 0.7081 to 0.7087 (n = 8) with an average of 0.7087. There was one high value of 0.7096.

2. Calcite matrix from the UGM3 and the UGM2 yielded ^{87}Sr/^{86}Sr values of 0.7081 to 0.7089 (n = 3) with an average of 0.7086.

3. Calcite cement ^{87}Sr/^{86}Sr values range from 0.7087 to 0.7101 (n = 4) with an average of 0.7100. One value (0.7113) showed a low signal during testing.

WELL	UNIT	DEPTH (m)	$^{87}Sr/^{86}Sr$	COMMENTS
01-09-70-03W5	HONDO	1157.3	0.7081	Calcite and dolomite
08-16-87-01W5	UGM2	892.2	0.7085	Calcite and dolomite
15-23-69-01W5	UGM3	1120	0.7090	Calcite and dolomite
10-35-73-04W5	UGM2	1120.5	0.7113	Calcite. Low signal
11-35-70-25W4	UIRE	895.05	0.7100	Calcite
08-16-87-01W5	UGM2	892.2	0.7087	Calcite
03-28-70-24W4	UGM2	855.7	0.7101	Calcite
15-17-71-25W4	HONDO	910.70	0.7081	Anhydrite
15-17-71-25W4	HONDO	913.5	0.7082	Anhydrite
10-35-73-04W5	UGM2	1118.5	0.7085	Anhydrite
02-30-79-04W5	UGM3	1068.5	0.7083	Anhydrite and Gypsum
08-16-87-01W5	UGM2	751.03	0.7082	Anhydrite
08-28-69-04W5	UIRE	1314.25	0.7096	Anhydrite
15-23-69-01W5	UGM3	1120	0.7087	Anhydrite
15-23-69-01W5	UGM3	1111.5	0.7082	Anhydrite

Table 5.3 Samples analyzed for strontium isotopes.

Plots of $^{87}Sr/^{86}Sr$ and $\delta^{18}O$ and $\delta^{13}C$ for the Grosmont are shown in Figures 5.9, 5.10, 5.11, and 5.12.
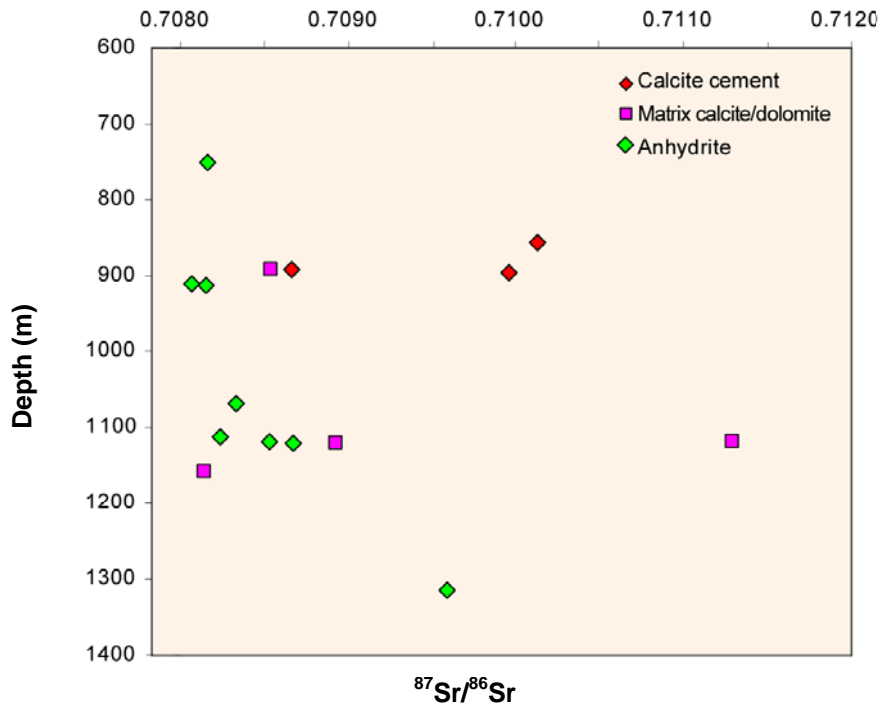
Figure 5.9 $^{87}Sr/^{86}Sr$ versus depth.
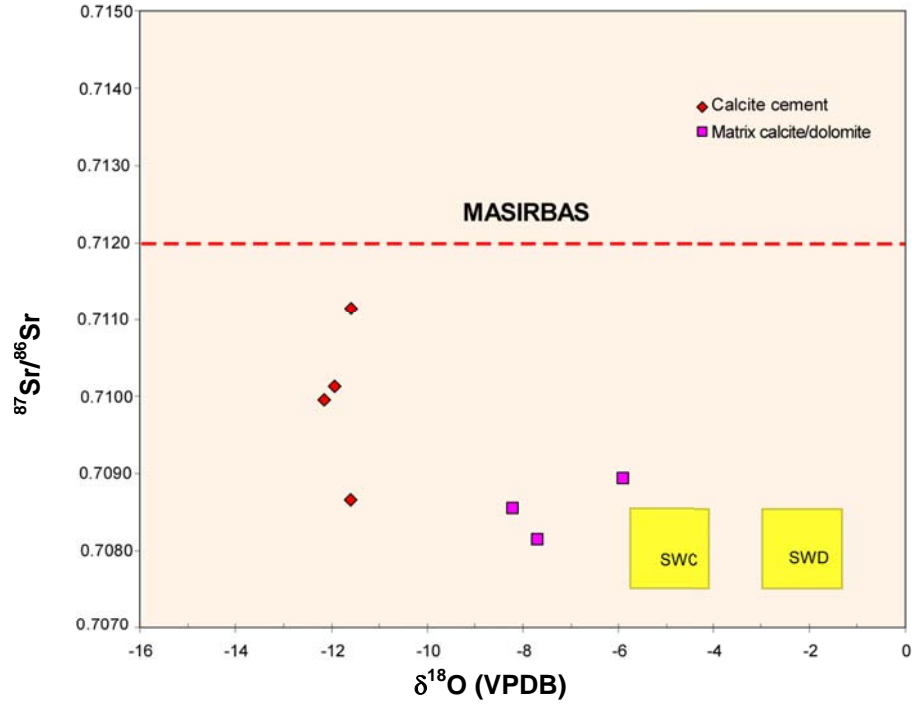
Figure 5.10 ^{87}Sr/^{86}Sr ratios versus δ^{18}O VPDB of calcite-dolomite mixed matrix and calcite cement in the Grosmont. All values are lower than the MASIRBAS. Boxes represent values calculated for dolomite (SWD) and calcite (SWC) formed in equilibrium with theoretical Late Devonian seawater at 25°C (Amthor et al., 1993; Drivet and Mountjoy, 1994; Marquez, 1994).
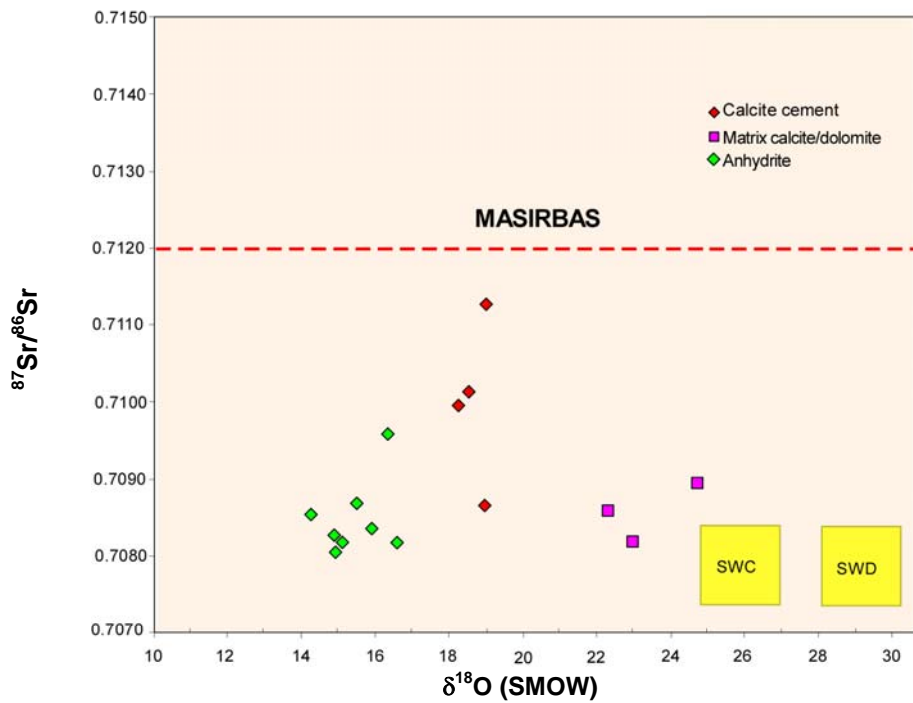
Figure 5.11 ^{87}Sr/^{86}Sr ratios versus δ^{18}O SMOW of calcite-dolomite mixed matrix, calcite cement and anhydrite.
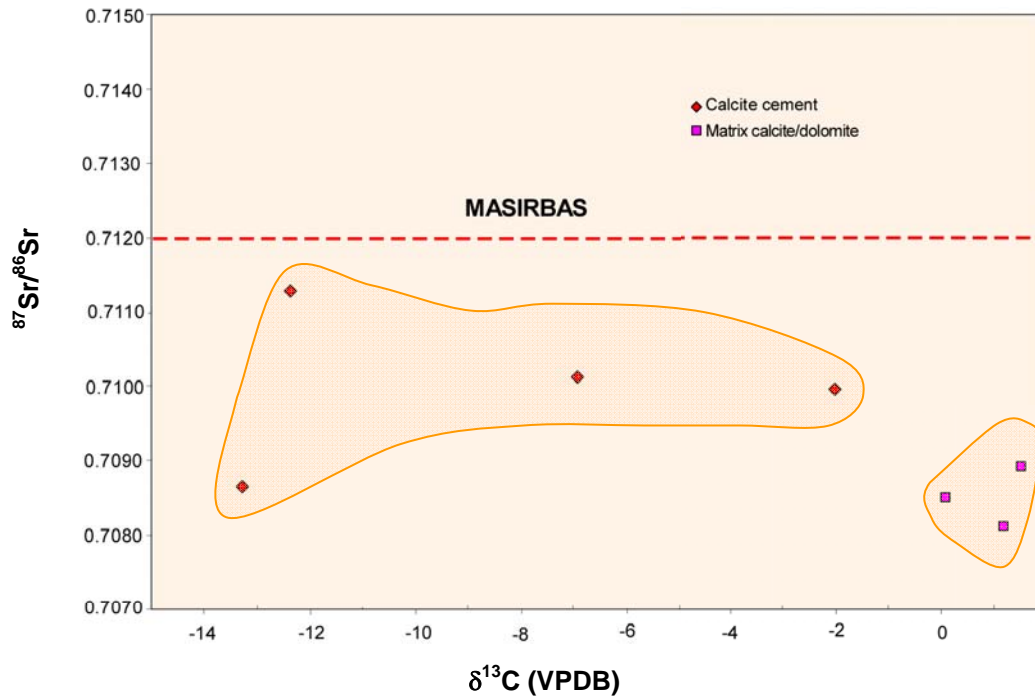
Figure 5.12 $^{87}Sr/^{86}Sr$ ratios versus $\delta^{13}C$ of calcite-dolomite mixed matrix and calcite cement in the Grosmont.

5.7 Interpretation of Geochemistry Results

5.7.1 Calcite and Dolomite Matrix

The baselines for both oxygen and carbon isotopic compositions of Late Devonian marine calcites were defined by previous authors (Hurley and Lohman, 1989; Veizer et al., 1999) (Figure 5.4). In the Grosmont, neither the calcite nor the dolomite samples fall into these ranges. Rather both calcite and dolomite values are significantly depleted in $\delta^{18}O$ relative to the marine reference values and slightly depleted (with one exception) for $\delta^{13}C$ (Figure 5.4). This indicates isotopic re-equilibration from meteoric water or from buried marine water of slightly elevated temperature. However, there are no clearly discernible stable isotopic trends with depths (Figure 5.5 and 5.6). On the other hand, the sparry

111

calcite cements are clearly distinct from the matrix samples for δ^{18}O (Figure 5.4 and 5.6), suggesting that they formed diagenetically from different fluids (further explained below).

The values for ^{87}Sr/^{86}Sr ratios of calcite-dolomite mixed matrix samples are slightly enriched in ^{87}Sr compared to the values for the Frasnian-Givetian stages, which suggests moderate ^{87}Sr release from silicate minerals (probably in the "shale breaks") during burial and concomitant isotopic re-equilibration.

5.7.2 Sparry Calcite Cement

The calcite cement δ^{18}O values are significantly lower than Late Devonian seawater δ^{18}O values and distinct from the matrix samples. This depletion of ^{18}O relative to seawater is likely due to precipitation from meteoric water or at elevated temperatures. The temperature of formation can be calculated with the equation (2) from section 5.3.

The mean obtained for sparry calcite cements (δ^{18}O$_C$) in this study is -11.7 ‰ VPDB. Assuming different values for meteoric water from Alberta (δ^{18}Ow) (-10, -14,-18, and +2 ‰ SMOW), there are four possible scenarios; the four scenario is the one using a value for gypsum brines from the Devonian (Figure 5.13):

1. For a δ^{18}Ow value of -10 ‰ SMOW, the temperature calculated is 21.0°C. Waters at that temperature could be associated with meteoric waters entering the Grosmont Formation via faults during the Cretaceous. Meteoric waters

during/after the Laramide orogeny could have entering the Grosmont through localized fractures; these waters favour formation of calcite crystals.

2. For a $\delta^{18}O_w$ value of -14 ‰ SMOW, representing meteoric waters during the Tertiary when Alberta had moved to higher latitudes due to plate tectonics, the temperature calculated is 6.3 °C. This temperature is too cold climatically for the Tertiary but is reasonable for groundwater of Tertiary origin during the Pleistocene interglaciar epochs, and for the Holocene. The present formation water temperature in the Grosmont reservoir in the Saleski area is approximately 15 °C (Barrett, K, personal communication, July 2010).

3. For a $\delta^{18}O_w$ value of -18 ‰ SMOW, which is $\delta^{18}O$ value of sub-recent rain water in Alberta (Connolly et al., 1990), the temperature calculated is -7.0°C. This temperature is impossible because the freezing point water is 0°C.

4. The presence of saddle dolomite in two wells suggest that temperatures in excess of ~80°C were reached at least locally, probably by relatively hot (hydrothermal) fluids ascending via faults. Assuming a $\delta^{18}O_w$ of +2‰ SMOW, which is representative of a mesohaline brine with salinity between that of normal seawater and gypsum-saturated brine (Knauth and Beeunas, 1986), yields a temperature of ~104 °C (Figure 5.13).

Without further study, option 1, 2, and 4 all appear feasible.
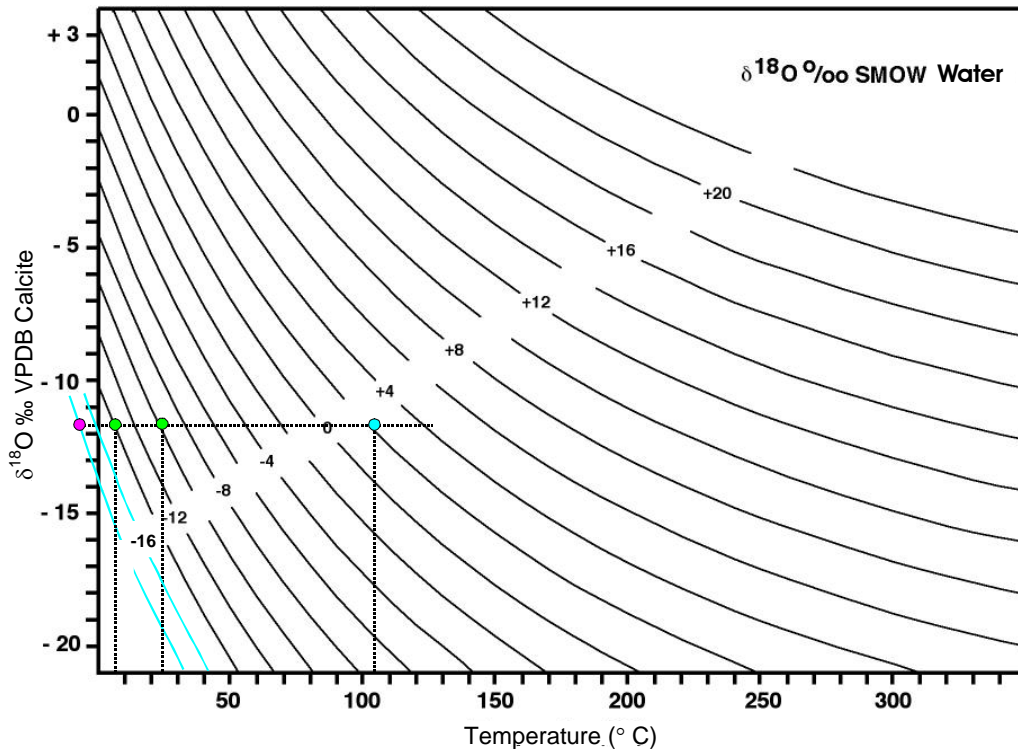
Figure 5.13 Plot of equilibrium relationship between temperature and isotope composition of water and calcite after Friedman and O'Neill (1977). Average of $\delta^{18}O$ for calcite cements is -11.7 ‰ VPDB. The temperature of waters forming calcite cement is calculated for four values of $\delta^{18}Ow$: -10, -14, -18, and +2‰ SMOW.

Values for $^{87}Sr/^{86}Sr$ in calcite cement samples range from 0.7081 to 0.7101. A single value of 0.7113 which is analytically suspected has been omitted from the data analysis. The range of 0.7081 to 0.7101 for the Grosmont/Hondo is more radiogenic than that of Middle Devonian seawater. 87 strontium enrichment may be attributed to an admixture of waters from basal through fractures. Machel and Cavell (1999) explained that rocks with values of $^{87}Sr/^{86}Sr > 0.7120$ (higher than the MASIRBAS) are formed from formation waters with a metamorphic source derived from the Precambrian. Values of $^{87}Sr/^{86}Sr$ obtained in this study are under 0.7120; however, the analyzed samples were formed from modified

114

Devonian seawaters that had interacted with siliciclastics (Devonian and Cretaceous) in the sedimentary succession (Figure 5.12).

5.7.3 Anhydrite

Late Devonian seawater is reported to have had a δ^{34}S average of 25 ‰ VCDT (Carpool et al., 1980). Anhydrite samples from the Hondo have δ^{34}S values between 23.7 ‰ and 27.4 ‰ VCDT, whereas δ^{34}S in samples from the Hondo, UGM3, and UGM2 have values ranging from 23.7 ‰ to 27.9 ‰; δ^{18}O values are between 14.3 ‰ and 16.6 ‰ SMOW (Figure 5.7). The values of oxygen are slightly higher than those of Late Devonian seawaters, probably due to the high salinity of the Hondo parent brines.

Values for ^{87}Sr/^{86}Sr suggested for Devonian seawater range from 0.7078 to 0.7082 (Figure 5.3). Anhydrites within the Grosmont Formation show values of 0.7081 to 0.7087, which indicates marine parentage from the Middle Devonian. A value of 0.7096 for ^{87}Sr/^{86}Sr corresponds to an anhydrite nodule (secondary) within argillaceous dolo-limestone of the Upper Ireton. Enrichment in strontium could be attributed to mixed waters from the upper units like the Nisku and/or Calmar Formations. Oxygen isotopic compositions of anhydrites did not follow any trend with depth (Figures 5.8 and 5.9).

CHAPTER 6

DISTRIBUTION AND DEPOSITIONAL ENVIRONMENT OF HONDO

6.1 Introduction

The spatial distribution of the Hondo sulphates and the Grosmont platform margin were reconstructed using 32 wells with core, 105 wells with cuttings, and a total of 140 wells with logs. Structural maps were constructed for the Upper Ireton, Upper Grosmont 3, and Upper Grosmont 2, and isopach maps were constructed for Upper Grosmont 3 and Upper Grosmont 3 with the Hondo, and five cross sections. A sedimentological interpretation for the Hondo is proposed based on lithofacies, distribution, integration of geochemical results, and comparison with modern examples of evaporitic basins.

6.2 Data

A total of 32 wells with core were described; five of them contain primary sulphates. These wells were used to establish the first framework to draw three cross sections following dip and two following the strike direction (Figure 6.1). Descriptions of cuttings were matched with log interpretations to better define the presence of gypsum and/or anhydrite, and to identify and locate the shale/marl units (SB1, SB2, and SB3) between the Grosmont members. A sulphate content of 25 to 35 percent classified an interval as part of the Hondo.

116
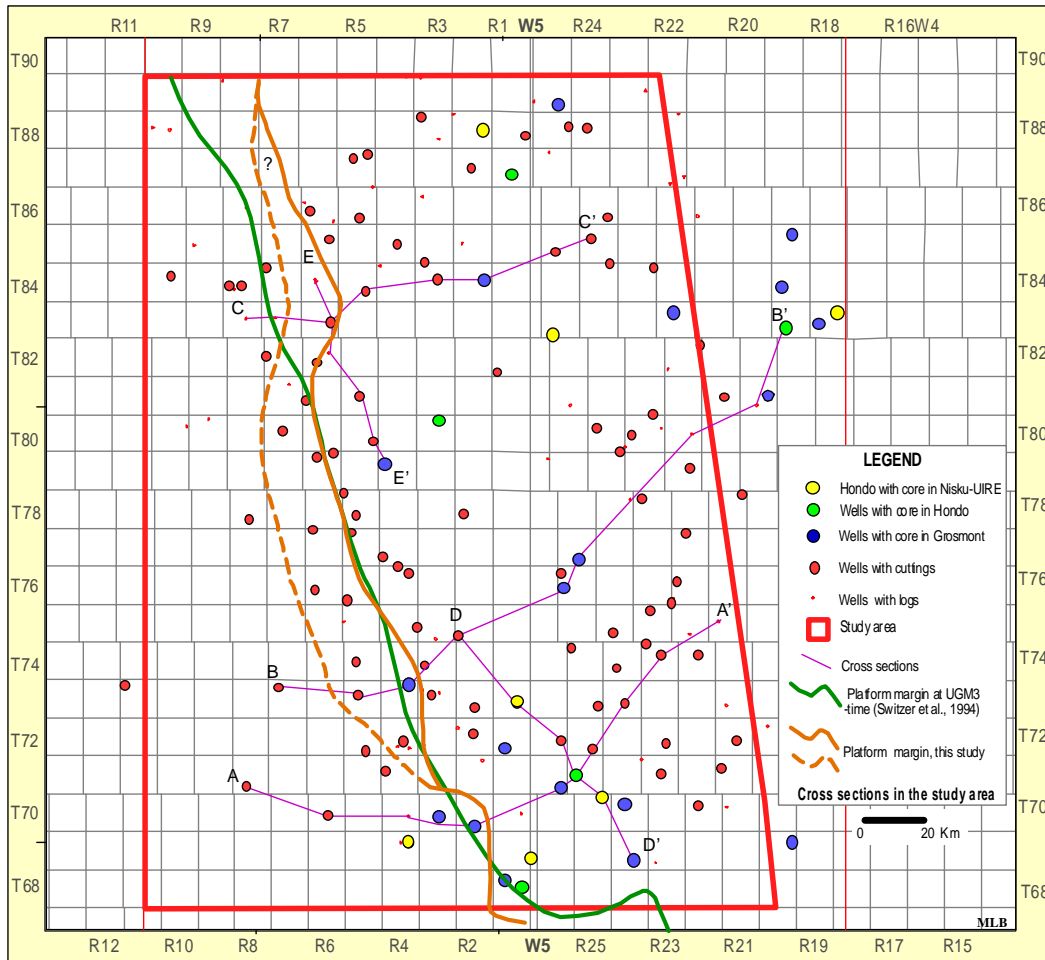
Figure 6.1 Location of the cross sections in the study area and Grosmont platform margin at UGM3-time, three solutions (see text for explanation).

6.3 Structural maps

A limitation in this study was the sporadic distribution of cored wells, most of them drilled only down to the sub-Cretaceous unconformity; also, the quality of some logs is questionable. Logs used for stratigraphic interpretation (gamma ray, resistivity and density logs) were matched with cuttings to interpret the presence of sulphates in the Grosmont as well as the presence of shale layers within the Grosmont Formation. Structural maps were drawn for Upper Ireton, Upper Grosmont 3, and Upper Grosmont 2.

6.3.1 Upper Ireton

The Upper Ireton Formation displays a regional strike of 160° in the northeast to 150° in the southwest. The dip is approximately 0.3° to the southwest. The structural map shows elevation ranges from 800 m below sea level in the southwest corner to 250 m above sea level close to the erosional edge (Figure 6.2).

6.3.2 Upper Grosmont 3

Upper Grosmont 3 shows a regional strike of 150° to 160° and a dip of 0.3° in the southwest (Figure 6.3) Elevation from the top of UGM3 varies from 700 m below sea level to 250 m close to the erosional edge.

6.3.3 Upper Grosmont 2

Upper Grosmont 2 shows a regional trend of 160°; local strikes vary from 130°to 150° in the northwestern corner. The dip of the formation is 0.3° southwest in the north and central parts and in the southwest increases to 0.5°. Elevation varies from 900 m below sea level in the southwest to 200 m above sea level in the northeast (Figure 6.4).
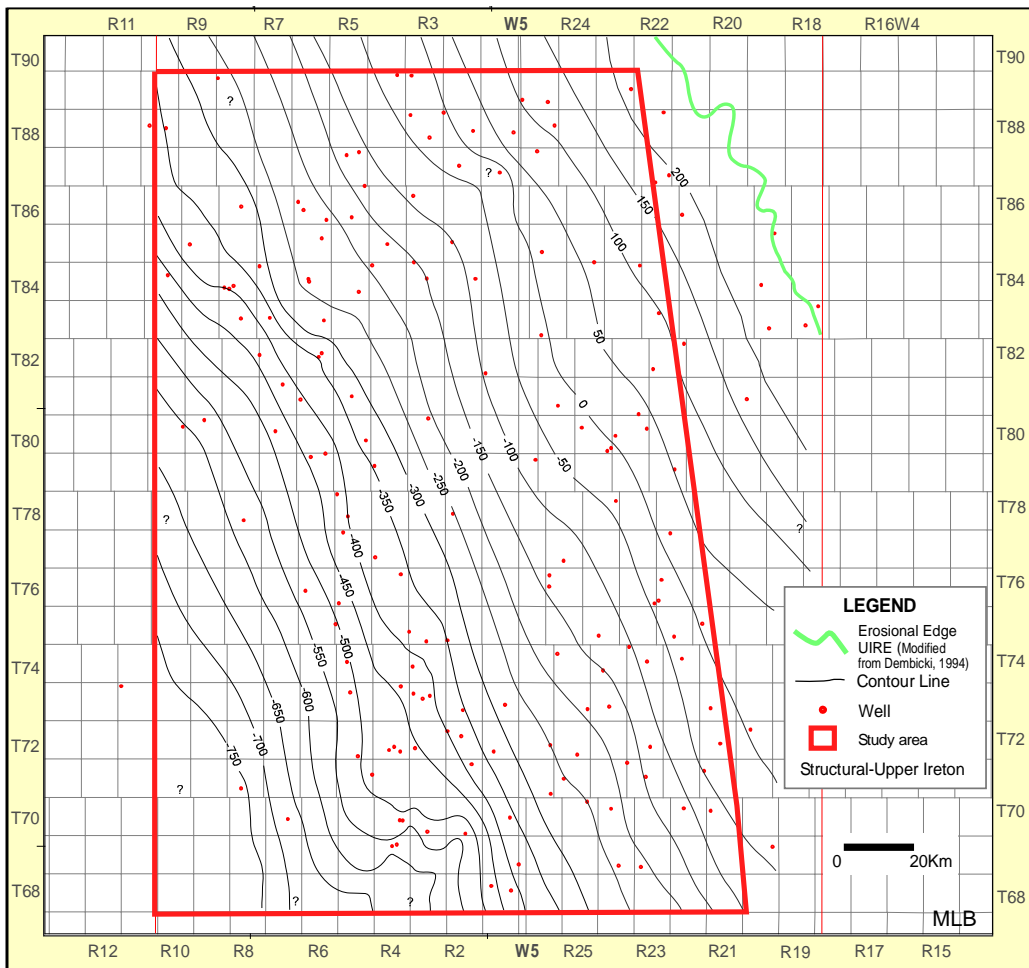
Figure 6.2 Structural map of the Upper Ireton.
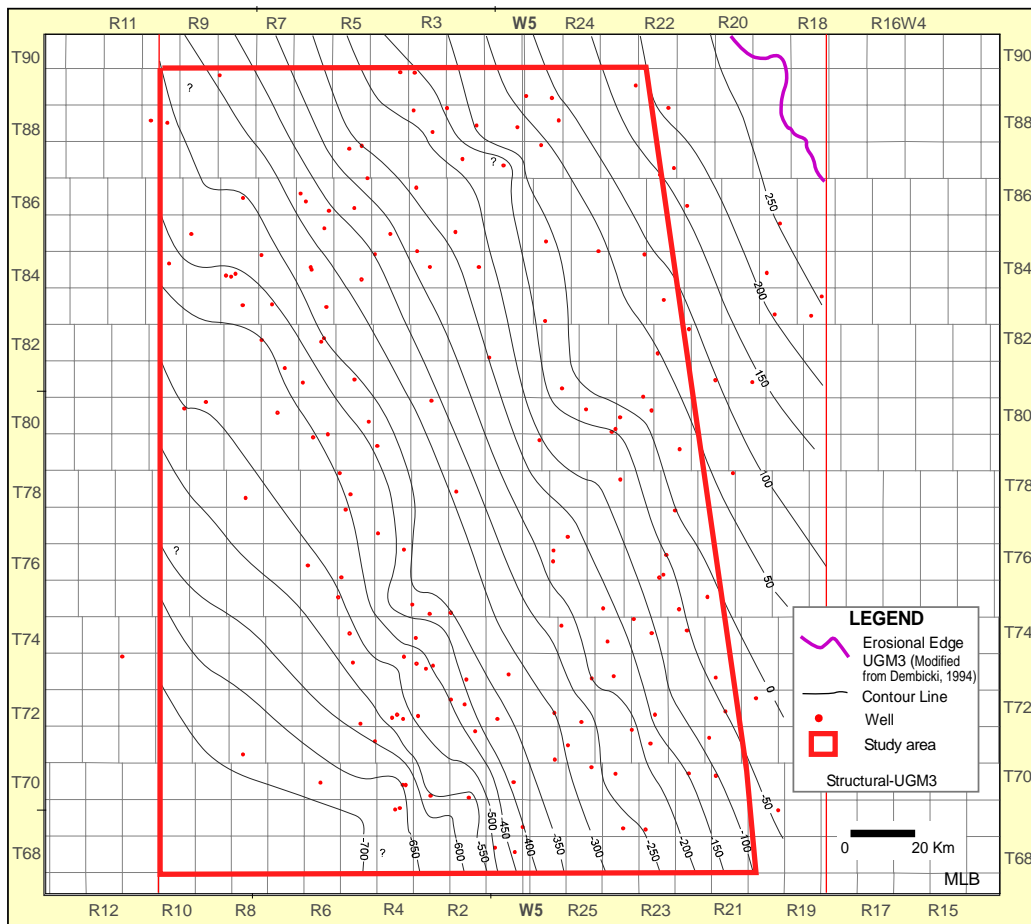
Figure 6.3 Structural map of the Upper Grosmont 3.

6.4 Isopach Maps

Isopach maps for Upper Grosmont 3 including and excluding the Hondo are shown in Figures 6.5 and 6.6, respectively. The thickness of the UGM3 varies from zero (0) at the southwest border and is uniform in the eastern part. In the central and northeastern areas, the thickness reaches about 60 m, being thickest in the central part of the Hondo loop (Figure 6.5).

120

Both isopach maps show decreasing thickness toward the platform edge and increasing thickness toward the center of the Hondo loop. The thickness of the Hondo varies from 35 m to 2 m, with an average thickness of 20.8 m.
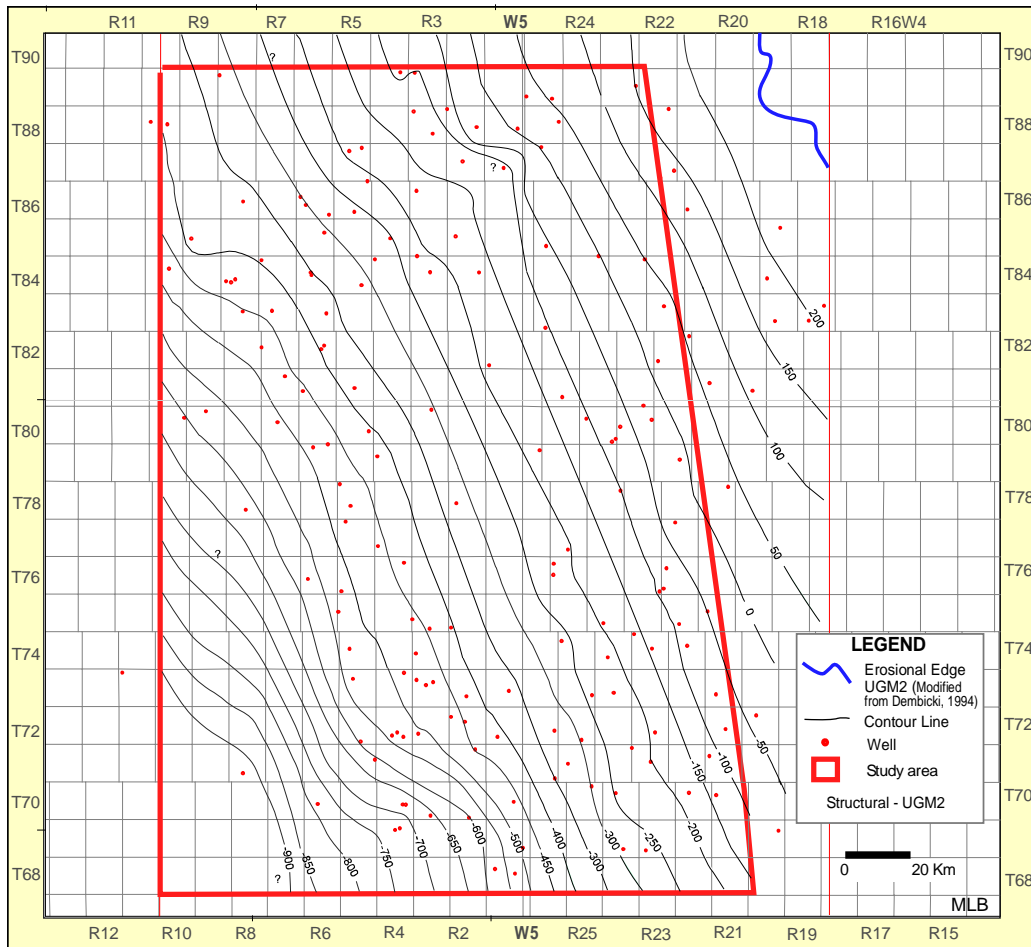
Figure 6.4 Structural map of the Upper Grosmont 2.
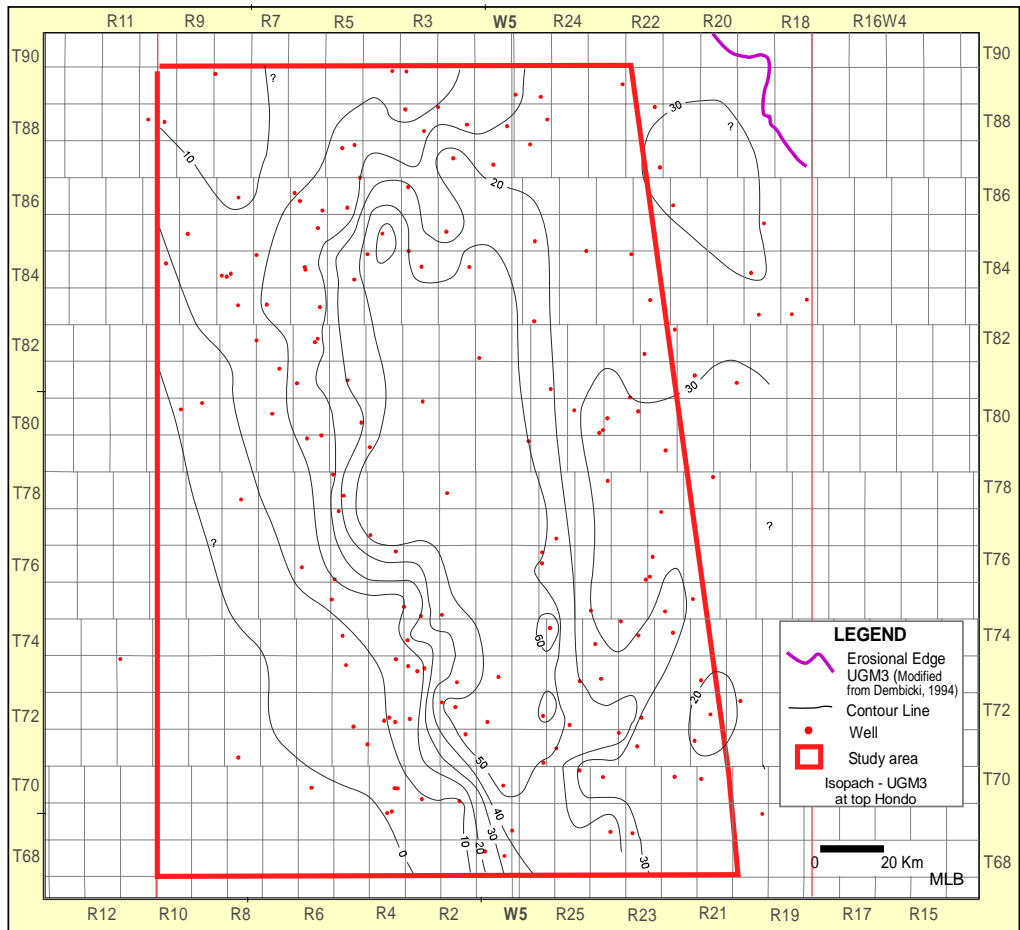
Figure 6.5 Isopach map Upper Grosmont 3 including Hondo.

6.5 Cross Sections

Five cross sections were constructed to illustrate the regional distribution of the Hondo sulphates and the Grosmont Formation. The wells were chosen based on core and cuttings suitability, and on the quality of available logs. Logs were taken from ACCUMAP and redrawn for better visual quality. Location of the cross sections is illustrated in Figure 6.1.
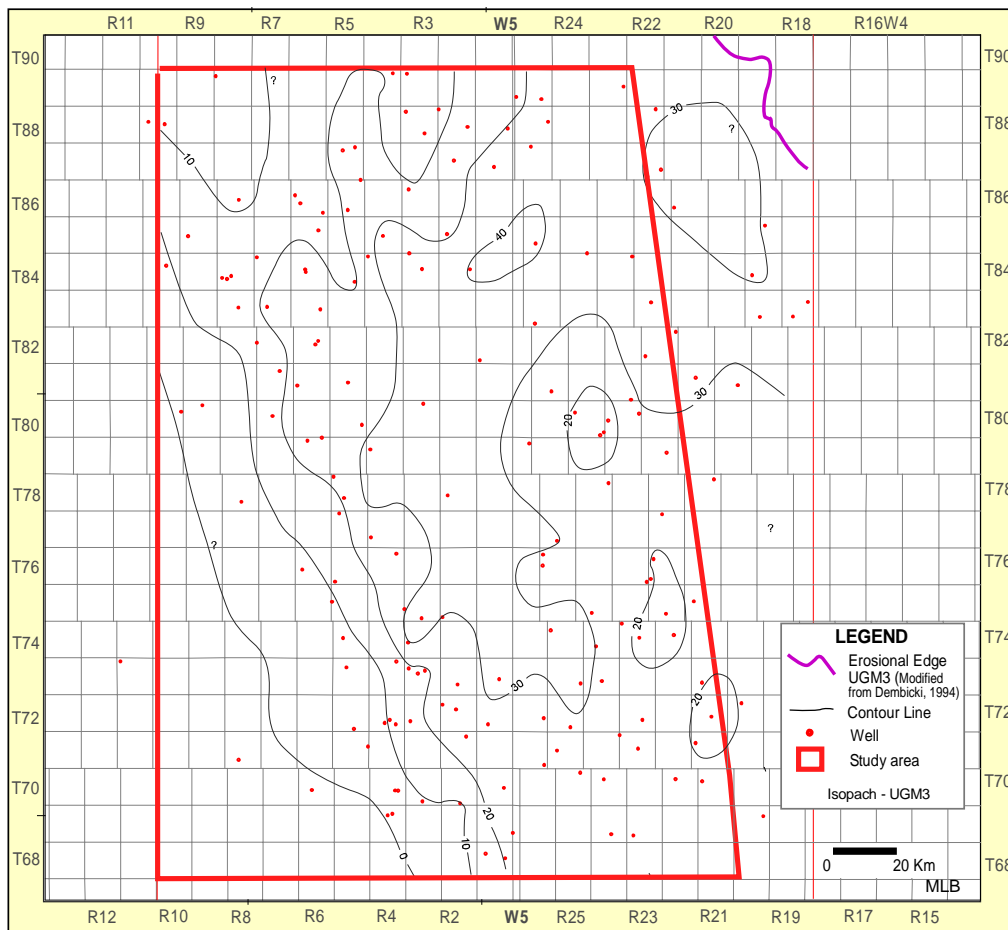
Figure 6.6 Isopach map Upper Grosmont 3 excluding Hondo.

The datum used in the cross sections is the top of the Upper Ireton. This datum is regionally continuous and easy to recognize on logs. Cross sections are drawn with a vertical exaggeration of up to 150X.

In most wells, the gamma-ray log was used in combination with a density (when available) or resistivity logs. Abbreviations used for the cross sections are:

LIRE: Lower Ireton Formation

UIRE: Upper Ireton Formation

SB1, SB2, and SB3: shale/marl layers between the Grosmont units

123

LGM: Lower Grosmont

UGM1: Upper Grosmont 1

UGM2: Upper Grosmont 2

UGM3: Upper Grosmont 3.

6.5.1 Dip Cross Sections

The dip cross sections A-A', B-B', and C-C' range from the Lower Ireton to the Upper Ireton (Figures 6.7 to 6.12). Section A-A' contains nine wells that stretch over 147.20 km, from well 06-09-71-08W5 to well 10-20-75-21W4. Farther north, section B-B' comprises ten wells over 186.00 km, from well 04-27-73-07W5 to well 10-17-84-19W4. Dip section C-C' covers 101.05 km, with nine wells from well 07-22-83-08W5 to well 04-32-85-23W4. In all three sections the Grosmont units become thinner basinward and the shale content increases to the west. The degree of uncertainty in delineating the extent of the Grosmont units in the west increases due to the lack of good quality logs in the western part of the study area.

In cross section A-A', between well 10-01-71-26W4 and well 06-03-70-02W5 there is an abrupt change in thickness of the Grosmont units, especially in Upper Grosmont 3 and Upper Grosmont 2. Also, the Upper Grosmont units in well 06-03-70-02W5 appear at a much higher level and closer to the datum than in well 10-01-71-26W4, providing for a "bulge" in the UGM3 strata between these wells. Furthermore, west of the interpreted fault, in wells 12-14-70-04W5, 10-28-70-06W5, and 06-09-71-08W5, the gamma logs suggest an increase of calcareous

content within the shale interval of the Lower Ireton. However, cuttings from the first two wells do not suggest that those intervals with high calcareous content are part of the Grosmont Formation and the cuttings of well 06-07-71-08W5 are of poor quality. In section B-B', logs of wells 10-35-73-04W5, 07-10-73-05W5, and 04-27-73-07W5 show the same increase in calcareous content but it is not apparent in the cuttings.

These three findings are interpreted as a product of syndepositional faulting. Further, supporting evidence for faulting along this part of section A-A' is the presence of saddle dolomite in well 01-09-71-03W5, located beside well 06-03-70-02W5 (Figure 6.7: the position of this well is indicated only schematically because no wireline logs are available for this well below the Upper Ireton). Saddle dolomite is generally recognized as a high-temperature type of dolomite that often forms from "hot" (greater than 80 °C) aqueous fluids. Thus, it is likely that the saddle dolomite found in well 01-09-71-03W5 formed from fluids that ascended from a fault near by, albeit most likely relatively late diagenetically (Chapter 4). In addition, the isolated occurrences of sparry calcite cement may well have formed from "hydrothermal" fluids as well (see Chapter 4 and 5). If so, these calcite cements provide additional evidence for faulting, albeit not syndepositionally. Thus, the presence of saddle dolomite and late sparry calcite cement are evidence for reactivation of the syndepositional faulting at the later time, most probably during the Cretaceous.

However, the interpretation of this faulting is somewhat tenuous considering the relatively wide well spacing, the vertical exaggeration of the

section, and the absence of seismic information. On the other hand, it is well known that the entire region is dissected by an orthogonal fault system (Lyatsky and Pana 2003; Wagner et al., 2010).

If correct, syndepositional faulting in this geographic and stratigraphic location (UGM3) provides a ready explanation for the presence of the Hondo evaporites. The region west of the interpreted fault would have been slightly elevated relative to the region to the east, providing accommodation space for the evaporite deposition. The faulting thus also delineates the location of the Grosmont platform margin at UGM3-time, as shown as a solid orange contour in Figure 6.1.

The interpreted syndepositional faulting is also present in sections B-B' and C-C', again roughly coinciding with the Grosmont platform margin. However, the "bulge" is not as pronounced as in section A-A', nor is the westward decrease in thickness as dramatic. For these reasons, the location of the faulting is not well defined. Rather, the faulting may have occurred in a zone delineated by the orange solid and dashed lines (Figure 6.1), suggesting that the platform margin was located in this zone and slightly raised at the time of UGM3 deposition.

Considering further that the LGM, UGM1, 2, and 3 all appear to be forming a "bulge" in the region of the platform margin, it appears that the fault was reactivated postdepositionally with the opposite sense of throw (down-thrown on the west). Late-diagenetic reactivation is also indicated by the presence of

saddle dolomite in well 08-16-87-01W5 indicated in section C-C'. The structural dip sections 6.10, 6.11, and 6.12 are consistent with this interpretation.

While the platform margin was delineated by syndepositional faulting at UGM3-time, it was located farther east and not necessarily controlled by faulting in earlier times. The presence of Hondo primary sulphates at the LGM level immediately east of the Leduc reef in section B-B' suggest that it was the reef that essentially formed the platform margin and provided accommodation eastward at LGM-time. Well 10-17-19-84W4 contains two narrow intervals with primary sulphates in the LGM, whereas primary sulphates can be inferred from log signatures in well 11-14-81-20W4.

These findings further indicate that the Grosmont platform margin had migrated westward between LGM and UGM3 times. This regional trend of platform progradation had already been recognized by Switzer et al. (1994), who provided contours for the platform margin also for Duvernay and Majeau Lake times located farther northeast (Figure 6.13). Switzer et al. (1994) also showed that the western edge of the Grosmont platform coincides with the reduction of thickness of UGM2 and mainly the UGM3 (Figure 6.14). Considering all available evidence one is left to conclude that the Grosmont platform margin migrated westward through time and can not be delineated with certainty in some parts of the region.
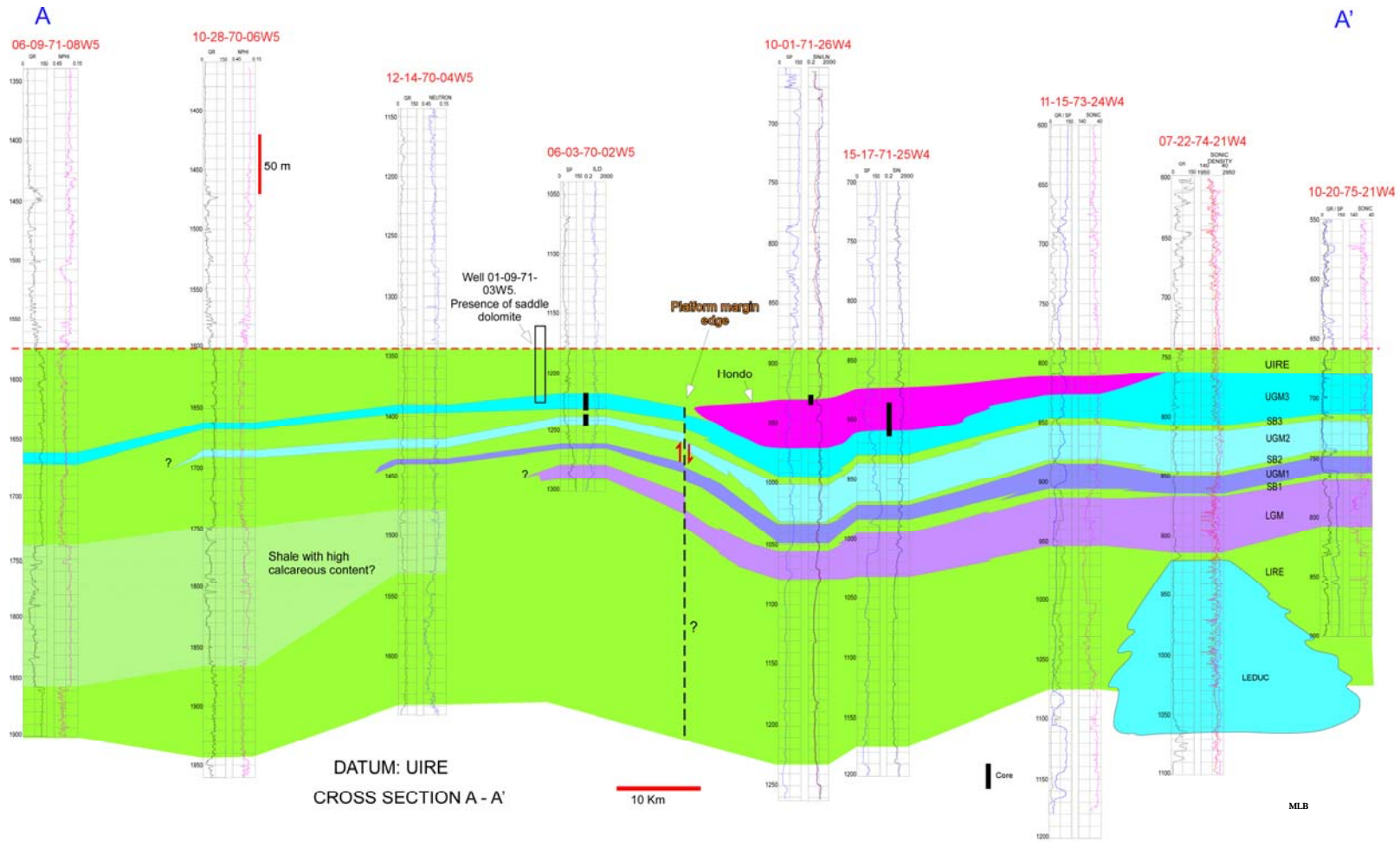
Figure 6.7 Stratigraphic cross section A-A'.
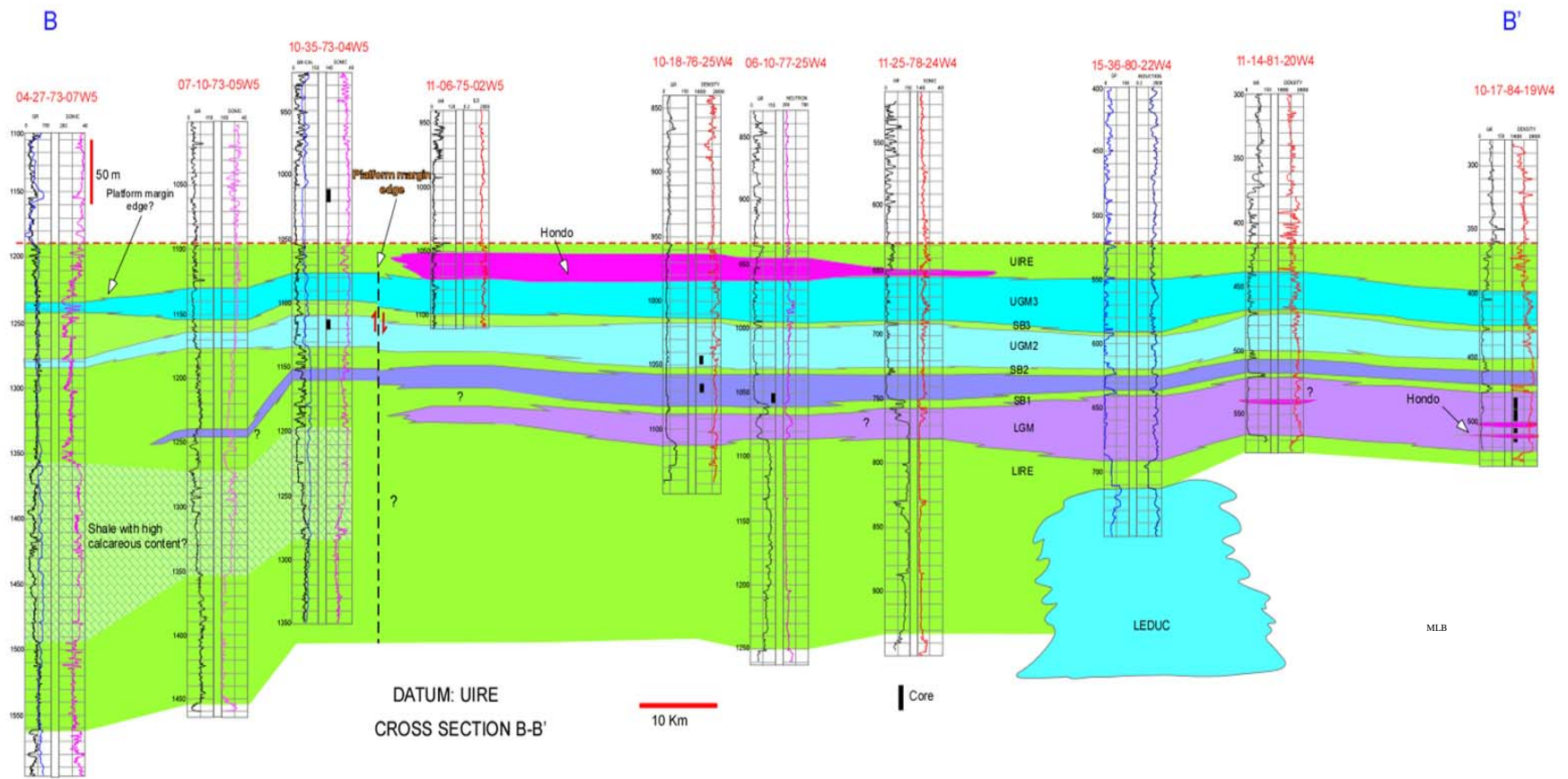
Figure 6.8 Stratigraphic cross section B –B'
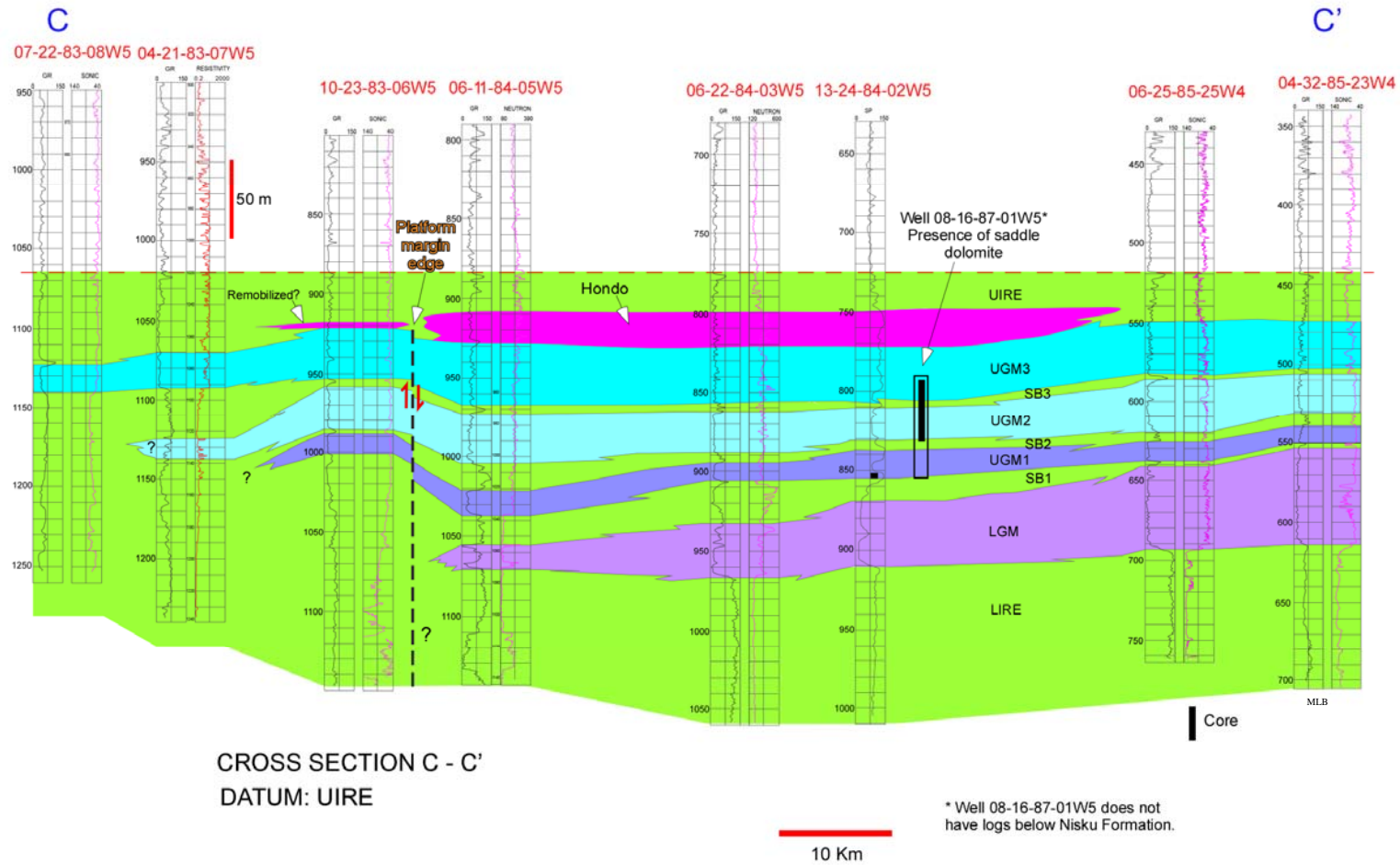
Figure 6.9 Stratigraphic cross section C-C'
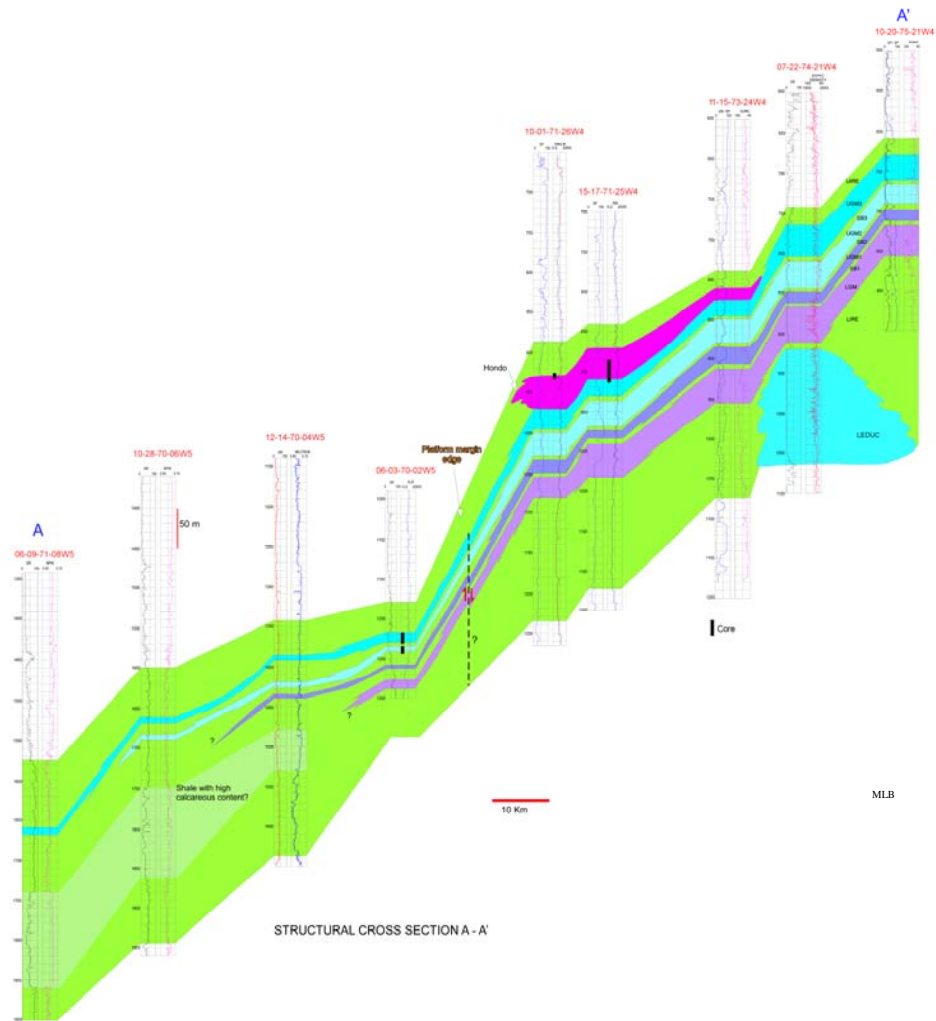
Figure 6.10 Structural cross sect

131

Figure 6.11.Structural

STRUCTURAL CROSS SECTION B - B'

Figure 6.11 Structural cross section B - B'.

129

132
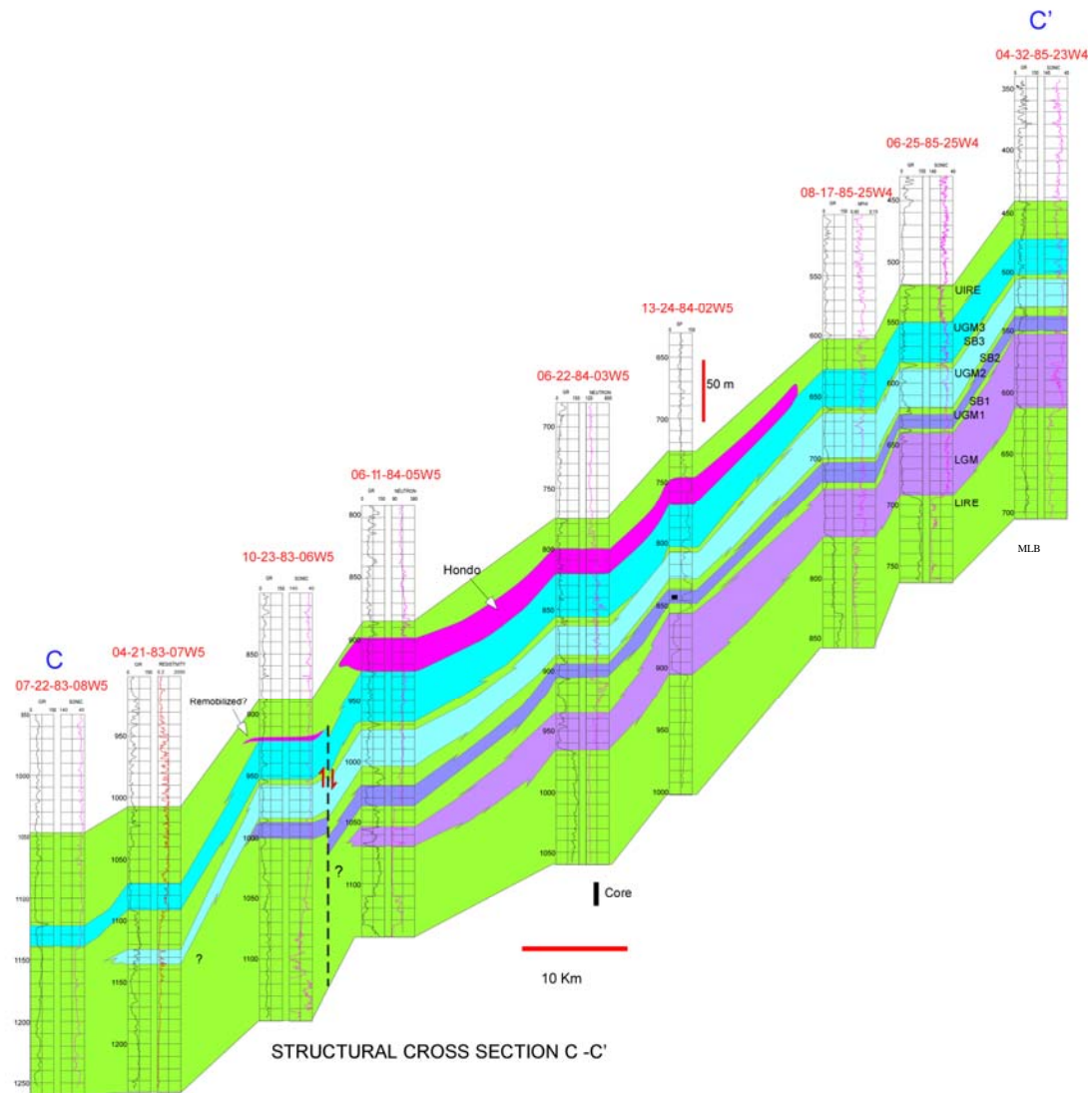
Figure 6.12 Structural cross section C-C'.
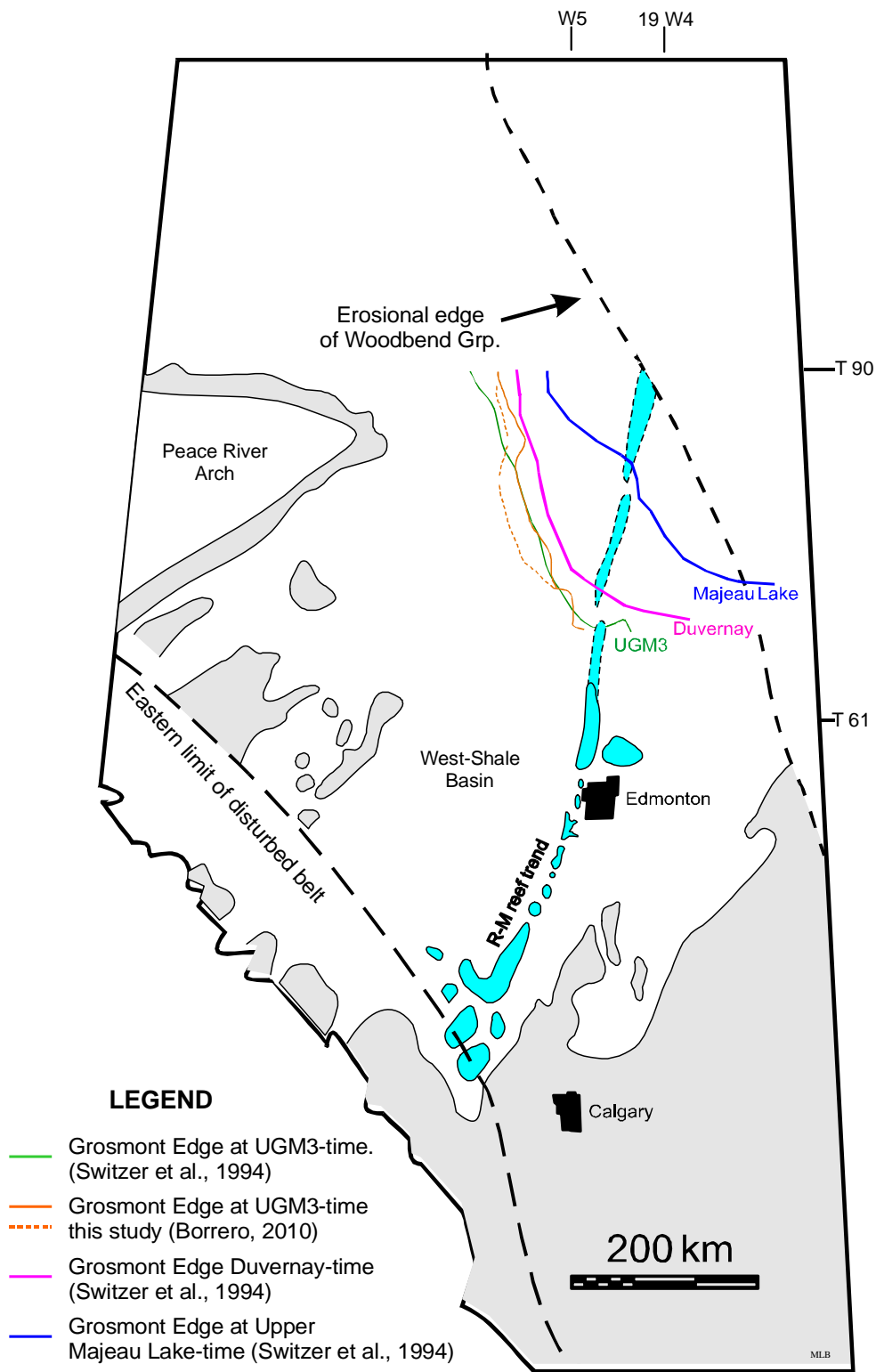
Figure 6.13 Simplified map of the Devonian in Alberta highlighting the western progradation of the Grosmont platform margin through time.
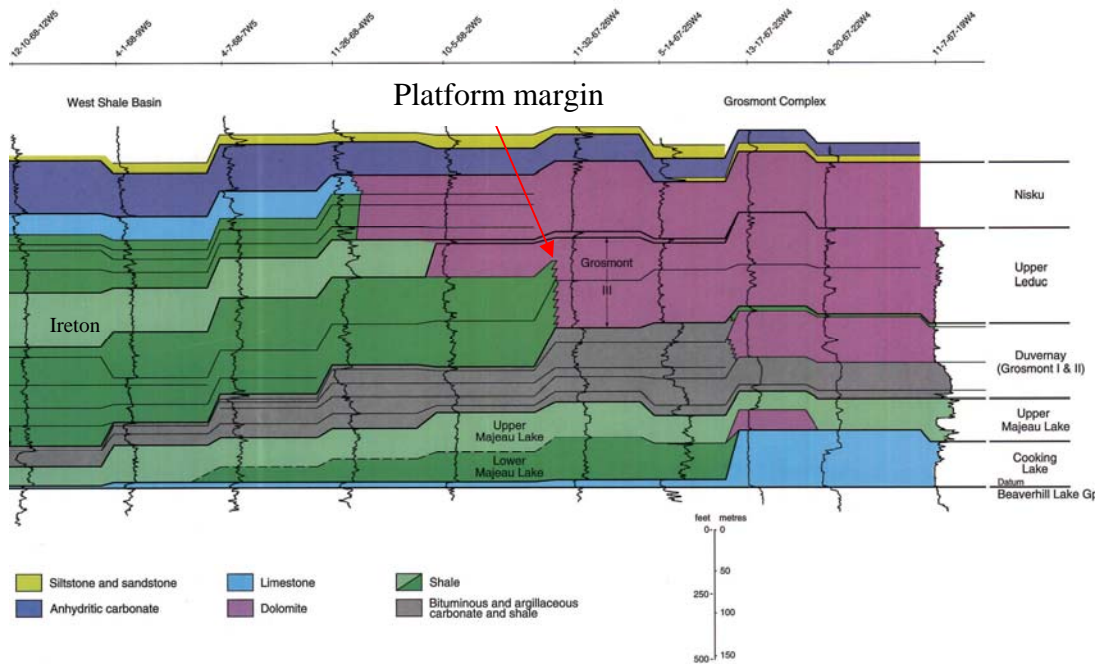
Figure 6.14 West-east cross section, showing Woodbend-Winterburn strata from Gold Creek to the Grosmont area (from Switzer et al., 1994).

6.5.2 Strike Cross Sections

Strike-direction cross sections D-D' and E-E' range from the Upper Ireton to the Lower Ireton Formation (Figures 6.15 to 6.18). Cross section D-D' covers 52.1 km from well 11-06-75-02W5 to well 04-15-69-24W4. The UGM3 and UGM2 conserve the thickness while the UGM1 and LGM get thicker in the central part of the study area. There is an increase in shale content toward the northwest part of the section. The thickness of the Hondo varies from approximately 30 m in the center to 10 m toward the borders. Cuttings in wells 11-06-75-02W5 and 16-15-73-01W5 have high shale content within the Grosmont Formation, and here the Grosmont units here are difficult to interpret.

Cross section E-E' extends 73.7 km, from well 06-21-84-06W5 to well 02-30-79-04W5. The thickness of the UGM1 and LGM decreases toward the northwest

of the section (Figure 6.16). The Hondo primary sulphates are present only in the southern part, with thickness up to 15 m. Cuttings for wells 06-21-84-06W5, 10-23-83-06W5, 02-22-82-06W5, and 16-16-81-05W5 show high shale content in the Grosmont interval, thus, interpretation of the Grosmont units in these wells was based mainly on logs.
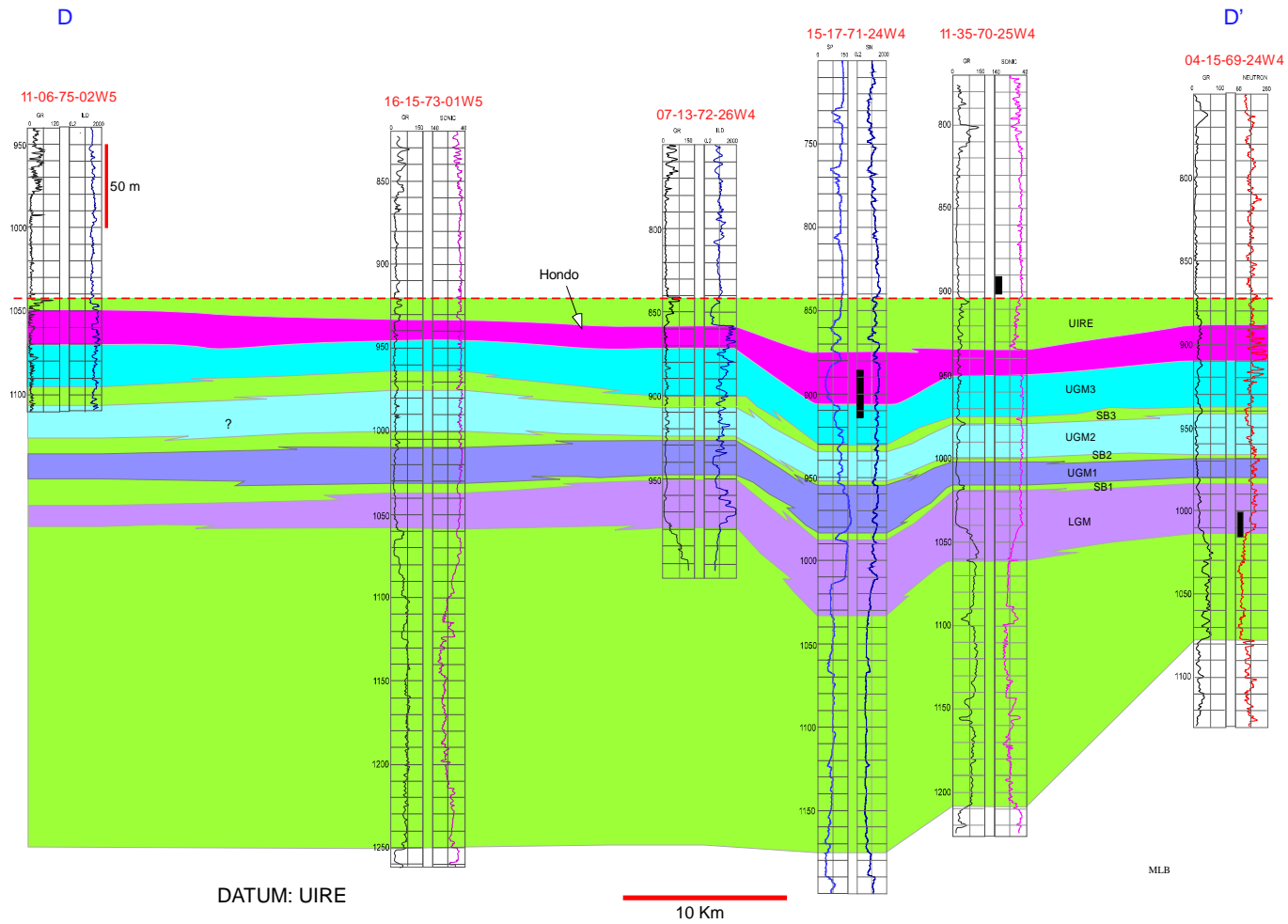
Figure 6.15 Stratigraphic cross section D-D'.
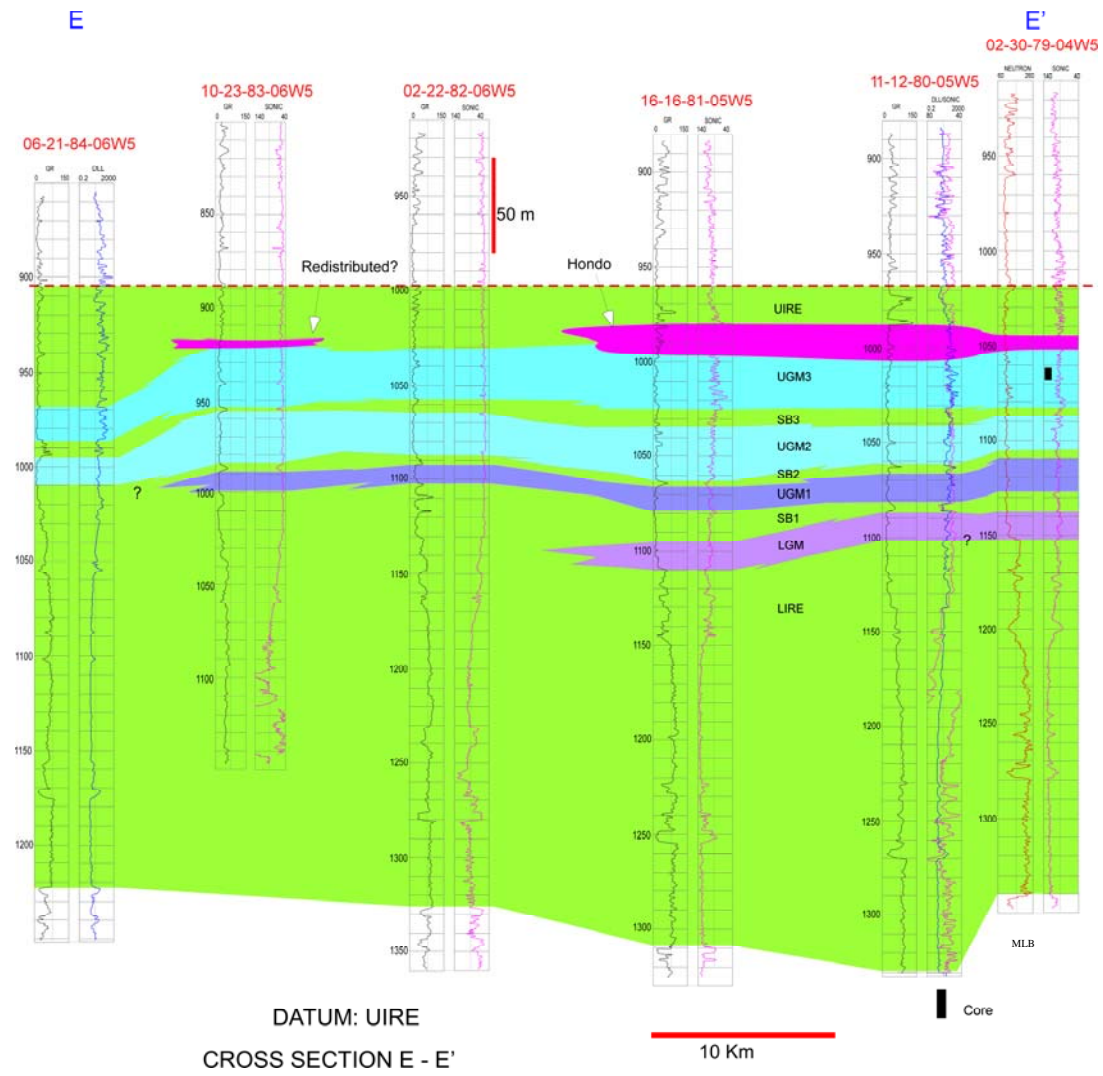
Figure 6.16 Stratigraphic cross section E-E'.
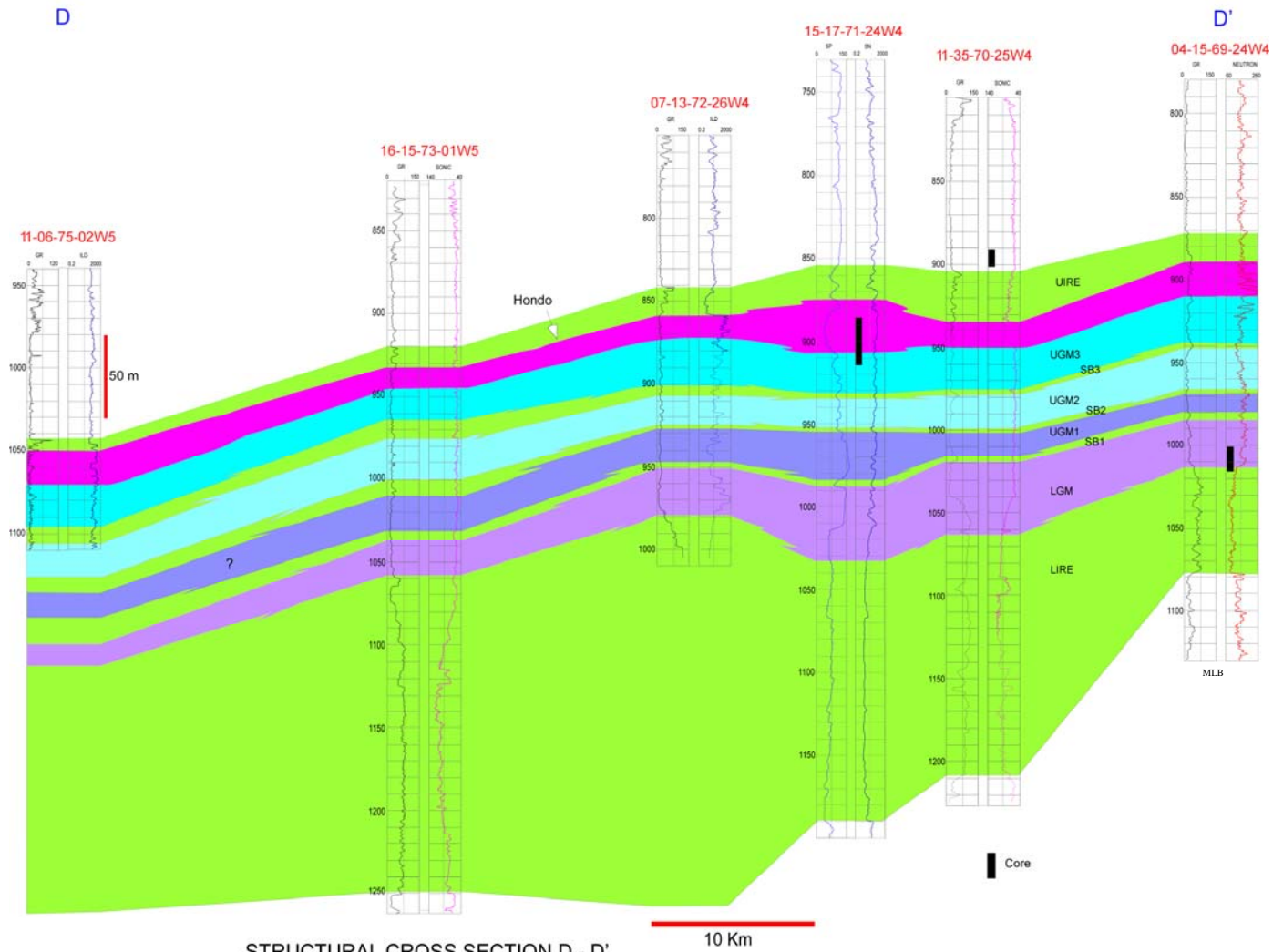
Figure 6.17 Structural cross section D-D'.
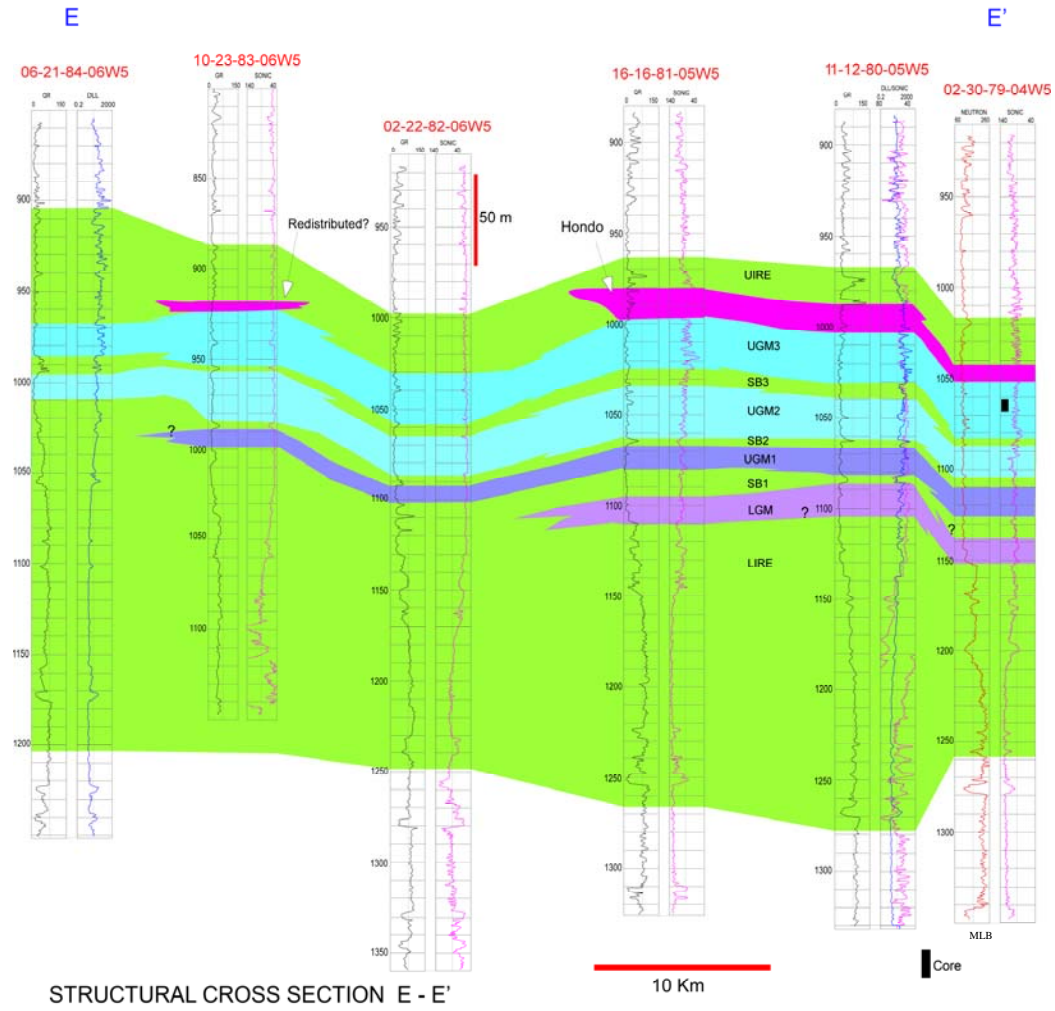
Figure 6.18 Structural cross section E-E'.

6.6 Hondo Depositional Environment

Interpretation of the depositional environment for the Hondo primary sulphates is based on the integration of core logging, petrography, isotopic geochemistry, and stratigraphic correlations. Comparison with modern examples of evaporitic basins is also useful.

Hondo primary sulphates in the UGM3 and LGM are interpreted to have been deposited in subaqueous salinas or lagoons, either in a series of relatively small ponds or in a large lagoon striking with an orientation of about 15° to 30° NW. Evaporite deposition was possible because depressions had formed near the platform margin at least during LGM time and again during UGM3 time.

The distribution of the Hondo primary sulphates in the Lower Grosmont and Upper Grosmont 3 is interpreted in two scenarios:

1. In "small ponds" with an average size of two by two or three townships (20x20 km to 20x30 km) (Figure 6.19); thickness varies from 5 to 35 m and differs from pond to pond.

2. In a larger pond or "lagoon" which includes the "small ponds" (Figure 6.19).
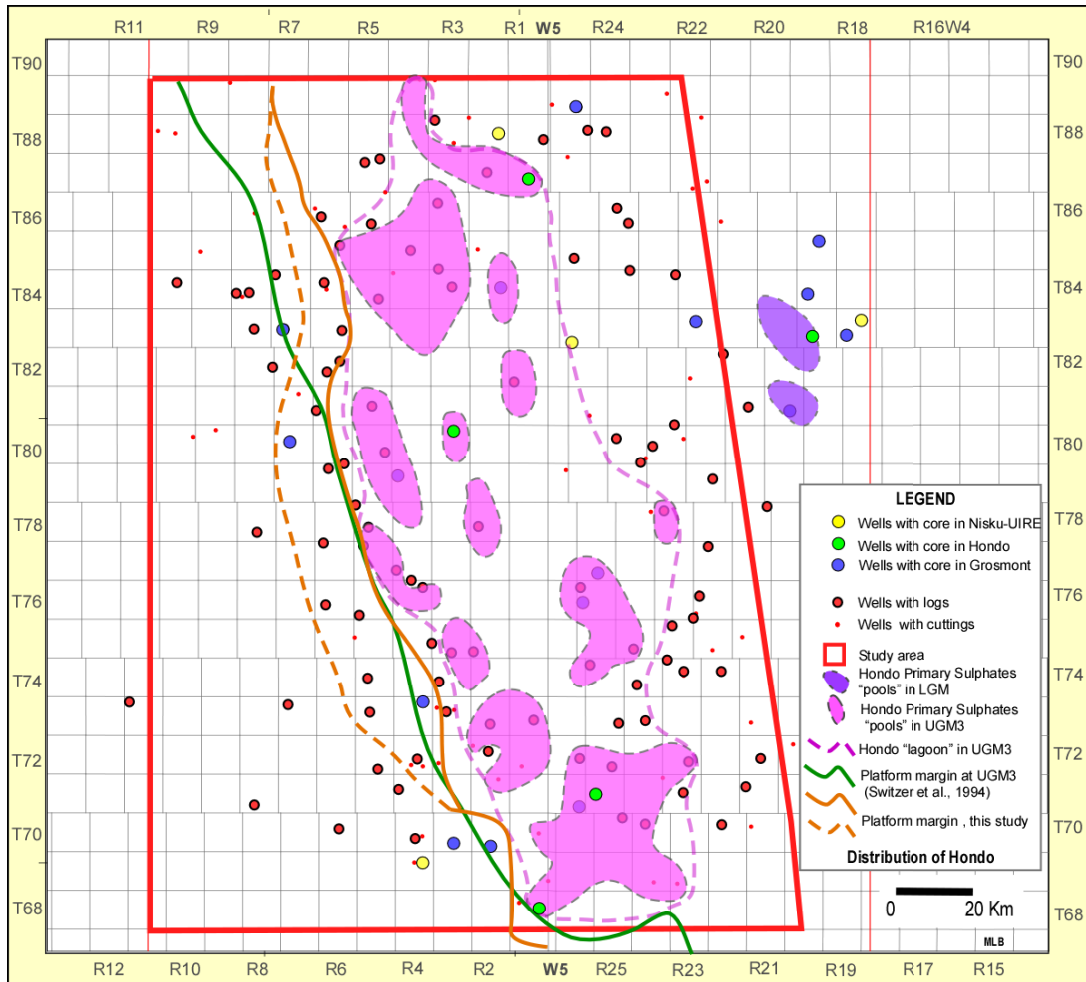
Figure 6.19 Geometry and distribution of the Hondo primary sulphates.

The "small ponds" represent the present distribution of Hondo primary sulphates. However, they may not correspond to the original distribution at the time of deposition. Dissolution in one or several phases, ranging from the time to deposition to the present, of the sulphates may have affected the original depositional distribution and geometry of the Hondo such that the small ponds are remnants of a large sheet of evaporites. Outside of the "Hondo lagoon" in the UGM3, in the northeastern part of the study area, many cores contain brecciated and bitumen-supported intervals (Figure 4.21). Such intervals may represent

142

sulphate removal. These intervals appear to be correlatable over tens of km outside of the study area to the north and northeast, where much better core control is available (Dembicki, 1994; Barrett and Hopkins, 2010). At least some bitumen-supported intervals within the Upper Grosmont 3 are probably dissolved parts of the Hondo, which are now filled with bitumen, as discussed in Chapter 4.

The size and lateral extent of regional evaporite deposition is relevant for two aspect of the Grosmont reservoir: 1) how much mesohaline to haline brine was available for reflux dolomitization (Jones et al., 2003); 2) did Hondo ever formed an effective seal for hydrocarbon migration and entrapment? While this study provides interesting leads, a detailed discussion of these questions is beyond the scope of this study.

Based on strontium, sulphur, oxygen, and carbon isotope data, the Hondo brines were of marine parentage, and the sulphates were precipitated from Late Devonian evaporated seawater. Salinities in the Hondo brines appear to have been between mesohaline (1–3 times salinity of seawater) and less than halite saturation (about 10 times salinity of seawater), providing for the widespread formation of dolomite and calcium sulphate (gypsum and/or anhydrite). Most Hondo primary sulphates likely were deposited as gypsum layers subaqueously. At times the brines must have exceeded halite saturation, as shown by the occasional presence of halite hoppers. Halite that was previously precipitated is now completely dissolved. No evidence of a shoreline was found in the cores described.

The main lithofacies in the Hondo primary sulphates correspond to laminated anhydrite and dolomudstone, interpreted to have been deposited in quiet waters at depths between 2 to 5 m within the photic zone. Intervals where many fine dolomitic layers are interbedded with comparatively few gypsum/anhydrite layers may have been formed during periods of increased rainfall or during a temporary decrease in salinity. Some distorted and synsedimentary breccias could have been formed during seasonal storms or by an enhance inflow of normal marine water.

The rate of deposition of the Hondo primary sulphates can be estimated by comparison with modern evaporite environments. The estimated depositional rates for evaporites and other types of sediment are shown in Table 6.1. Using these rates, deposition of the Hondo primary sulphates might have taken place within a short interval, as little as 750 to 30,000 years.

Type of sediments	Environment	Accumulation Rate
Sulphates and Carbonates	Sabkha (supratidal)	1 m /1000 yrs Progradation 1 km /1000 yrs
Sulphates	Shallow subaqueous	1-40 m /1000 yrs
Sulphates	Deep subaqueous	1-2 m /1000 yrs
Halite	Shallow subaqueous	10-100 m /1000 yrs
Halite	Deeper subaqueous	1-10 m /1000 yrs
Reefal carbonates	Shallow water	1-3 m/1000 yrs
Non-reefal carbonates	Shelf	1-3 cm /1000 yrs
Pelagic carbonates	Deep sea (Jurassic>)	0.05-0.1 cm /1000yrs

Table 6.1 Estimated depositional rates: evaporites and several other types of sediments (from Schreiber and Hsu, 1980).

144

6.7 MODERN ANALOGS

In terms of scale, there are no recent evaporite depositional analogous to Hondo primary evaporites. However, limited comparison can be drawn between the Hondo, the Arabian Gulf region and the Great Bahama Bank.

In the southern part of the Arabian Gulf, the Abu Dhabi region has been recognized as a coastal *sabkha* (Alsharhan and Kendall, 1994; Warren, 2006). *Sabkha* (sebkha or sabkhah) is an Arabic word for a salt flat and describes extensive, barren, salt-encrusted, and periodically flooded coastal and inland mudflats. It also implies intrasediment evaporitic growth under a flat geomorphic surface (Warren and Kendall, 1985).

Conditions for a sabkha environment are a combination of the following parameters:

1. Semiarid climate with common day time high temperatures of 40 to 50°C.

2. Low humidity conditions, precipitation lower than 5 cm/year with the presence of frequent winds.

3. Marine restrictions or enclosed basins, where outflow is lower than inflow.

4. Low input of terrigenous sediments.

These conditions are common in near-equatorial terrains that are generally dry but may have short wet seasons; these terrains constitute the largest areas of formation of present and ancient evaporites (Curtis et al., 1963; Evans et al. 1969; Butler et al., 1982; Sonnenfeld, 1984; Evans, 1995; Steinhoff and Strohmenger, 1999). During the Middle to Late Devonian (Givetian-Famennian), Alberta was located close to the equator and climatic conditions were likely the same as

present conditions in the Middle East. Although the physical and chemical conditions at the time of evaporation could have been very similar to those ones in the Abu Dhabi coast, the Hondo sulphates were not formed in a sabkha environment. This is clearly indicated by the evaporite facies recognized in core (Chapter 3) and by the spatial distribution as shown in Figure 6.19.

The Great Bahamas Bank can be considered an analog in size for the Grosmont platform (Figure 6.20). However, no evaporites analogous to those in the Hondo are forming or have formed in the Great Bahama Bank. The likely reason for the absence of evaporite deposition on the Great Bahama Bank is the absence of a "sill" or raised platform edge, which could restrict inflow and outflow of seawater sufficiently for evaporation to create mesohaline or haline brines.
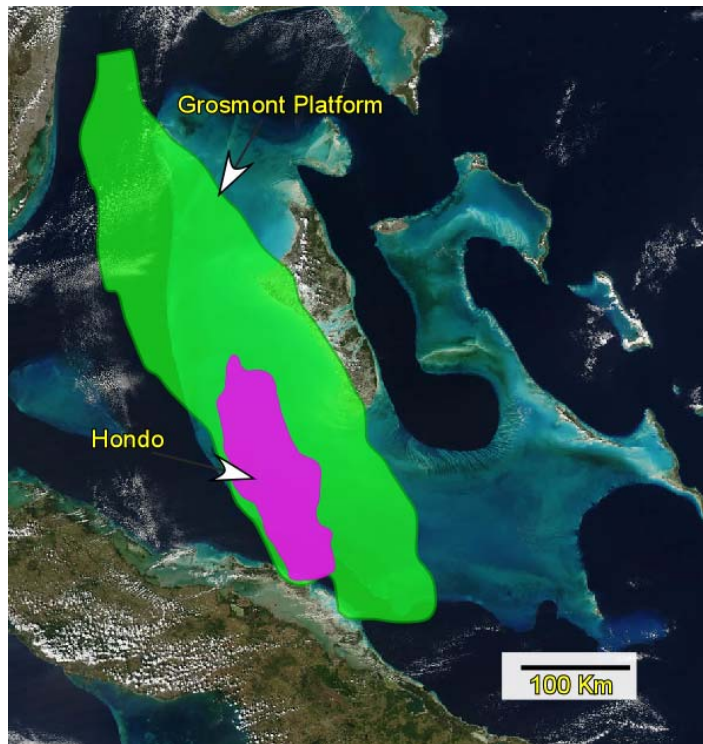
Figure 6.20 Great Bahamas Bank represents an analog in size for the Grosmont Formation (photograph taken from www.maps.google.ca).

CHAPTER 7

CONCLUSIONS AND FUTURE WORK

7.1 Conclusions

This study set out to provide new insights into the depositional environment and distribution of the Hondo, its relationship with the Grosmont Formation, and to supplement the understanding of the geometry and oil trapping characteristics in the Grosmont, and five specific objectives as follows:

1. Delineation of the spatial distribution of Hondo evaporites.

2. Better define the western margin of the Grosmont platform.

3. Investigate the sedimentological and diagenetic characteristics of the Hondo.

4. Determine the depositional and sedimentological evolution of the Hondo evaporites, and to suggest possible recent analogs for the Hondo.

5. Determine the role of the Hondo evaporites as a potential reservoir seal.

All of these objectives have been successfully addressed.

Objective 1:

The Hondo primary sulphates presently occur in a number of relatively small ponds of about 10-30km x 10-30 km, with thicknesses of a few meters each. If these ponds represent the depositional distribution, the Hondo primary evaporites were deposited in a series of small, shallow subaqueous salina ponds. Alternatively, the Hondo primary evaporites were deposited in an extensive

lagoon, and their present distribution represents the remnants after post-depositional (mainly karstic) dissolution.

Objective 2:

a) The western margin of the Grosmont platform can be defined in the southern part of the study area on the bases of several characteristics, including: 1) thickness reduction of Grosmont units from east to west; 2) a "bulge" where sedimentology predicts a ramp profile; 3) decrease in carbonate content from east to west; 4) sporadic occurrence of late-diagenetic saddle dolomite and sparry calcite cements. In the central and northern part of the study area the above characteristics cannot define the platform margin any more accurately than in a band that is two to three townships wide. Despite these short comings, the newly defined platform margin roughly coincides with the platform margin as previously shown in Geological Atlas of the Western Canada Sedimentary Basin (Switzer et al., 1994).

b) The location of the platform margin appears to have migrated from east to west through time.

c) During LGM time the platform margin was defined by the underlying Leduc reef trend. During UGM3 time the platform margin was defined by syndepositional faulting several townships farther west.

Objective 3:

a) Evaporite minerals in the Hondo are gypsum and anhydrite, the latter being the most abundant. Halite was formed locally. Its former presence is indicated only by occasional hopper molds.

b) The sulphates can be grouped in three categories: primary sulphates, secondary sulphates, and diagenetic anhydrite. The first group shows primary depositional features in five lithofacies: laminated anhydrite and dolomudstone, mosaic anhydrite with microbial mats, enterolithic anhydrite/contorted bedded anhydrite, displacive-nodular anhydrite, and disrupted bedding anhydrite and breccias. Secondary sulphates are represented by anhydrite nodules and/or as cement in molds and in fractures throughout the Grosmont, especially in the UGM3, the UGM1, and the LGM.

c) The Grosmont Formation was deposited in four major depositional cycles, represented by the Lower Grosmont (LGM) and Upper Grosmont 1, 2, 3, respectively. Belyea (1952) considered the Hondo evaporites to be a separate formation. However, the Hondo primary sulphates, or "evaporites," are part of the Upper Grosmont 3 (UGM3) and Lower Grosmont, where the evaporites occur in place of the normal carbonate facies.

d) Considering that the Hondo is stratigraphically is replacing carbonate facies within the UGM3 and LGM, the diagenesis of the Hondo must be considered in the context of the diagenesis of the entire Grosmont Formation. The most important diagenetic processes were dolomitization, dissolution (mainly during karstification, but probably also earlier), anhydritization-gypsification, chemical

149

compaction, dolomite cementation, calcite cementation and fracturing, and oil/bitumen emplacement.

e) Two types of dolomites are recognized in the Hondo/Grosmont: R1 which was formed syndepositionally or during shallow-burial by brine reflux, whereas R2 was formed postdepositionally by recrystallization of R1, or directly by relatively warm fluids during burial.

f) The presence of few crystals of saddle dolomite and possible hydrothermal calcite cements in two wells suggests that "hot" fluids ascended through localized fractures.

g) Calcite cement was formed either from meteoric water (during the Laramide orogeny or in the Tertiary period) or at elevated temperatures from fluids ascending via faults.

Objective 4:

a) The location of primary Hondo evaporite deposition in the UGM3 near the western edge of the Grosmont platform is best explained by syndepositional faulting, which may have raised the platform margin to such an extent that a lagoon formed between the platform margin and a paleo-shoreline much farther to the east (now eroded). On the other hand, deposition of Hondo evaporites in the Lower Grosmont, farther east on the Grosmont platform, was facilitated the presence of the Leduc reef-trend, which created restricted conditions to the east.

b) Hondo deposition took place under semi-arid to arid conditions. A possible modern analog with respect to climatic conditions is the Abu Dhabi coast in the

Arabian/Persian Gulf. In terms of the size of the carbonate platform, the Great Bahama Bank provides a recent analog, albeit without evaporite deposition.

c) The brines that formed the Hondo evaporites are of marine parentage, based on strontium, sulphur, oxygen, and carbon isotope data. The salinity of the evaporated sea water ranged from mesohaline (1-3x salinity of seawater) to halite saturation (about 10x salinity of seawater).

Objective 5:

The role of the Hondo as a "seal" for hydrocarbon migration and entrapment is difficult to assess because it cannot be ascertained whether the evaporites (sulphates and halite) originally formed a regionally extensive deposit on the scale of the entire study area, and how much was removed by post-depositional dissolution. In the eastern part of the Grosmont platform, the Hondo evaporites appear to have been dissolved, replaced by solution-collapse breccias and "bitumen supported intervals", which is a peculiar rock type that consist of bitumen-cemented, fine- to medium-crystalline dolomite crystals. On the other hand, in the western part of the study area the Hondo primary sulphate "pools" may form effective reservoir seals on the scale of the sizes of these "pools". However, it is likely that hydrocarbons passed around these "pools' wherever the carbonates had sufficient permeability.

7.2 Future Work

1. The presence of saddle dolomite in wells 01-09-70-03W5 and 08-16-87-01W5 suggests the presence of faulting in the areas around these wells. Future work should attempt to find the location of more faults with a variety of methods, including, but not restricted to, petrography (identification of more saddle dolomite and hydrothermal calcite cements), and seismic.

2. Evaluate the possibility that hot fluids migrated from the Precambrian basement along reactivated faults into the Devonian strata in the area of the Grosmont platform. Fluid inclusions analysis of saddle dolomite and other dolomites could provide information on timing of dolomitization processes; fluid inclusions in the sulphates could provide a measure of the salinity at the time when the original minerals were formed. Cathodoluminiscence would be useful in identifying the timing of dolomitization. These investigations could enhance understanding of diagenetic processes in the study area.

REFERENCES

AL-AASM, I.S., TAYLOR, B.E., AND SOUTH, B., 1990, Stable isotope analysis of multiple carbonate samples using selective acid extraction. Chemical Geology, v.80, p. 199-125.

ALSHARHAN, A.S. AND KENDALL, C., 1994, Depositional Setting of the Upper Jurassic Hith Anhydrite of the Arabian Gulf: An Analog to Holocene Evaporites of the United Arab Emirates and Lake MacLeod of Western Australia, American Association of Petroleum Geologists Bulletin, v. 78, p. 1075 – 1096.

AMIEUX, P., 1980, Exemple d'un passage des black shales aux evaporites dans le Ludien (Oligocene Inferieur, du basin de Mormoiron (Vaucluse, Sud-Est de la France, Bulletin Centre de Recherches Exploration-Production Elf Aquitaine, 4: 281-307.

AMTHOR, J.E., MOUNTJOY, E.W., AND MACHEL, H.G., 1993, Subsurface dolomites in Upper Devonian Leduc buildups, central part of Rimbey-Meadowbrook reef trend, Alberta, Canada, Bulletin of Canadian Petroleum Geology, v. 41, p. 164-185.

AMTHOR, J.E., MOUNTJOY, E.W., AND MACHEL, H.G., 1994, Regional-scale porosity and permeability variations in Upper Devonian Leduc buildups: implications for reservoir development and prediction in carbonates, American Association of Petroleum Geologists Bulletin, v. 78, p. 1541-1559.

ARMSTRONG, S.C., STRUCHIO, N., AND HENDRY, N.J., 1998, Strontium isotope evidence on the chemical evolution of pore waters in the Milk River aquifer, Alberta, Canada, Applied Geochemistry, v.13, p. 463-467.

ANDRICHUK, J.M., 1958, Stratigraphy and facies analysis of Upper Devonian reefs in Leduc, Stettler, and Redwater areas, Alberta, American Association of Petroleum Geologists Bulletin, v. 42, p. 2189-2222.

ARTHUR, M., ANDERSON, T., KAPLAN, I., VEIZER, J AND LAND, L., 1983, Stable isotopes in sedimentary geology. SEPM short course No. 10. Dallas.

ARVIDSON, R.S., AND MACKENZIE, F.T., 1999, The dolomite problem: Control of precipitation kinetics by temperature and saturation state, American Journal of Science, v. 299, p. 257-288.

BARRET, K., AND HOPKINS, J., 2010, Stratiform Carbonate Breccias of the Grosmont Formation, Alberta, Abstract, AAPG Conference, Calgary.

BELYEA, H.R., 1952, Notes on the Devonian System of the north-central plains of Alberta. Geological Survey of Canada, Paper 52-27.

BELYEA, H.R., 1956, Grosmont Formation in the Loon Lake area, Journals of Alberta Society of Petroleum Geologists, v 4, p 66-69.

BELYEA, H.R., 1964, Upper Devonian, part II, Woodbend, Winterburn and Wabamun Groups, *in* McCrossan, R.G., and Glaister R.P., eds., Geological History of Western Canada: Alberta. Society of Petroleum Geologists, Calgary, p. 66-68.

BLAKEY, 2010, Middle Devonian, *in* Paleogeography and Geologic Evolution of North America. Retrieved from http://jan.ucc.nau.edu/~rcb7/namD385.jpg.

BLOUNT, C. W., AND DICKSON, F.W., 1969, The solubility of anhydrite ($CaSO_4$, in $NaCl-H_2O$ from 100 to 450°C and 1 to 1000 bars, Geochimica et Cosmochimica Acta, 33, p. 227–245.

BRASS, G.W., 1976, The variation of the marine $^{87}Sr/^{86}Sr$ ratio during Phanerozoic time: interpretation using a flux model, Geochimica et Cosmoschimica Acta, v.40, p.721-730.

BROOKS, P W., FOWLER, M G., AND MACQUEEN, R. W., 1988, Biological marker conventional organic geochemistry of oilsands/heavy oils, Western Canada Basin, Organic Geochemistry, v. 12, p. 519–538.

154

BUDD, D.A., 1997, Cenozoic dolomites of carbonate islands: their attributes and origin, Earth-Science Reviews, 42, p.1-47.

BURKE, W.H., DENISON, R.E., HETHERINGTON, E.A., KOEPNICK, R.B., NELSON, H.F., AND OTTO, J.B., 1982, Variation of seawater $^{87}Sr/^{86}Sr$ throughout Phanerozoic time, Geology, v.10, p.516-519.

BURROWES, G., 1977, Sedimentation and diagenesis of back-reef deposits, Miette and Golden Spike buildups, Alberta. Unpub. M.Sc. Thesis. McGill University, Montreal, 307 p.

BUTLER, G.P., KENDALL, C.G.ST.C., HARRIS, P.M., 1982. Recent evaporites from the Abu Dhabi coastal flats, *in*: Handford, G.R., Loucks, R.G., Davies, G.R., eds., Depositional and Diagenetic Spectra of Evaporites. Society of Economic Paleontologists and Mineralogists Core Workshop, v. 3, p. 33– 64.

CARPENTER, A, B., 1980, The chemistry of dolomite formation 1: The stability of dolomite, Concepts and Models of Dolomitization, i*n* Zenger, D.H., et al., eds., SEPM Special Publication. 28, p. 111–121.

CHOQUETTE, P., AND JAMES, N., 1990, Limestones: The burial diagenetic environment, *in* Mcllreath, I., and Morrow, D., eds., Diagenesis. Geosciences Canada reprint series, Ontario, p. 75-112.

CIMOLAI, M.P., SOLANKI, S.C., EDMUNDS, N.R., 2009, Passive Reservoir Heating for Improved Bitumen Recovery, Canadian Society Petroleum Conference, paper 2009-145.

CLAYTON, R.N., SKINNER, H.C., BERNER, R.A. AND RUBINSON, M., 1968, Isotopic compositions of recent South Australian lagoonal carbonates, Geochimica et Cosmochimica Acta, v 32, p. 983–988.

CLAYPOOL, E., HOLSE, W.T., KAPLAN, I.R; SAKAI, H., AND ZAK, T., 1980, The age curves of sulfur and oxygen isotopes in marine sulfate and their mutual interpretation, Chemical Geology, v.28, p. 199–260.

CODY, W.R., and HULL, A.B., 1980, Experimental growth of primary anhydrite at low temperatures and water salinities: Geology, v. 8, p. 505-509.

CONNOLLY, C. A., WALTER, L. M., BAADSGAARD, H., AND LONGSTAFFE, F., 1990, Origin and evolution of formation waters, Alberta Basin, Western Canada Sedimentary Basin. II. Isotope systematics and water mixing, Applied Geochemistry, v. 5, p. 397–413.

COPLEN, T. B.M., AND KROUSE, H. R., 1998, Sulphur isotope data consistency improved, Nature, v.392, p. 32.

CRAIG, H., 1957, Isotopic standards for carbon and oxygen and correction factors for mass-spectrometric analysis of carbon dioxide, Geochimica et Cosmochimica Acta, v. 12, p. 133–149.

CRAIG, H., 1961, Isotopic variations in meteoric waters, Science, v.133, p. 1702-1703.

CRUFT, T. ., AND CHAO, P. C., 1970, Nucleation kinetics of the gypsum-anhydrite system, 3rd Symposium on Salt, Cleveland, Northern Ohio Geological Society, p. 109–118.

CURTIS, R., EVANS, G., KINSMAN, D., AND SHEARMAN, D., 1963, Association of dolomite and anhydrite in the recent sediments of the Persian Gulf, Nature, v. 197, p. 679–680.

CUTLER, W.G., 1983, Stratigraphy and sedimentology of the Upper Devonian Grosmont Formation, Alberta, Canada, Bulletin of Canadian Petroleum Geology, v.31, p. 282-325.

DAVIES, G.R., AND LUDLAM, S.D., 1973, Origin of laminated and graded sediments, Middle Devonian of western Canada, Geological Society of America Bulletin, v. 84, p. 3527-3546.

DEAN, W.E., AND ANDERSON, R.Y., 1982, Continuous subaqueous deposition of the Permian Castile Evaporites, Delaware Basin, Texas and New

Mexico, *in* Handford, C.R., Loucks, R.G., and Davies, G.R., eds., Depositional and Diagenetic Spectra of Evaporites—A Core Workshop: Society of Economic Paleontologists and Mineralogists, Core Workshop 3, p. 324-353.

DEMBICKI, E., 1994, The Upper Devonian Grosmont Formation: well log evaluation and regional mapping of heavy oil carbonate reservoir in northeastern Alberta, unpublished M.Sc. Thesis, University of Alberta, Edmonton, 221p.

DEMBICKI, E.A., AND MACHEL, H.G., 1996, Recognition and delineation of paleokarst zones by the use of wireline logs in the bitumen-saturated Upper Devonian Grosmont Formation of northeastern Alberta, Canada, American Association of Petroleum Geologists Bulletin, v. 80, p. 695-712.

De GROOT, K, 1967, Experimental dedolomitisation. Journal Sedimentary Petrology, 37, I216-I22O.

DRIVET, E., AND MOUNTJOY, E., 1997, Dolomitization of the Leduc Formation Upper Devonian,, southern Rimbey-Meadowbrook reef trend, Alberta, Journal of Sedimentary Research, v. 67, p. 411-423.

ENERGY RESOURCES CONSERVATION BOARD (ERCB)., 2010, Energy Reserves 2009 and Supply/Demand Outlook 2010-2019, Statistical Series, ST98-2010.

EVAMY, D., 1967, Dolomitization and the Development of Rhombohedral Pores in Limestones, Journal of Sedimentary Research, v.37, p. 1204–1215.

EVANS, G. 1995, "The Arabian Gulf: a modern carbonate-evaporite factory; a review", Cuadernaos de Geologia Iberica, v. 19, p. 61-96.

EVANS, G., SCHMIDT, V., BUSH, P., NELSON, H., 1969. Stratigraphy and geologic history of the sabkha, Abu Dhabi, Persian Gulf, Sedimentology, v. 12, p. 145– 159.

FRIEDMAN, G.M., 1973, Petrographic data and comments on the depositional environment of the Miocene sulfates and dolomites at Sites 124, 132 and 134, western Mediterranean Sea, i*n* Ryan, W., et al., eds., Initial Reports of the Deep Sea Drilling Project, v. 13, Part 2, p. 695-708.

FRIEDMAN I. AND O'NEIL J.B., 1977, Compilation of stable isotope fractionation factors of geochemical interest, *in* . Fleischer, M., eds., Data of Geochemistry. US Geological Survey., Prof. Paper 440-KK, 6th ed.

FOLK, R.L., 1965, Some aspects of recrystallization in ancient limestones, *in* Pray, L.C., and Murray, R.C., eds., Dolomitization and Limestones Diagenesis, SEPM Special Publications, v 13, p. 14–48.

FLÜGEL, E., 1982, Microfacies Analysis of Limestones, New York, Springer-Verlag, 633 p.

GARRELS, M., AND PERRY, E., 1974, Cycling of carbon, sulfur, and oxygen through geologic time, *in* Goldberg, E., eds., The Sea, v. 5. Wiley-Interscience, p. 330-336.

GILLIVRAY, J.G., AND MOUNTJOY, E.W., 1975, Facies and related reservoir characteristics Golden Spike reef complex, Alberta, Bulletin of Canadian Petroleum Geologist, v. 23, p.753-809.

GREGG, J.M., AND SIBLEY, D.F., 1984, Epigenetic dolomitization and the origin of xenotopic dolomite texture, Journal of Sedimentary Petrology, v.54, p.908-931.

HARDIE, L. A., 1967, The gypsum-anhydrite equilibrium at one atmosphere pressure. *American Mineralogist Journal*, v. 52, p.172-200.

HARDIE, L. A., 2003, Anhydrite and Gypsum, *in* Middleton, G., eds., Encyclopedia of sediments and sedimentary rocks. Kluwer Academic Publishers, Dordrecht, Netherlands, p. 16-18.

HARRISON, R., 1982, Geology and production history of the Grosmont carbonate pilot project, Alberta, Canada, *in* Meyer, R., Wynn, J., and

Olson, J., eds., The future of heavy crude and tar sands: Second international conference on heavy crude and tar sands, Caracas, Venezuela, February 7-17, v 1, p. 199-204.

HARRISON, R., 1984, The bitumen-bearing Paleozoic carbonate trends of northern Alberta, *in* Meyer, R., Early, J., Barnea, J., and Johnston, L., eds., Convention Exploration for heavy crude oil and bitumen, AAPG Research conference, Santa Maria, California.

HARRISON, R., AND MCINTYRE, B., 1981, The geologic setting of the Grosmont thermal recovery project, northeastern Alberta: Alberta oil sands technology and Research Authority seminar on advances in petroleum recovery and upgrading technology, Calgary, May 24-26, 11p.

HAYS, P. D., AND GROSSMAN, E. L., 1991, Oxygen isotopes in meteoric calcite cements as indicators of continental palaeoclimate, Geology, v. 19, p. 441- 444.

HEAD, I., JONES, D., AND LARTER, S., 2003, Biological activity in the deep subsurface and the origin of heavy oil. Nature, p. 1-36.

HEIN, F. J., 2006, Heavy oil and oil tar, sands in North America; an overview and summary of contributions, Natural Resources Research, New York, v. 15, no. 2, p. 67-84.

HEIN, F., MARSH, R., AND BODDY, M., 2008, Overview of the Oil Sands and Carbonate Bitumen of Alberta: Regional Geologic Framework and Influence of Salt-Dissolution Effects, Search and Discovery Article No. 10144, 2008.

HOLSER,W.T., KAPLAN, I.R., SAKAI, H AND ZAK, I., 1979, Isotope geochemistry of oxygen in the sedimentary sulfate cycle, Chemical Geology, v.25, p. 1–17.

HOFFMANN, C. F., AND STRAUSZ, O. P., 1986, Bitumen accumulation in Grosmont Platform complex, Upper Devonian, Alberta, Canada, American Association of Petroleum Geologists, v.70, p. 1113-1128.

HUEBSCHER., H., 1996, Regional controls on stratigraphic and diagenetic evolution of Woodbend Group carbonates, North-central Alberta, Canada, unpublished PhD. Thesis, University of Alberta, 231p.

HUEBSCHER, H., AND MACHEL, H.G., 2004, Reflux and Burial dolomitization in the Upper Devonian Woodbend Group of North-central Alberta,Canada: Extended Abstract, Dolomite Conference, CSPG, Calgary.

HUNT, J.M., 1996, Petroleum Geology and Geochemistry, 2nd edition. W.H Freeman, New York, 743 p.

HURLEY, N.F., AND LOHMANN, K.C., 1989, Diagenesis of Devonian reefal carbonates in the Oscar Range, Canning Basin, western Australia, Journal of Sedimentary Petrology, v. 59, p. 127-145.

INTERNATIONAL STRATIGRAPHIC GUIDE., 1994, International subcomission on stratigraphic classification of IUGS, International commission on stratigraphy. Amos Salvador Editor. Boulder, Colorado.

ISOTOPE SCIENCE LABORATORY, DEPARTMENT OF PHYSICS AND ASTRONOMY, UNIVERSITY OF CALGARY., 2010, Sulfur Isotope analyses by Continuous-Flow Isotope Ratio Mass Spectrometry. (online). Available from: http://www.ucalgary.ca/uofcisl/files/uofcisl/Prism_34S.doc. Accessed 2010 July.

ISOTOPE SCIENCE LABORATORY, UNIVERSITY OF CALGARY., 2010, Analysis of δ^{13}C & δ^{18}O values of carbonate minerals. (online). Available from: http://www.ucalgary.ca/uofcisl/files/uofcisl/VG903_carbs.doc. Accessed 2010 July.

JONES, G.D., SMART, P.L., WHITAKER, F.F., ROSTRON, B.J., AND MACHEL, H.G., 2003, Numerical modeling of reflux dolomitization in the Grosmont platform complex (Upper Devonian), Western Canada sedimentary basin, American Association of Petroleum Geologists Bulletin, v. 87, p. 1273-1298.

KEITH, M. L., AND WEBER, J. N., 1964, Carbon and oxygen isotope composition of selected limestones and fossils, Geochimical et Cosmochimica Acta, v. 28, p. 1787–1816.

KENDALL, A., 1992, Evaporites. Response to sea level changes, *in* Walker, R., and James, N., eds., Facies models, Geoscience Canada Reprint Series 1, Toronto, p. 375-409.

KNAUTH, L. P., AND BEEUNAS, M., 1986, Isotope Geochemistry of Fluid Inclusions in Permian Halite with Implications for the Isotopic History of Ocean Water and the Origin of Saline Formation Waters, Geochimical et Cosmochimica Acta, v. 50, p. 419-433.

LAND, L., 1980, The isotopic and trace element geochemistry of dolomite: the state of the art, *in* Zenger. D., Dunham, J., and Ethington, R., eds., Concepts and Models of dolomitization. SEPM. Special publication, v.28, p. 87-110.

LAND L., 1983, The application of stable isotopes to studies of the origin of dolomite and to problems of diagenesis of clastic sediments, *in* Arthur, M., eds., Stable Isotopes in Sedimentary Geology. SEMP, Short Course, 10, 4-1 to 4-22.

LARTER, S., HUANG, H., ADAMS, J., BENNETT, B., JOKANOLA, O., OLDENBURG, T., JONES, M., HEAD, I., RIEDIGER, C. AND FOWLER, M., 2006, The controls on the composition of biodegraded oils in the deep subsurface: Part II - Geological controls on subsurface biodegradation fluxes and constraints on reservoir-fluid property prediction. American Association of Petroleum Geologist Bulletin, v.90, p. 921-938.

LEACH, D.L., PLUMLEE, G.S., HOFSTRA, A. H., LANDIS, G.P., ROWAN, R.L AND VIETS, J. G., 1991, Origin of late dolomite cement by CO_2-saturated deep basin brines: Evidence from the Ozark region, central United States, Geology, v.19, p. 348-351.

LIND, I. L., 1993, Loading experiments on carbonate ooze and chalk from Leg 130, Ontong Java Plateau, *in* Berger, W.., Kroenke, J., and Mayer, L., et

al., eds., Proceedings of the Ocean Drilling Program,, Scientific Results, v. 130.

LOUCKS, R.G., AND LONGMAN, M.W., 1982, Lower Cretaceous Ferry Lake anhydrite, Fairway Field, east Texas, product of shallow-subtidal deposition, *in* Handford, C., Loucks, R., and Davies, G., eds., Depositional and diagenetic spectra of Evaporites. SEPM, Calgary, Core Workshop No. 3, p. 130-173.

LUCIA, J.F., 2004, Origin and petrophysics of dolostone pore space, *in* Braithwaite, C., Rizzi, G., and Darke, G., eds., The Geometry and Petrogenesis of Dolomite Hydrocarbon Reservoirs. Geological Society of London, Special Publication 235, p. 141-155.

LUO, P., AND MACHEL, H. G., 1995, Pore size and pore throat types in a heterogeneous dolostone reservoir, Devonian Grosmont Formation, Western Canada Sedimentary Basin, American Association of Petroleum Geologists, v. 79, p.1698-1720.

LYATSKY, H; AND PANA, D., 2003, Catalogue of Selected Regional Gravity and Magnetic Maps of Northern Alberta, The Alberta Energy and Utilities Board/Alberta Geological Survey (EUB/AGS), Report 56.40 p.

MACHEL, H.G., 1985, Facies and diagenesis of the Upper Devonian Nisku Formation in the subsurface of central Alberta. Unpublished PhD. Thesis, McGill University, Montreal, 392 p.

MACHEL, H. G., 1987, Saddle dolomite as a by-product of chemical compaction and thermochemical sulphate reduction, Sedimentary Geology, v.15, p.936-940.

MACHEL, H.G., 1993, Anhydrite nodules formed during deep burial, Journal of Sedimentary Petrology, v.63, p. 83-90.

MACHEL, H. G., 1997, Recrystallization versus neomorphism, and the concept of 'significant' recrystallization in dolomite research, Sedimentary Geology, v.113, p. 161-168.

162

MACHEL, H. G., 1999, Effects of groundwater flow on mineral diagenesis, with emphasis on carbonate aquifers, Hydrogeology Journal, v.7, p.94-107.

MACHEL, H. G., 2004, Concepts and models of dolomitization - a critical reappraisal, *in* Braithwaite, C., Rizzi, G., and Darke, G., eds., The geometry and petrogenesis of dolomite hydrocarbon reservoirs, Special Publication of the Geological Society of London.

MACHEL, H. G., AND CAVELL, P. A., 1999, Low-flux, tectonically-induced fluid flow "hot flash", into the Rocky Mountain Foreland Basin, Bulletin of Canadian Petroleum Geology, v.47, p.510-533.

MACHEL, H. G., AND HAWLADER, H., 1990, Diagenesis and reservoir characteristics of the heavy-oil carbonate trend in western Canada-Preliminary Investigations of facies, diagenesis, porosity, and bitumen saturation of the Grosmont Formation, AOSTRA, reports 2 to 7. 169p.

MACHEL, H. G., AND HUNTER, I., 1994, Facies models for Middle to Late Devonian shallow marine carbonates with comparisons to modern reefs - a guide for facies analysis, Facies, v. 30, p. 155-176.

MACHEL, H. G., AND LONNEE, J., 2002, Hydrothermal dolomite – a product of poor definition and imagination, Sedimentary Geology, v. 152, p. 163-171.

MACHEL, H.G., AND MOUNTJOY, E.W., 1986, Chemistry and environments of dolomitization – a reappraisal, Earth Science Reviews, v.23, p. 175-222.

MAIKLEM, W., BEDOUT, D., AND GLAISTER, R., 1969, Classification of anhydrite: a practical approach, Bulletin of Canadian Petroleum Geology, v.17, p. 194-233.

MARQUEZ, X. M., 1994, Reservoir geology of Upper Devonian Leduc Buildups, Deep Alberta Basin, unpublished Ph.D. Thesis, McGill University, Montreal, 281 p.

MATTES, B., AND MOUNTJOY, E., 1980, Burial dolomitization of the upper Devonian Miette buildup, Jasper National Park, Alberta, *in* Zenger, D.H., et al., eds., Concepts and Models of Dolomitization. SEPM, Tulsa. v. 28**,** p. 259-297.

MCCROSSAN, R.G., 1961, Resistivity mapping and petrophysical study of Upper Devonian inter-reef calcareous shales of central Alberta, Canada, American Association of Petroleum Geologist Bulletin, v.45, p. 441-470.

MEIJER DREES, N.C., 1986, Evaporitic deposits of western Canada, Geological Survey of Canada, paper 85–20, 118 p.

MORROW, D.W., 1990, Part 2: Dolomitization models and ancient dolostones. In: I.A. McIlreath & D.W. Morrow (Eds., *Diagenesis*. Geoscience Canada, Series 4: 125-140.

MOSSOP G., AND SHEARMAN, D., 1973, Origins of secondary gypsum rock, Institute of Mining and Metallurgy Transactions, Section B, v. 82, p. 147–154.

MOSSOP, G., AND SHETSEN, I., 1994, *in* Geological Atlas of the Western Canada sedimentary Basin, Canadian Society of Petroleum Geologists and Alberta Research Council, 504p (Compilers).

MOUNTJOY, E. W., QING, H., AND MCNUTT, R., 1992, Sr isotopic composition of Devonian dolomites, western Canada: significance regarding sources of dolomitizing fluids, Applied Geochemistry, v.7, p.59-75.

MURRAY, R. C., 1964, Origin and diagenesis of gypsum and anhydrite, Journal of Sedimentary Petrology, v. 34, p. 512-523.

O'NEIL, R. O., CLAYTON, R. N., AND MAYEDA, T. K., 1969, Oxygen isotope fractionation in divalent metal carbonates, Journal of Chemical Physics, v. 51, p. 5547–5558.

PARK, W.C. and SCHOT, E.H., 1968, Stylolites: Their nature and origin, Journal of Sedimentary Petrology, v. 38, p. 175–191.

PAYTON, A., KASTER, M., CAMPBELL, D., AND THIEMENS, H., 1998, Sulfur isotopic composition of Cenozoic seawater sulfate, Science, v. 282, p. 1459-1461.

PIERRE, C., 1994, Stable isotope tracers of conditions of evaporites sedimentation and diagenesis, *in* Technical Committee, GRECO (CNRS)., eds., Evaporite sequences in petroleum exploration, v. 52, p 146-160.

PIERRE, C., AND FONTES, J. C., 1978, Isotope composition of Messininan sediments from the Mediterranean Sea as indicators of paleoenvironments and diagenesis, Initial Reports of the Deep Sea Drilling Project 42, p. 635-650.

PICHA, F., 1978, Depositional and diagenetic history of Pleistocene and Holocene oolitic sediments and sabkhas in Kuwait, Persian Gulf, Sedimentology, v. 25, p.427-450.

PONSNJAK, E., 1940, Deposition of calcium sulfate from sea water, American Journal of Science, v. 238, p. 559-568.

POTMA, K., WEISSENBERGER, J., WONG, P & MURRAY, G., 2001, Toward a sequence stratigraphic framework for the Frasnian of the Western Canadian Basin, Bulletin of Canadian Petroleum Geology, v. 49, p. 37-85.

RADKE, B. M., AND MATHIS, R. L., 1980, On the formation and occurrence of saddle dolomite, Journal of Sedimentary Petrology, v. 50, p. 1149-1168.

REZNIK, I.J., GAVRIELI, I., GANOR, J., 2009, Kinetics of gypsum nucleation and crystal growth from Dead Sea brine, Geochimica et Cosmochimica Acta, v. 73, p. 6218-6230.

RITTENHOUSE, G., 1971, Mechanical compaction of sands containing different percentages of ductile grains: a theoretical approach, Bulletin of the American Association of Petroleum Geologists, v. 55, p. 92-96.

ROUCHY, J., MONTY, P., BERNET-ROLLANDE, M., MAURIN, A., AND PERTHUISOT, J., 1985, Genese de corps carbonatés diagénétiques par réduction de sulfates dans le Miocène evaporitique du Golfe de Suez et de la Mer Rouge. *C. R.* Academic. Science, Paris, v.301, p.1193-1198.

ROOT, K G., 2001, Devonian Antler fold and thrust belt and foreland basin development in the southern Canadian Cordillera: implications for the Western Canada Sedimentary Basin, Bulletin of Canadian Petroleum Geologists, v. 49, p. 7-36.

SANZ-RUBIO, E., SANCHEZ-MORAL, S., CANAVERAS, J., CALVO, J. AND ROUCHY, J., 2001, Calcitization of Mg-Ca carbonate and Ca-sulphate deposits in a continental Tertiary basin Calatayud Basin, NE Spain, Sedimentary Geology, v.140, p.123-142.

SCHREIBER, B. C., 1978, Environments of subaqueous gypsum deposition, *in* Dean, W., and Schreiber, B.C., eds., Marine Evaporites. Society of Economic Paleontologist and Mineralogists, Oklahoma., short Course Notes 4, p. 43-73.

SCHREIBER, B. C., AND HSU, K. J., 1980, Evaporites,Developments in Petroleum Geology, vol.2.Applied science, England, p. 87–138.

SCHREIBER, B. C, AND KINSMAN, D., 1975, New observations in the Pleistocene evaporites of Montallegro, Sicily and a modern analog, Journal of Sedimentary Petrology, v. 45, p. 469-479.

SCHREIBER, B. C., AND TABAKH, M. E., 2000, Deposition and early alteration of evaporites, Sedimentology, v. 47, p. 215–238.

SCHOLLE, P. A., AND D. S. ULMER-SCHOLLE., 2003, A Color Guide to the Petrography of Carbonate Rocks: Grains, textures, porosity, diagenesis: Tulsa, OK, American Association of Petroleum Geologists Memoir 77, 474 p.

166

SHEARMAN, D. J., 1963, Recent anhydrite, gypsum, dolomite, and halite from the coastal flats in the Arabian shore of the Persian Gulf. Geological Society of London, v. 1607, p. 63-65.

SHEARMAN, D. J., 1970, Recent halite rock, Baja California, Mexico: Institute of Mining and Metallurgy, Transactions, series B, v. 79, p. 155-162.

SHEARMAN, D. J., 1985, Syndepositional and late diagenetic alteration of primary gypsum to anhydrite, *in*. Schreiber, B.C., eds., Sixth International Symposium on Salt. Salt Institute, Alexandria, Virginia., v. 1, p. 41-50.

SHINN, E. A., AND ROBBIN, D. M., 1983, Mechanical and chemical compaction in fine-grained shallow-water limestones: Journal of Sedimentary Petrology, v. 53, p. 695–618.

SIBLEY, D.F. AND GREGG, J.M., 1987, Classification of dolomite rock textures, Journal of Sedimentary Petrology, v. 57, p. 967-975.

SONNENFELD, P., 1984, Brines and evaporites. New York, N.Y. Academic Press, 631 p.

STEINHOFF, I., AND STROHMENGER, C., 1999, Facies differentiation and sequence stratigraphy in ancient evaporite basins—an example from the basal Zechstein (Upper Permian of Germany), Carbonates and Evaporites, v. 14, p. 146-181.

STOAKES, F. A., 1980, Nature and control of shale basin fill and its effect on reef growth and termination: Upper Devonian Duvernay and Ireton Formations of Alberta, Canada, Bulletin of Canadian Petroleum Geology, v. 28, p. 345-410.

SWITZER, S., HOLLAND, W., CHRISTIE, D., GRAF, G., HEDINGER, A., MCAULEY, R., WIERZBICKI, R., AND PACKARD, J., 1994, Devonian Woodbend-Winterburn strata of the Western Canada Sedimentary Basin,

in Mossop, G., and Shetsen, I., eds., Geologic Atlas of the Western Canada Sedimentary Basin.Calgary, Canadian Society of Petroleum Geologists and Alberta Research Council, p. 165-195.

THERIAULT, F., 1988, Lithofacies, diagenesis, and related reservoir properties of the Upper Devonian Grosmont Formation, northern Alberta, Bulletin of Canadian Petroleum Geology, v. 36, p. 52-69.

THERIAULT, F., AND HUTCHEON, I., 1987, Dolomitization and calcitization of the Devonian Grosmont Formation, northern Alberta, Journal of Sedimentary Petrology, v. 57, p. 955-966.

TUCKER, M., AND WRIGHT, P., 1990, Carbonate Sedimentology. Oxford, London. Blackwell Scientific Publications, 481 p.

VEIZER, J., AND COMPSTON, W., 1974, $^{87}Sr/^{86}Sr$ composition of seawater during the Phanerozoic, Geochimica et Cosmochimica Acta, v.38, p. 1461-1484.

VEIZER, J., HOLSER, W.T. AND WILGUS, C.K., 1980, Correlation of $^{13}C/^{12}C$ and $^{34}S/^{32}S$ secular variations, Geochimica et Cosmochimica. Acta v. 44, p. 579-587.

VEIZER, J., ALA, D., AZMY, K., BRUCKSCHEN, P., BUHL, D., STRAUSS, H., 1999. $^{87}Sr/^{86}Sr$, $\delta^{13}C$ and $\delta^{18}O$ evolution of Phanerozoic seawater, Chemical Geology, v. 161, p. 59-88.

WAGNER, P., NELSON, R., LONNEE, J., COSTELLO, M., WHALE, R., MCKINZIE, W., JENNINGS, J., BALZARINI, M., REED, D., AL BAHRY, A., AND WATSON, R., 2010, Fracture Characterization of a Giant Unconventional Carbonate Reservoir, Alberta, Canada. Abstract, AAPG Conference, Calgary.

WANLESS, H. R., 1979, Limestone response to stress: pressure solution and dolomitization, Journal of Sedimentary Petrology, v. 49, p. 437-462.

WARRAK, M., 1974, The petrology and origin of dedolomitised veined or brecciated carbonated rocks, the cornieules, in the Fréjus region, French Alps, J. Geol. Geol. Soc. London, v. 130, p. 229–247

WARREN, J. K., 2006, Evaporites; sediments, resources and hydrocarbons. Berlin, Germany. Springer. 1035 p.

WARREN, JOHN., AND KENDALL, C., 1985, Comparison of Sequences Formed in Marine Sabkha (Subaerial) and Salina (Subaqueous) Settings – Modern and Ancient, American Association Petroleum Geologists Bulletin, v. 69, p. 1013 - 1023.

WENDTE, J.C., 1992, Evolution of the Judy Creek complex, a late middle Devonian isolated platform-reef complex in west-central Alberta, *in* Wendte, J., Stoakes, F., and Campbell, C., eds., Devonian–Early Mississippian Carbonates of the Western Canada Sedimentary Basin: A Sequence Stratigraphic Framework. SEMP, Short Course Notes No. 28, p. 89–125.

WENDTE, J. C, 1994, Cooking Lake platform evolution and its control on Late Devonian Leduc reef inception and localization, Redwater, Alberta, Bulletin of Canadian Petroleum Geology, v. 42, p. 499–528.

WHALEN, M., EBERLI, G., BUCHEM, V., MOUNTJOUY, E., & HOMEWOOD, P., 2000, Bypass margin, basin-restricted wedges, and platform-to-basin correlation, Upper Devonian, Canadian Rocky Mountains: implications for sequence stratigraphy of carbonate platform systems, Journal of Sedimentary Research, v. 70, p. 913-936.

ZHAO., Y., 2009, Petrophysical properties of Bitumen from the Upper Devonian Grosmont Reservoir, Alberta, Canada, unpublished M.Sc. Thesis, University of Alberta. 183 p.

APPENDIX 1: LIST OF WELL INTERVALS WITH CUTTINGS THAT HAVE BEEN INVESTIGATED

Well	Interval (metres)
02-29-68-01W5	1127.8 - 1139.0
10-28-68-01W5	1036.2 - 1140.0
02/15-23-68-01W5	1096 -1127.0
05-25-69-20W5	530.0 - 731.52
06-08-69-23W4	792.5 - 980.0
04-15-69-24W4	1005.8 - 1020
08-29-69-04W5	1230.0 - 1455.0
15-27-69-04W5	1215.0 - 1480.0
03-28-70-24W4	800.0 - 952.5
11-35-70-25W4	807.7 - 1050
02-23-70-01W5	854.0 - 1139.0
06-03-70-02W5	1075.0 - 1215.0
01-09-70-03W5	1036.3 - 1170.43
06-28-70-22W4	701.0 - 917.5
10-14-70-04W5	1200.9 - 1307.6
07-30-71-21W4	542.5 - 777.2
13-22-71-23W4	740.7 - 944.8
16-36-71-24W4	749.8 - 963.2
15-17-71-25W4	750.0 - 1012.0
10-01-71-26W4	829.1 - 1009.0
12-35-71-02W5	870.0 - 1140.0
06-09-71-08W5	1745.0 -1795.0
11-15-72-21W4	560.8 - 765.1
06-14-72-23W4	649.2 - 731.5
01-10-72-25W4	765.1 - 999.7
07-13-72-26W4	750.0 - 980.0
05-09-72-01W4	850.3 - 1039.4
02-28-72-02W4	870.0 - 1120.0
14-30-72-02W5	899.2 - 1164.3
10-28-72-20W4	563.9 - 679.7
10-16-73-21W4	570.0 - 579.0
11-15-73-24W4	691.9 - 902.2
16-12-73-25W4	740.0 - 855.0
16-15-73-01W5	832.1 - 1079.0
16-09-73-02W5	887.0 - 1018.3 quality?
04-27-73-03W5	948.0 - 1036.3 quality?
10-35-73-04W5	969.2 - 1140.0
07-22-74-22W4	600.5 - 789.4
02/07-22-74-23W4	687.0 - 887.0
14-31-74-23W4	731.5 - 920.5
04-16-74-24W4	740.7 - 947.9
10-30-74-25W4	847.3 - 1079.0
10-18-74-03W5	1060.7 - 1341.1
10-20-75-21W4	575.0 -770.0

10-09-75-24W4	813.8 - 1018.0
11-06-75-02W5	955.0 - 995.0, 1035.0 - 1110.0
11-06-75-02W5	600.5 - 789.4
10-04-75-03W5	950.0 - 1110.0
04-19-75-05W5	1204.0 - 1298.4
06-18-75-03W5	1234.4 - 1453.9
11-06-76-22W4	685.8 - 768.1
12-29-76-22W4	690.0 - 735.0
01-01-76-23W4	780.3 - 853.4
10-18-76-25W4	883.9 - 1039.4
14-30-76-25W4	951.0 - 1188.7
02-35-76-04-W5	1057.7 - 1313.7
10-06-76-05W5	1173.5 - 1310.6 lost of circulation, quality?
06-10-77-25W4	930.0 - 1100.0
06-33-77-22W4	545.0 - 710.0
10-07-77-04W5	1024.2 - 1191.8
14-32-77-06W5	1060.7 - 1188.7
11-32-77-05W5	1040.0 - 1220.0
11-25-78-24W4	566.9 - 746.8
11-17-78-02W5	790.0 - 1050.0
04-16-78-05W5	1057.7 - 1180.0
11-31-78-05W5	1050.0 - 1175.0
11-17-78-08W5	804.7 - 1054.6
12-10-78-08W5	914.4 - 1493.5
01-27-79-22W4	454.2 - 660.0
07-36-79-26W4	471.5 - 475.0
02-30-79-04W5	914.4 - 1008.9
12-33-79-06W5	1015.0 - 1213.1
10-18-80-23W4	472.4 - 481.6
06-29-80-24W4	442.0 - 515.0
11-34-80-03W5	709.0 - 979.6
11-12-80-05W5	978.4 - 1063.8
02-02-80-06W5	1069.9 - 1216.2
02-21-80-07W5	1082.0 -1188.7
11-10-81-25W4	521.3 - 527.3
16-16-81-05W5	890.1 - 1106.4
10-18-81-06W5	890.1 - 1176.5 quality?
10-07-82-22W4	500.0 - 680.0
10-06-82-01W5	612.6 - 856.5
04-19-82-07W5	1008.9 - 1149.1
13-24-84-02W5	589.8 -847.3
06-22-84-03W5	923.5 - 1103.4
10-23-83-06W5	819.9 - 990.6
04-21-83-07W5	923.5 - 1091.2
07-22-83-08W5	999.7 - 1130.8
14-35-84-24W4	405.4 - 688.9
06-22-84-03W5	774.2 - 944.9
02/10-31-84-04W5	853.4 - 1082.0

06-11-84-05W5	826.0 - 1042.4
11-21-84-06W5	780.0 - 970.0 quality?
06-31-84-07W5	890.0 - 1063.8
15-08-84-08W5	954.0 - 1072.9 quality?
04-16-84-08W5	960.0 - 1100.0 lots of cavings
02-27-84-10W5	963.2 - 1054.7
03-05-85-03W5	743.7 - 957.0
06-15-85-04W5	792.5 - 999.7
10-23-85-06W5	819.9 - 1057.7
06-10-86-05W5	1063.7 - 1112.5
11-01-86-06W5	1230.0 - 1590.1
10-19-86-06W5	1230.0 - 1495.0
09-06-86-07W5	917.5 - 966.2